Elevated source SF6-tracer dispersion experiments in the Copenhagen area

Gryning, Sven-Erik

Publication date:
1981

Document Version
Publisher's PDF, also known as Version of record

Risø-R-446

RISØ

Risø-R-446

Elevated Source SF_6-Tracer Dispersion Experiments in the Copenhagen Area

Sven-Erik Gryning

Risø National Laboratory, DK-4000 Roskilde, Denmark
November 1981

RISØ-R-446

ELEVATED SOURCE SF_6-TRACER DISPERSION EXPERIMENTS IN THE COPENHAGEN AREA

Sven-Erik Gryning

Abstract. Atmosperic dispersion experiments were carried out in the Copenhagen area under neutral and unstable conditions in order to study the atmosperic dispersion process in a built-up area. The tracer sulphurhexafluoride was released without buoyancy from a tower at a height of 115 m, and then collected at ground-level positions in up to three crosswind series of tracer sampling units, positioned 2-6 km from the point of release.

A description is given of the developed tracer technique and the instrument system for the determination of the three-dimensional fluctuating wind velocity used in these experiments.

The dispersion parameters were estimated from the measured tracer concentration distribution and compared with the dispersion parameters that can be calculated from the measured atmospheric parameters by various standard methods. Some of these methods have been in common use for a long time, while others reflect the current stage of research. Theoretical aspects of the various methods are considered and discussed in the

(continue on next page)

November 1981

Risø National Laboratory, DK 4000 Roskilde, Denmark

light of the experimental results. Based on the experiments, a semiempirical model is devised for predicting the lateral and vertical dispersion parameters for elevated point sources in an urban area under neutral and unstable conditions.

This report also contains a review of the fundamentals of dispersion theory. The more significant experimental campaigns reported in the literature are discussed briefly.

UDC 551.511:621.o39.85

The present thesis is submitted to the Technical University of Denmark in partial fulfilment of the requirements for the degree of lic. techn. (Ph.D.). Associate Professor Sven Hadvig acted as reponsible supervisor. Lic. techn. Niels E. Busch and mag. scient. Leif Kristensen functioned as supervisors.

ISBN 87-550-0828-3
ASSN 0106-2840

Risø Repro 1982

CONTENTS

A report that documents the experiments described herein will be published as: SVEN-ERIK GRYNING and ERIK LYCK. Elevated source SF_6-tracer dispersion experiments in the Copenhagen area. Data report. Risø-R-467.

PREFACE

The study presented in this report was carried out in close co-operation between the Air Pollution Laboratory of the Danish National Agency of Environmental Protection and the Meteorology Section of Risø National Laboratory.

1. INTRODUCTION

Usually the atmosphere is very efficient in dispersing pollutants released into it. This has resulted in its universal use as a pollutant depository. However, there are situations in which the dispersing ability is substantially reduced. In the common attempts to secure a generally acceptable air-quality, the existence of such situations led to increasing demands for improvements in the understanding of the atmospheric dispersion process. The demands are especially pronounced during periods of industrial expansion, bringing along an increased use of the atmospheric depository as well as a public concern for the environment.

The transport and dilution of effluents is almost entirely caused by the motion of the air, which can be thought of as a chaotic motion of eddies of all sizes. The eddies that can disperse pollutants are effectively fed from the shear of the mean wind and the warming of the ground by the sun, which creates the turbulence that is constantly evolving, propagating, breaking, stretching, and dissipating. Predictions of the spread of a plume are therefore closely linked to and of equal difficulty as the prediction of the behaviour of this complicated eddy motion. Intuitively, this makes predictions of the spread of effluents in the atmosphere a rather complicated task. In reality, purely theoretical attempts to describe the dispersion process have been rather unsuccessful, whereas some success has been obtained with entirely empirical approaches. At the present state of the art, the more successful methods are based on a combination of theoretical considerations and empirical approaches.

The study that is presented in this report was initiated primarily in order to gain insight into the characteristics of the dispersion process over a city. Much effort was put into measurements that describe the fluctuations in the air-motion, but also measurements that describe the energetics of the atmosphere were attempted.

A thorough measuring programme that deals with atmospheric dispersion, requires the possibility of using a tracer technique in order to test the models that are being used for describing the dispersion process. A tracer technique was developed and tested in two experimental campaigns that were carried out at Risø National Laboratory. As the Risø site is located on a peninsula in the Roskilde Fjord, these pilot experiments provided the possibility of studying dispersion over a non-homogeneous terrain. The results have been published (Gryning et al., 1978; Gryning and are reviewed in the appendix.

This report concentrates on full-scale elevated-source tracer dis persion experiments that were carried out in the Copenhagen area. It includes a description of the developed tracer technique, the meteorological measurements that were carried out during the experiments, and the analysis of that experimental data. Finally, based on the results from the experiments, a simple model is devised to calculate the spread of a plume of effluents that have been released from an elevated source in a built-up area in neutral and unstable conditions.

Preliminary and fragmentary parts from the analysis of the experimental results contained herein have been presented at symposia (Gryning et al., 1980b; Gryning and Lyck, 1980c), and have formed part of a course (Gryning and Lyck, 1980d).

2. DISPERSION THEORY

This chapter deals with aspects of the description of the atmospheric dispersion process. Fundamentals are reviewed of various purely theoretical plume-dispersion theories; the effects of time-averaging on the plume properties are discussed including a short presentation of some basic properties of relative dispersion. Also treated is the dependence on the spread of a plume of some micrometeorological parameters, and a number of practical applicable methods for the prediction of the spread of a plume are presented.

2.1. Dispersion models

Material released into the atmosphere will disperse more or less rapidly under the influence of the turbulent eddies. The theoretical description of the atmospheric dispersion process has not yet been uniquely formulated in the sense that a single physical model explaining all important aspects of the problem still has to be developed. Instead, the theoretical efforts have been devoted to basically four types of models. These are:

1) the closure models, of which a special case is the gradient transfer approach (also called first-order closure)
2) the statistical theory models
3) the Lagrangian similarity theory models, and
4) the mixed-layer similarity theory models for dispersion under convective conditions.

Historically, the theories were formulated in the aforementioned sequence. In the closure models, the dispersion process is formulated in terms of the equation of conservation of the dispersed material. The statistical theory is a kinematic approach in which the spreading of material due to atmospheric dispersion is described in terms of the statistical properties of the fluid motion. Most recently, similarity theories have been developed.

In these models the physical parameters that are expected to control the dispersion process are postulated, and formulas that relate atmospheric dispersion to the postulated parameters are derived by dimensional analysis. These theories include descriptions of dispersion from ground-level sources, called Lagrangian similarity theories. Recently theories for elevated sources have been formulated that describe the atmospheric dispersion process under strongly convective conditions; these are called mixed-layer scaling theories.

2.1.1. Closure models

All closure models rest on an equation for the conservation of the material that is being dispersed. Denoting the instantaneous concentration of material by χ, the continuity equation reads

$$\frac{d\chi}{dt} = \text{sources} + \text{sinks} \qquad (2.1)$$

which, in words, simply states that the concentration of material in a volume of the fluid following the fluid motion changes due only to the action of sources or sinks inside the volume. In order to describe the behaviour of the mean concentration, and possibly get a suitable measure of the statistical deviation from the mean at a specific position x_i, where x_1, x_2, and x_3 are the horizontal along-wind, horizontal crosswind and vertical direction in a Cartesian co-ordinate system, the instantaneous concentration and wind velocity are decomposed according to the Reynold convention:

$$u_i = \bar{u}_i + u_i' \qquad (2.2)$$

$$\chi = \bar{\chi} + \chi'$$

where an overbar denotes averaging and the prime the deviation from the average; u_i is the instantaneous value of the i'th component of the wind velocity. The Reynolds decomposition scheme requires that it be possible to define a suitable average value. A discussion of the necessary conditions which a quantity

must fulfil in order for the decomposition to be valid, can be found in Panofsky (1979). When applying the decomposition to (2.1), the concentration of material at a specific position, x_i, is governed by

$$\frac{\partial(\bar{\chi} + \chi')}{\partial t} + (\bar{u}_i + u_i') \frac{\partial(\bar{\chi} + \chi')}{\partial x_i} = \text{sources} + \text{sinks} \quad (2.3)$$

where the usual summation convention of repeated indices is assumed. In order to obtain an expression for the average concentration the equation is ensemble averaged, yielding

$$\frac{\partial \bar{\chi}}{\partial t} = - \bar{u}_i \frac{\partial \bar{\chi}}{\partial x_i} - \frac{\partial(\overline{u_i'\chi'})}{\partial x_i} + \text{sources} + \text{sinks} \quad (2.4)$$

(1) (2) (3)

Equation (2.4) states that the change in time of the mean concentration at a specific position (Term 1), is due to advection of material with the mean flow field (Term 2) plus the divergence of the turbulent fluxes of material (Term 3) plus sources and sinks. Solving (2.4) with respect to the mean concentration requires knowledge of the flow field, which, for example, can be obtained either from measurements on a specific flow field, from mathematical descriptions of the flow-field or by obtaining simultaneous solutions of the equations of motion (the Navier-Stokes equations) with appropriate boundary conditions. Besides sources and sinks the turbulent fluxes of material must also be known.

First-order closure models. In attempts to solve (2.4) when the mean wind field is known, some success has been obtained by assuming proportionality between the turbulent fluxes of material and the mean gradient of the material, thus

$$\overline{u_i'\chi'} = - K_{ij} \frac{\partial \bar{\chi}}{\partial x_j} \quad (2.5)$$

where K_{ij} are the constants of proportionality, called the Austauch coefficients or diffusivities. Because $\overline{u_i'\chi'}$ and

$\partial\bar{\chi}/\partial x_j$ are vectors, the diffusivities constitute a second rank tensor. This expression is vastly simplified by the assumption that the off-diagonal elements in the tensor equal zero. It should be kept in mind, however, that there is no a priori reason to expect the off-diagonal elements in the tensor to be zero as pointed out in Lettau (1952), and in turn cited in Corrsin (1974). With the off-diagonal elements equal to zero, (2.4) reduces to

$$\frac{\partial\bar{\chi}}{\partial t} = -\bar{u}_i \frac{\partial\bar{\chi}}{\partial x_i} + \frac{\partial}{\partial x_i}\left(K_i \frac{\partial\bar{\chi}}{\partial x_i}\right) + \text{sources} + \text{sinks} \qquad (2.6)$$

which is the form in which (2.4) most often is presented when closed at 1st order. Here we write for convenience $K_{11} = K_1$, $K_{22} = K_2$ and $K_{33} = K_3$. With constant but not necessarily equal values of K_i the type of dispersion process implied by (2.6) is called Fickian.

The significance of (2.6) naturally rests on the physical significance of the assumption that the flux of material adequately can be described as in (2.5). It is characteristic for the dispersion process in the atmosphere that the plume will be acted on by the whole spectrum of turbulent fluctuations. Only the fluctuations that are of the actual size of the plume will disperse it in the sense of broadening, however, whereas the fluctuations on a length scale larger than the plume will move the whole plume without broadening. It is evident that such a complicated dispersion process, with a multitude of length scales involved, cannot be expected to be adequately described by (2.5) except under special circumstances. Such a case is vertical dispersion from a ground-level source, where both the plume dimensions and the turbulent fluctuations are limited by the presence of the ground. In this case the magnitude of the vertical length scale of the turbulence is about equal to height of the plume at every position downwind.

A solution to (2.6) in the special case of anisotropic dispersion with constant but different values of K_i and with the mean wind velocity, $\bar{u}_1$, constant with height, was first found by Roberts (1923) (cited by Sutton (1953)) for a continuous point

source in the absence of boundaries as

$$\bar{\chi}(x_1,x_2,x_3) \simeq \frac{Q}{4\pi\, x_1 \sqrt{K_2K_3}} \exp\left[-\frac{\bar{u}_1}{4x_1}\left(\frac{x_2^2}{K_2}+\frac{x_3^2}{K_3}\right)\right] \qquad (2.7)$$

where Q is the material release rate. The importance of this expression is that the shapes of the dispersed material in the crosswind and vertical direction are Gaussian distributions being characterized by the standard deviations

$$\sigma_y = \left\{2K_2 \frac{x_1}{\bar{u}_1}\right\}^{\frac{1}{2}} \qquad (2.8)$$

$$\sigma_z = \left\{2K_3 \frac{x_1}{\bar{u}_1}\right\}^{\frac{1}{2}}$$

where σ_y and σ_z are the standard deviations in the crosswind and vertical directions, respectively. Thus, constant K-theory predicts that the size of a plume be proportional to the square root of the travel time, t, since $t = x_1/\bar{u}_1$. Comparison with results from full-scale atmospheric dispersion experiments shows that σ_y and σ_z grows proportionally with x^p, where p lies in the range 0.75-1 in near neutral conditions. Therefore, the equivalent values of K_i must increase systematically with time of travel. The reason is that in the atmosphere eddies of all sizes are present, but constant K_i infers that eddies of only one general size exists as is the case in the molecular diffusion process, for example. This has brought about a number of numerical and analytical efforts to solve (2.6) with variable K_i (see for example Berkowicz and Prahm (1979)).

On the vertical concentration distribution from ground-level sources. The shape of the vertical concentration distribution will be investigated by means of the expression for an infinite crosswind line sources, emitting at a constant rate. Because the x_1 direction is in the direction of the mean wind, the advection term in (2.6) reduces to $\bar{u}_1 \frac{\partial \bar{\chi}}{\partial x_1}$, the crosswind

dispersion term vanishes due to the nature of the sources; neglecting along-wind dispersion as well as sources and sinks, (2.6) reduces to

$$\bar{u}_1 \frac{\partial \bar{\chi}}{\partial x_1} = \frac{\partial}{\partial x_3}\left(K_3 \frac{\partial \bar{\chi}}{\partial x_3}\right) \tag{2.9}$$

This equation can be solved for power-law functions of K_3 and $\bar{u}_1$

$$K_3(x_3) = (K_3)_o \left(\frac{x_3}{(x_3)_o}\right)^p$$

$$\bar{u}_1(x_3) = (\bar{u}_1)_o \left(\frac{x_3}{(x_3)_o}\right)^m \tag{2.10}$$

where $(K_3)_o$ and $(\bar{u}_1)_o$ are the values of K_3 and $\bar{u}_1$ at the height $(x_3)_o$. These expressions can be brought to fit actual profiles reasonably well. For a ground-level source, the boundary conditions yield

$$\bar{\chi} \to 0 \quad \text{as} \quad x_1, x_3 \to \infty$$

$$\bar{\chi} \to \infty \quad \text{at} \quad x_1^2 + x_3^2 \to 0$$

$$K_3 \frac{\partial \bar{\chi}}{\partial x_3} \to 0 \quad \text{as} \quad x_3 \to 0, \; x_1 > 0$$

Roberts solution (1923), as cited by Sutton (1953), reads for $(x_3)_o$ as the length unit

$$\bar{\chi}(x_1, x_3) = \frac{Qr}{(\bar{u}_1)_o \Gamma(s)} \left[\frac{(\bar{u}_1)_o}{r^2 (K_3)_o x_1}\right]^s \exp\left[-\frac{(\bar{u}_1)_o x_3^r}{r^2 (K_3)_o x_1}\right] \tag{2.11}$$

where Q is the emission per unit length, $r = m-p+2$ and $s = (1+m)/(m-p+2)$. The solution is valid for $m-p+2 > 0$. Thus, the vertical concentration distribution is an exponential function of the height raised to the power r. For $r = 2$, the distribution is Gaussian.

The power m varies in neutral conditions approximately from 0.1 over smooth terrain to about 0.4 at greater surface roughness. The power decreases as the air turns more unstable. The diffusivity coefficient, K_3, in neutral air varies linearly with height, causing $p = 1$. Typical values of p, m, r, and s are shown in Table 2.1 (Panofsky, 1979).

Experimental studies of ground-level source dispersion resulted in values of r in the range 1.1 to 1.5 (Elliott, 1961; Nieuwstadt and van Ulden, 1978), which is fairly consistent with the listed values in Table 2.1. Experimental values of r as small as 0.67, which constitute the free convective limit, have not been reported, but may well exist. The Gaussian solution, $r = 2$, is not represented in Table 2.1, which covers only neutral and unstable conditions, but this concentration distribution may well exist under stable conditions.

Table 2.1. Typical values of the parameters in the power laws for K_3 and $\bar{u}_1$, (2.10), and in the solution of the diffusion equation for a linesource, (2.11).

parameter	neutral smooth	neutral rough	moderately unstable	free convection
p	1	1	1.1	1.33
m	0.14	0.4	0.1	0
r	1.14	1.4	1	0.67
s	1	1	1.1	1.5

On the vertical concentration distribution from elevated sources

Use of (2.9) to calculate the vertical concentration distribution for an elevated source is not generally accepted, contrary to the situation for the ground-level sources. This is associated essentially with the height variation of the scale of the vertical component of the turbulence. As discussed before, successful application of K-theory requires that the length scales of the turbulence are sufficiently small compared with the length scales of the plume. This is typically the case for vertical dispersion from ground-level sources, as the vertical length scale of the turbulence varies linearly with height and therefore always will be comparable with the length scale of the plume. For elevated sources, this is not the case. Initially the vertical size of the plume is small compared with the vertical length scale of the turbulence, but downwind from the source, a progression takes place from the initial stage to a stage where the plume acts as originating from a ground-level source. Until this last stage is reached, K-theory is inadequate.

Nevertheless, solutions to (2.9) for an elevated source have been worked out by Smith (1957). The solution turns out to be exceedingly complicated, and bearing in mind the fundamental difficulties of this method, it is mainly of academic interest. To gain an impression of the vertical shape of the concentration distribution observations have to be investigated. Table 2.2 is a part of a table taken from Pasquill (1957a), where it is concluded that an assumption of Gaussian shape of the vertical concentration distribution is unlikely to be too greatly in error as long as the plume is not too far downwind of the position of the ground-level maximum concentration, and the plume still retains features that can be attributed to the elevation of the source. The non-Gaussian shapes appear downwind when the concentration distribution has a tendency to resemble that for ground-level sources.

Table 2.2. Evidence of the shape of the vertical concentration distribution from elevated point sources, Pasquill (1975a).

Nature of data	Gaussian or not	Reference
Tracer distribution 100-150 m from elevated source	yes	Hay and Pasquill (1957)
Properties at maximum in ground-level concentration from an elevated source of pollution*	yes	Pasquill (1974)
Lidar studies of power station plumes	yes	Hamilton (1969)

*This analysis involves the "image source" model for the effect of the boundary on the vertical distribution.

Higher order closure models. From a physical point of view, a more satisfactory treatment of the dispersion process can be obtained by giving up the K-theory assumption of proportionality between the local concentration gradient and the flux, and instead directly include the fluxterms, $\overline{u_i \chi'}$, in the calculations (second-order closure). In order to close the system, triple correlations must then be expressed in terms of already known variables. Several attempts to solve the problem of turbulent dispersion along this line are under way, all characterized by a rather high level of complexity, but none of these attempts has yet yielded readily usable results for calculating concentration distributions.

2.1.2. Statistical dispersion theory

The statistical dispersion theory was founded by G.I. Taylor (1921). Most textbooks reference Taylor directly without derivation when stating the fundamental formula. Therefore, it is justifiable here to rederive the formula. It is derived for the crosswind component only.

Consider a homogeneous, stationary fluid, that is, a fluid in which the statistical properties of the motion at every point at all times are the same. The Lagrangian autocorrelation function, $R_{L,v}(\xi)$, with time lag ξ is defined as

$$R_{L,v}(\xi) = \frac{\overline{v'(t) \cdot v'(t + \xi)}}{\overline{v'^2}} \tag{2.12}$$

where $v'(t)$ is the crosswind velocity for a specific air parcel at time t, and $v'(t + \xi)$ is the crosswind velocity for the same parcel of air at time $t + \xi$. Because we look at crosswind dispersion, $\bar{v} = 0$. Thus, $R_{L,v}(\xi)$ is the correlation coefficient between the value of v' for an air parcel at any instant, and the value of v' for the same air parcel after an interval of time, ξ. Due to the assumption of homogeneity and stationarity, it is irrelevant to specify the time and place for the measurements, as $R_{L,v}(\xi)$ depends only on time differences. Equation (2.12) is equivalent to

$$\int_0^t \overline{v'(t) \cdot v'(t + \xi)} d\xi = \overline{v'^2} \int_0^t R_{L,v}(\xi) d\xi \tag{2.13}$$

which can be transformed to

$$\overline{v'^2} \int_0^t R_{L,v}(\xi) d\xi = \overline{v'(t) \int_0^t v'(t + \xi) d\xi} \tag{2.14}$$

but the right-hand side is the mean of the crosswind distances that the air-parcels have travelled in time t, multiplied by

the velocity at the same time. Thus (2.14) can be expressed as

$$\overline{v'^2} \int_0^t R_{L,v}(\xi)d\xi = \overline{v'(t)\cdot Y} \qquad (2.15)$$

where Y is the distance traversed by an air parcel in time t. But

$$\overline{v'(t)\cdot Y} = \frac{1}{2}\frac{d}{dt}(\overline{Y^2}) \qquad (2.16)$$

which infers that (2.15) can be written

$$\overline{Y(T)^2} = 2\,\overline{v'^2} \int_0^T \int_0^t R_{L,v}(\xi)d\xi dt \qquad (2.17)$$

The quantity $\overline{Y(T)^2}$ is the mean-square crosswind distance travelled by the air parcels in the time T; consequently it is a measure of the spread of the plume. Equation (2.17) is Taylor's (1921) dispersion formula. It is characteristic for this formula that it reduces the problem of dispersion in homogeneous, stationary turbulence, to considerations of the correlation between the wind velocity of an air parcel at one instant to its velocity at a time ξ later.

When T is so small that $R_{L,v}(T)$ can be set equal to 1, (2.17) reduces to

$$\int_0^T \int_0^t d\xi dt = \frac{1}{2}T^2$$

Thus

$$\overline{Y(T)^2} = \overline{v'^2} \cdot T^2 \quad \text{for small T.} \qquad (2.18)$$

The lateral spread is proportional to T for small T. For large values of T, $R_{L,v}(T)$ will effectively be equal to 0. By in-

troducing the Lagrangian time scale, $t_{L,v}$

$$t_{L,v} = \int_0^\infty R_{L,v}(\xi)d\xi \tag{2.19}$$

(2.17) can be written

$$2\,\overline{v'^2}\int_0^T t_{L,v}\,d\xi = 2\,\overline{v'^2}\;T\;t_{L,v}$$

Thus

$$\overline{Y(T)^2} = 2\,\overline{v'^2}\;t_{L,v}\;T \quad \text{for large } T \tag{2.20}$$

For large times of travel T, the crosswind spread is proportional to $T^{\frac{1}{2}}$.

A reformulation of Taylor's formula was published by Kampé de Fériet (1939). Integration of (2.17) by parts yields

$$\overline{Y(T)^2} = 2\,\overline{v'^2}\int_0^T 1\left\{\int_0^t R_{L,v}(\xi)d\xi\right\}dt$$

$$\overline{Y(T)^2} = 2\,\overline{v'^2}\left\{\left[t\int_0^t R_{L,v}(\xi)d\xi\right]_0^T - \int_0^T t\,R_{L,v}(t)dt\right\}$$

$$\overline{Y(T)^2} = 2\,\overline{v'^2}\left\{T\int_0^T R_{L,v}(\xi)d\xi - \int_0^T \xi\,R_{L,v}(\xi)d\xi\right\}$$

which leads to Kampé de Fériet's form of Taylor's formula

$$\overline{Y(T)^2} = 2\,\overline{v'^2}\int_0^T (T-\xi)R_{L,v}(\xi)d\xi \tag{2.21}$$

The autocorrelation function is related to the variance spectra by the inverse Fourier transform

$$R_{L,v}(\xi) = \int_0^\infty F_{L,v}(n) \cos(2\pi n\xi) dn \qquad (2.22)$$

where $F_{L,v}$ is the normalized Lagrangian power spectrum for the lateral wind velocity and n is the frequency. Substituting (2.22) into (2.21) yields

$$\overline{Y(T)^2} = 2\,\overline{v'^2} \int_0^T (T - \xi) \int_0^\infty F_{L,v}(n) \cos(2\pi n\xi) dn d\xi \qquad (2.23)$$

Because the Fourier integral in (2.22) is convergent, it is possible to change the order of integration. Thus, (2.23) can be written

$$\overline{Y(T)^2} = 2\,\overline{v'^2} \int_0^\infty F_{L,v}(n) \left\{ \int_0^T (T - \xi) \cos(2\pi n\xi) d\xi \right\} dn \qquad (2.24)$$

Integration of the bracket by parts yields

$$\int_0^T (T - \xi) \cos(2\pi n\xi) d\xi = \left[- \frac{\cos(2\pi n\xi)}{(2\pi n)^2} \right]_0^T$$

which enables us to write (2.24) as

$$\overline{Y(T)^2} = 2\,\overline{v'^2} \int_0^\infty F_{L,v}(n) \frac{1-\cos(2\pi nT)}{(2\pi n)^2} dn$$

which is a form of (2.21) that can be found also in Kampé de Fériet (1939). This expression can be further reduced to

$$\overline{Y(T)^2} = T^2\,\overline{v'^2} \int_0^\infty F_{L,v}(n) \left(\frac{\sin(\pi nT)}{\pi nT} \right)^2 dn \qquad (2.25)$$

In this form, the expression displays a basic property of atmospheric dispersion from a continuous point source. For short travel times, the integral becomes close to unity which implies that wind velocity oscillations of all frequencies contribute to the dispersion of the plume. For larger values of T, the low frequency oscillations of the wind velocity will be dominant in the dispersion process. As the size of the plume dimensions increases with the travel time, the efficiency of the smaller eddies in further dispersion of the plume decreases.

2.1.3. Lagrangian similarity theory

Lagrangian similarity theory is based on the idea that the properties of a plume dispersed by the atmosphere remain self-similar throughout the flow, meaning that the characteristic shape of the plume is the same all over, and only the size of the plume is altered as it grows downwind from the source. This infers, for example, that the vertical concentration distribution of material from a ground-level source should differ by only a scaling factor throughout the flow, leaving the shape unaltered. The calculations of the scaling factor rest on Monin-Obukhov similarity theory, which restricts the range of applications of Lagrangian similarity theory to dispersion in the surface layer. The growth of the plume in the vertical direction is known to be described well by the scaling factor derivable from Monin-Obukhov theory (Horst, 1979; Nieuwstadt and van Ulden, 1978), but the scaling works poorly for the plume growth in the crosswind direction. When applied only for the vertical concentration distribution, the self-similarity assumption yields

$$\frac{\bar{\chi}(z)}{\bar{\chi}_o} = f_s\left(\frac{z}{\hat{z}}\right) \qquad (2.26)$$

where $\bar{\chi}(z)$ is the concentration at the height z, $\bar{\chi}_o$ the concentration at ground-level, and $\hat{z}$ is defined by

$$\hat{z} = \frac{\int_0^\infty z\bar{\chi}(z)dz}{\int_0^\infty \bar{\chi}(z)dz} \tag{2.27}$$

In this way, $\hat{z}$ becomes a function of the downwind distance from the source. Monin-Obukhov similarity theory states that the properties of the atmospheric turbulence in the surface layer are determined by only the height z, surface shear stress τ, sensible heat flux H, acceleration of gravity g, and temperature $\bar{T}$, and the quantities ρ and c_p, being density of air and specific heat of air at constant pressure, respectively. A characteristic velocity, called the friction velocity u_*,

$$u_* = \left(\frac{\tau}{\rho}\right)^{\frac{1}{2}} \tag{2.28}$$

as well as a characteristic length, called the Monin-Obukhov length L,

$$L = -\frac{u_*^3}{k\left(\frac{g}{\bar{T}}\right)\left(\frac{H}{\rho c_p}\right)} \tag{2.29}$$

can be formed from the quantities. The constant $k \approx 0.4$ is the so-called von Kármán constant. Note that g and $\bar{T}$ appear in the combination $g/\bar{T}$, which is called the buoyancy parameter. Lagrangian similarity theory proposes that the rate of change of the mean height of the plume can be expressed as a function of the friction velocity and the Monin-Obukhov length through

$$\frac{d\hat{z}}{dt} = a\, u_*\, G\left(\frac{\hat{z}}{L}\right) \tag{2.30}$$

a being a constant chosen so that G is unity in neutral conditions. This infers that the average height of the plume is proportional to the time of travel. Chaudry and Merony (1973) extended the Lagrangian similarity theory to include dispersion in unstable conditions. It was shown theoretically by use of

K-theory and by assuming equality between the diffusivities of material and heat that (2.30) can be written

$$\frac{d\hat{z}}{dt} = b\, u_* \, \phi_h^{-1} \left(\frac{\hat{z}}{L}\right) \tag{2.31}$$

where b is a slowly varying function of stability that in practice can be set equal to von Kármán's constant, and ϕ_h is the dimensionless temperature gradient defined by

$$\phi_h\left(\frac{z}{L}\right) = \frac{kz}{T_*} \frac{\partial \bar{\theta}}{\partial z}$$

where

$$T_* = - \frac{H}{c_p \rho u_*}$$

and $\bar{\theta}$ is the potential temperature. In the limit of free convection (2.31) must be independent of u_*. As the Monin-Obukhov length is proportional to the friction velocity to the third power, then ϕ_h theoretically in the condition of free convection should obey

$$\phi_h\left(\frac{\hat{z}}{L}\right) \propto \left(\frac{\hat{z}}{L}\right)^{-\frac{1}{3}} \tag{2.32}$$

Substitution of (2.32) into (2.31) leads to

$$\frac{d\hat{z}}{dt} = A\hat{z}^{\,1/3} \tag{2.33}$$

which upon integration yields

$$\hat{z} = C\, T^{3/2} \tag{2.34}$$

Here A and C are constants and T the time of travel. Thus, in conditions of free convection the plume height is proportional to $T^{3/2}$.

Instead of expressing the vertical plume height in terms of time of travel, it can be written in terms of the downwind distance x. The mean horizontal velocity of material, dx/dt,

that have travelled a distance x, is given by

$$\frac{dx}{dt} = \frac{\int_0^\infty \bar{\chi}(z)\bar{u}(z)dz}{\int_0^\infty \bar{\chi}(z)dz} \qquad (2.35)$$

The velocity, dx/dt, is equal to the wind velocity at height $c\hat{z}$

$$\frac{dx}{dt} = \bar{u}(c\hat{z}) \qquad (2.36)$$

where the precise value of c depends on the actual vertical concentration distribution and the wind velocity profile. However, c is known empirically to be a rather weak function of these parameters and is approximated well by a constant value of $c \simeq 0.6$. According to Businger (1973) the mean wind velocity at height $c\hat{z}$ can be expressed as

$$\bar{u}(c\hat{z}) = \frac{u_*}{k}\left[\ln\left(\frac{c\hat{z}}{z_o}\right) - \psi\left(\frac{c\hat{z}}{L}\right)\right] \qquad (2.37)$$

where z_o is the so-called roughness length and ψ is a dimensionless function only of z/L that describes the effect of stability. Under neutral conditions, $\psi(o)$ equals zero; this infers a logarithmic mean wind profile. Combining equations (2.31), (2.36), and (2.37), and setting b=k, yields

$$\frac{d\hat{z}}{dx} = \frac{k^2}{\phi_h\left(\frac{\hat{z}}{L}\right)}\left[\ln\left(\frac{c\hat{z}}{z_o}\right) - \psi\left(\frac{c\hat{z}}{L}\right)\right]^{-1} \qquad (2.38)$$

To give an example, the value of c will be calculated for a neutral wind profile with the dispersed material completely mixed between the ground, taken as the height of the roughness length z_o, and a capping inversion at height z_i. Calling the concentration of material $\bar{\chi}$, the mean velocity of the plume reads

$$\frac{dx}{dt} = \frac{\int_{z_o}^{z_i} \bar{\chi} \cdot \frac{u_*}{k} \ln\left(\frac{z}{z_o}\right) dz}{\int_{z_o}^{z_i} \bar{\chi} dz} \qquad (2.39)$$

Because $z_o << z_i$

$$\frac{dx}{dt} = \frac{u_*}{kz_i} \int_{z_o}^{z_i} \ln\left(\frac{z}{z_o}\right) dz \qquad (2.40)$$

which upon integration yields

$$\frac{dx}{dt} = \frac{u_*}{k} \ln\left(\frac{2}{e} \cdot \frac{\hat{z}}{z_o}\right) \qquad (2.41)$$

where $\hat{z} = z_i/2$. This shows that the mean velocity of the plume in question equals the mean wind velocity at the height $z = \frac{2}{e}\hat{z}$ or $c \simeq 0.74$. If the concentration distribution is not constant with height, but the concentrations are larger close to the ground as is usually the case for ground-level sources, the value of c will be reduced further below 2/e.

Under neutral conditions, (2.38) reduces to

$$\frac{d\hat{z}}{dx} = \frac{k^2}{\ln\left(\frac{c\hat{z}}{z_o}\right)} \qquad (2.42)$$

or

$$\int_{z_o}^{\hat{z}} \ln\left(\frac{cz}{z_o}\right) dz = k^2 \int_{o}^{x} dx \qquad (2.43)$$

which can be integrated to yield

$$\frac{x}{z_o} = \frac{\hat{z}}{z_o k^2}\left[\ln\left(\frac{c\hat{z}}{z_o}\right) - 1 + \frac{z_o}{\hat{z}}\left(1 - \ln c\right)\right] \qquad (2.44)$$

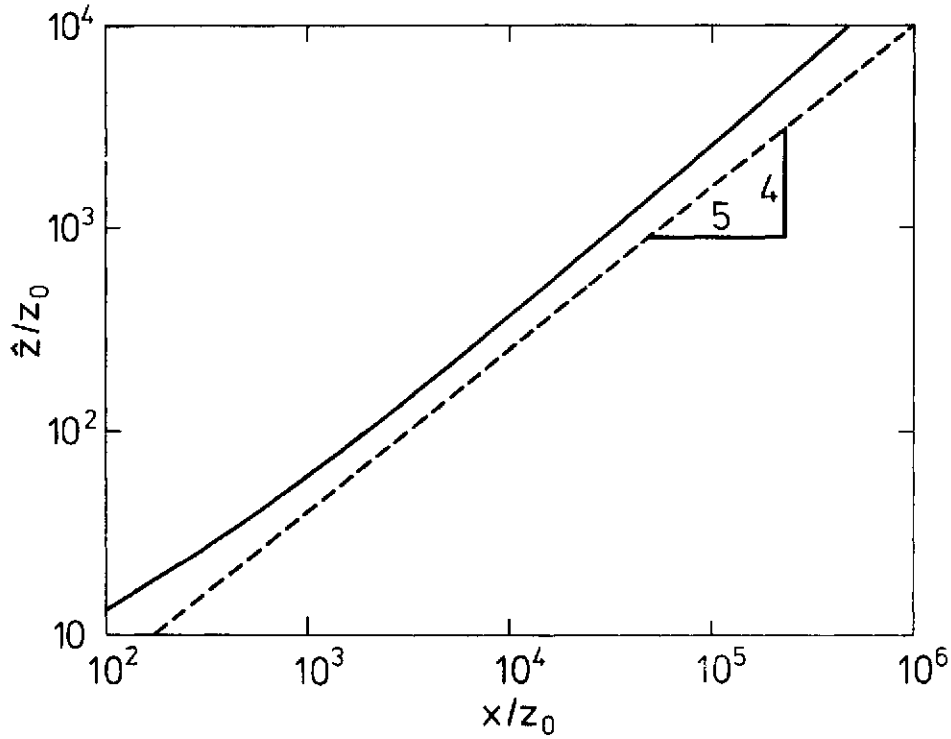

Fig. 2.1. Normalized mean plume height, $\hat{z}/z_0$ as a function of normalized downwind distance, x/z_0, according to (2.44) with c = 0.6. This relation is valid under neutral conditions only. Experiments show that $\hat{z}$ varies approximately as $x^{0.8}$. The dashed line illustrates the relation $\hat{z} \propto x^{0.8}$, and the predictions of (2.44) are seen to be well in accordance with the $x^{0.8}$ behaviour.

Experiments show that $\hat{z}$ varies approximately as $x^{0.8}$ in neutral air, which is well in accordance with (2.44) and Fig. 2.1.

2.1.4. Dispersion in the convective boundary layer

The convective boundary layer consists of the part of the planetary boundary layer, where the dispersion processes are controlled primarily by convective motion of the air, created by upward-directed surface heat flux. Wind-shear-generated mechanical turbulence is responsible only for a minor part of the mixing and cannot compete with the thermal convective plumes for control of the dispersion processes. The depth of the convective boundary layer is limited by the height of the lowest

inversion. A similar well-defined lower limit does not exist, because the wind-shear-produced mechanical turbulence gradually increases downward, and is completely predominant over the thermalproduced turbulence close to the ground. Often, the lower limit of the convective boundary layer is defined as the height, where the wind-shear-driven production of turbulent energy equals the production of convective-type turbulent energy. This height is about the size of -L, where L is the Monin-Obukhov length.

The flow pattern in the convective boundary layer is controlled by more or less distinct large eddies with relatively long lifetimes, (Kaimal et al., 1976). The eddies are created by thermal plumes that arise randomly in space and time. They entrain air close to the ground and transport it upward, thus creating local regions near the ground with strong horizontal convergence as illustrated in Fig. 2.2. This phenomenon is known as the sweep-up effect. Above the ground, relatively

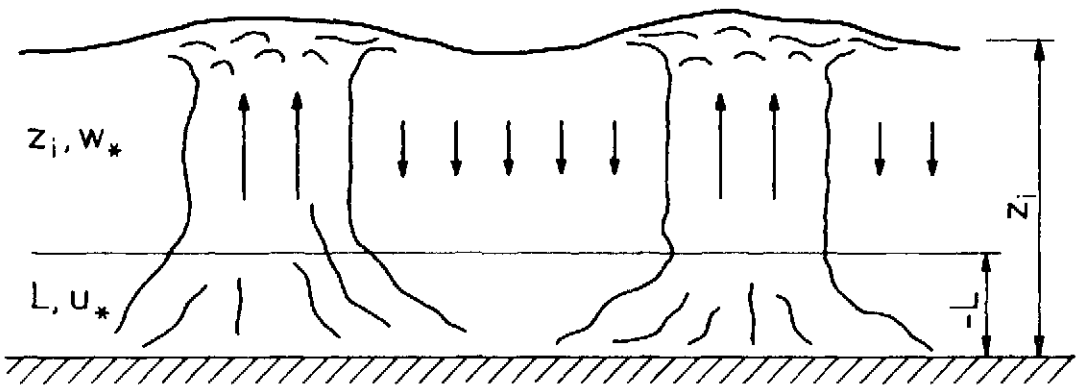

Fig. 2.2. Under convective conditions the dispersion process will be highly influenced by mechanical turbulence from the ground up to the height -L, and will be controlled by the structure of the convective cells in the layer that extends from the height -L up to the capping inversion at height z_i. Scaling parameters in the two layers are shown. The figure also illustrates that regions of slowly sinking air cover a broader area than those with upward-directed air motion.

narrow regions with strong updraft of warm air, sucked up close to the ground, alternates broader regions with slowly sinking air, brought down from the cooler region above. Air-pollutants emitted close to the ground, air likely to be sucked up in the thermal plumes, and the air just above the ground will be replaced with air coming from the outside region. If the air pollutants originally are enclosed in a narrow region compared with the horizontal size of the thermal plumes, sweep-up of the plume will replace the polluted air close to the ground with cleaner air from outside.

When the transport of upward heat flux is so relatively small that wind-shear-induced mechanical turbulence plays a significant role, the large-scale eddies will tend to arrange themselves in lines, roughly aligned with the mean wind-direction, the so-called vortex rolls, (Lemone, 1973).

Parameterization of dispersion in the convective boundary layer.

Parameterization of the atmospheric dispersion processes in a convective boundary layer has been proposed by Deardorff and Willis (1975). The approach rests basically on the assumption that the structure of the convective boundary layer is determined by the mixing depth, z_i, and by the positive kinematic surface heat flux, $(\overline{w'T'})_o$. Defining the length scale as z_i, dimensional analysis gives for the characteristic velocity scale

$$w_* = \left(\frac{g}{\bar{T}} z_i (\overline{w'T'})_o\right)^{1/3} \qquad (2.45)$$

where $g/\bar{T}$ is the usual bouyancy parameter for an ideal gas. A condition was introduced by Willis and Deardorff (1978) to assure that the mean wind-velocity is effectively constant with height throughout the convective boundary layer. This condition that expresses that the atmosphere is not too close to being neutral is

$$-\frac{z_i}{L} > 10 \qquad (2.46)$$

Simulation of the ability of the convective boundary layer to disperse and mix was performed by Deardorff and Willis. The experiments took place in a tank, where the working fluid was water. The chamber had transparent sidewalls, the lower chamber surface was an aluminium plate heated from below by circulating warm water. Prior to an experiment, the chamber was filled with an appropriate amount of water, and an overlaying stable layer was then formed by carefully floating in layers of increasingly warmer water. This upper layer would act as an upper limit for the motion in the lower part of the fluid. Convective motion in the water was initiated by heating the aluminium bottom of the tank. When the convective motion was fully established, neutrally buoyant droplets with an average diameter of 0.8 mm were released along the centerline, extending the length of the chamber, and the lateral and vertical spread of the droplets were determined as a function of time by means of a photographic technique. When the particles reached the sidewalls, the experiment was stopped.

The full series of pictures displayed how the droplets, released as an instantaneous line source, disperse as a function of time. By use of the scaling parameters z_i and w_*, the appropriate dimensionless distance X, is given by

$$X = (w_*/z_i)t \tag{2.47}$$

where t is the time elapsed from the start of the experiment.

By assuming that Taylor's hypothesis is applicable, the transformation can be made between the measured dispersion from the instantaneous line source to a simulated continuous point source in the presence of a significant mean wind velocity. The transformation requires that the dispersion in the direction of the mean wind is small compared to the effect of advection. The required limitations for this approach to be valid has been established to be (Willis and Deardorff, 1978)

$$1.2 < \frac{\bar{u}}{w_*} < 6 \tag{2.48}$$

Violation of the left side of the expression indicates that the mean wind is not much larger than the eddy velocities, which again implies that the upstream turbulent dispersion will be significant. If $\bar{u}$ is too large for (2.48) to be satisfied, then the wind shear becomes important in the bulk of the convective boundary layer and competes with the thermal convection for control over the dispersion process. In the Pasquill stability classification, the conditions roughly correspond to stability classes A and B (Deardorff and Willis, 1975).

By use of the scaling parameters, lengths are made dimensionless as

$$Y = \frac{y}{z_i} \quad , \quad Z = \frac{z}{z_i} \tag{2.49}$$

where y and z are lateral and vertical distances, respectively. The dimensionless concentration, $\bar{C}$, of the released material reads

$$\bar{C} = (z_i^2 \, \bar{u}/Q)\bar{\chi} \tag{2.50}$$

where $\bar{\chi}$ is the actual concentration, measured in mass per unit volume, and Q is the source strength of the continuous point source. The crosswind-integrated value of $\bar{C}$ is denoted by

$$\bar{C}^Y = \int_{-\infty}^{\infty} \bar{C}(X,Y,Z)\,dY \tag{2.51}$$

Dimensionless results from a series of tank experiments reported by Willis and Deardorff (1976) and (1978) are shown in Fig. 2.3. The dimensionless source heights, h/z_i, in the two experiments, are 0.067 and 0.25, h being the actual source height.

Comparison of the crosswind-integrated concentrations for $h/z_i = 0.067$ and $h/z_i = 0.25$ shows that the source height is of great importance for the dispersion until the line of maximum concentration reaches ground-level. By considering this point as a virtual origin, Willis and Deardorff (1978) point out

that beyond this origin - which for $h/z_i = 0.067$ is very close to the source and for $h/z_i = 0.25$ situated at a dimensionless distance $X \simeq 0.4$ from the source - the crosswind-integrated concentration fields are remarkably similar. In both cases, the concentration maximum remains close to the ground level for a dimensionless distance of $\Delta X \simeq 0.4$ beyond the virtual origin before being swept up.

For the elevated source, $h/z_i = 0.25$, Fig. 2.3 shows that close to the source the line of maximum concentration descends until it reaches ground level. This behaviour was first pointed out by Lamb (1978) where it was explained by the organized nature of the flow in the convective boundary layer. Throughout most of the layer, except close to ground-level and the inversion base, horizontal regions with downdraft occupy a greater area than those with updraft. Because of the greater areal coverage of downdraft, a majority of the material that is emitted at the elevated source begins to descend immediately after release, and this descent continues for a relatively long period due to the relative long lifetime of the convective cells. Thus, close to the source, the greatest concentration of material will be found on a descending path.

Material released rather close to the surface will, if released into an updraft region, begin to ascend immediately, and if released into the more likely downdraft region, move approximately horizontally until it reaches an updraft region and is swept up. After sufficient travel time, most of the material has entered updraft regions and the path of the plume centerline ascends toward the base of the inversion.

Thus, the line of maximum concentration of material released from an elevated source must first descend close to ground level before moving more horizontally to be finally swept up by the thermal plumes. For near surface releases, the descending part of the process is eliminated.

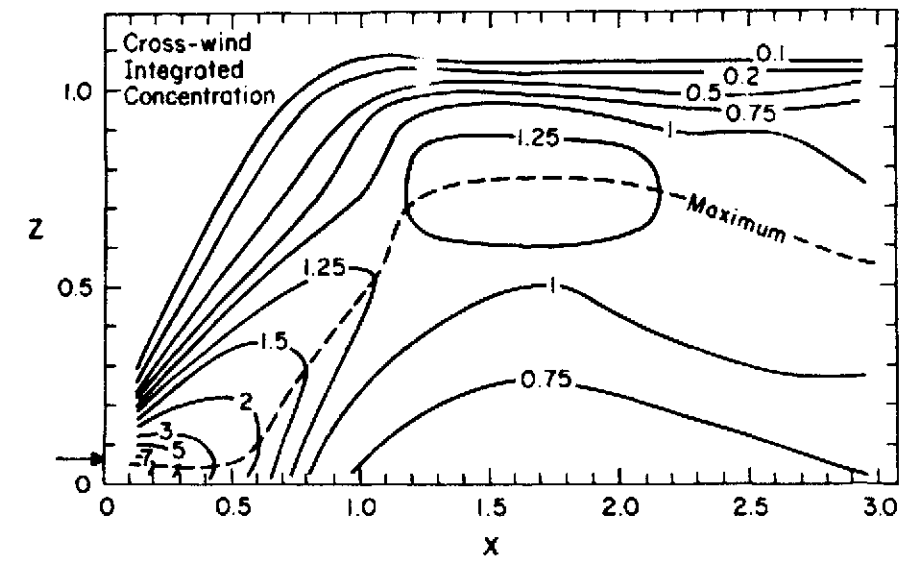

(a)

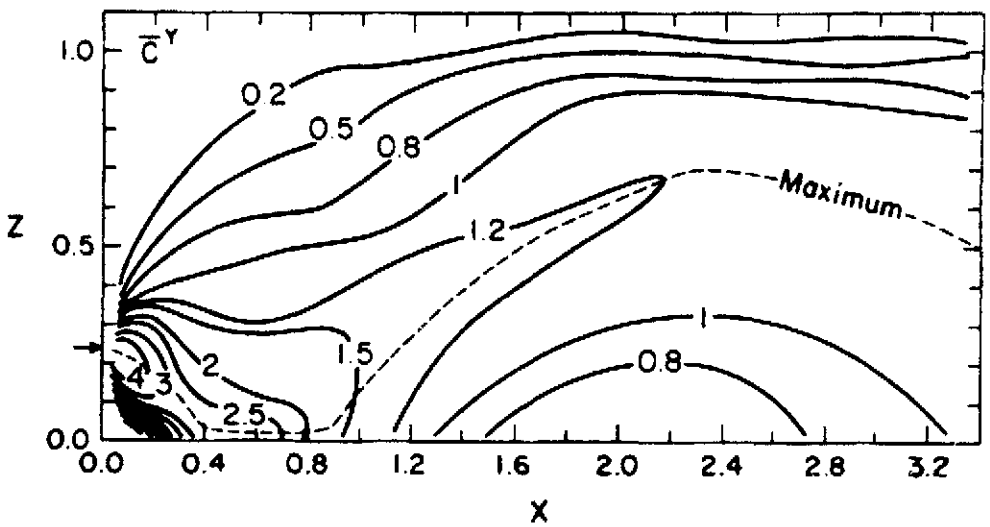

(b)

Fig. 2.3. Dimensionless crosswind-integrated concentrations $\bar{C}^Y$, as functions of the dimensionless height Z, and the dimensionless distance X

a) for the dimensionless source height $h/z_i = 0.067$, according to Willis and Deardorff (1976),

b) for the dimensionless source height $h/z_i = 0.25$, according to Willis and Deardorff (1978).

2.2. The concept of averaging time

The period over which a plume is averaged (or sampled) is of great significance; short averaging times are associated with narrow plumes of high concentrations of the released material while long averaging times will cause the plume to be spread over a large angular sector resulting in low concentrations of the released material. In the first chapter the influence of the averaging time on the proporties of the plume will be investigated by means of Taylor's statistical theory for the dispersion of plumes. In the next chapter, some characteristic features of the instantaneous outline of a plume will be discussed. This will be done in the framework of the theory of the dispersion of a cluster of particles.

2.2.1. Absolute dispersion

Taylor's dispersion formula which is restricted to homogeneous, stationary turbulence constitutes the basis for the discussion. It was assumed in the derivation of Taylor's formula that the Lagrangian power-spectrum of the wind velocity could be used to describe the motion of single air-particles followed over a period of time long enough for all velocity fluctuations, however low in frequency, to exert their effect statistically.

The effect of a finite averaging time, τ, has been modelled by Ogura (1957). His result reads

$$\overline{Y(T)^2} = T^2\,\overline{v'^2}\int_0^\infty F_{L,v}(n)\left\{1-\left(\frac{\sin\pi n\tau}{\pi n\tau}\right)^2\right\}\left(\frac{\sin\pi nT}{\pi nT}\right)^2 dn\ , \quad (2.52)$$

which is identical to Taylor's dispersion formula except for the high-pass filtering of the spectrum. The Lagrangian spectrum is multiplied by a low-pass filter function that originates from the travel time of the plume, and a high-pass filter function that is due to the finite averaging time. The high-pass filter serves to eliminate those fluctuations whose periods are long compared with the averaging time. They do not contribute to the dispersion of the plume, but their role is basically that of

determining the plume centerline. The shapes of the low- and high-pass filters are illustrated in Fig. 2.4. When $T << \tau$, the filter cut-off frequencies are widely separated, but increasing the time of travel T, keeping τ constant, implies that the two cut-off frequencies will approach each other and finally overlap, causing the breakdown of the model. A reasonable restriction on T and τ for avoiding collapse of the method might be

$$T \leq \tau$$

as suggested in Pasquill (1974).

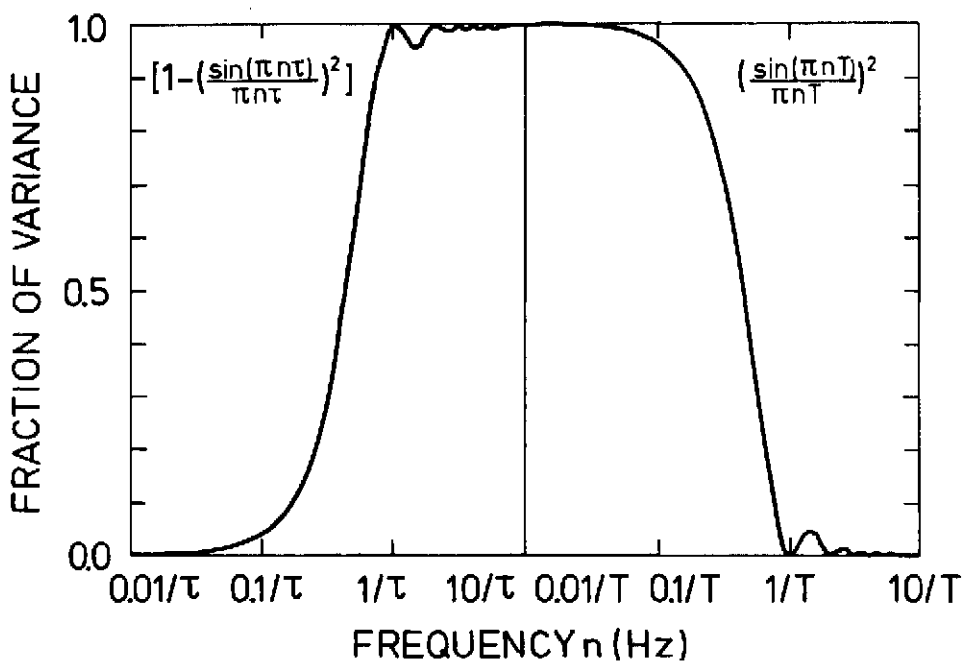

Fig. 2.4. Illustration of the shapes of the high- and low-pass filter functions that forms part of (2.52). The left-hand side of the figure indicates the fraction of the variance of a sinusoidal fluctuation of frequency n being high-pass filtered with the averaging time τ. The right-hand side indicates the effect on the variance when the fluctuation of frequency n is low-pass filtered with the time T. The highpass filters are due to the finite averaging time, and the low-pass filter describes the effect of the travel time (or downwind distance) on the plume.

When Taylor's formula is no longer applicable due to violation of the restrictions on τ and T, the description of the dispersion process rests on the theory of relative dispersion. This theory basically characterizes the instantaneous outline of the plume, but can be extended to include a finite averaging time. The dispersion of the plume will be represented by the separation between the trajectories of two simultaneously released particles. The variance of the separation is then used as a measure of the instantaneous spread of the plume. When the plume is sampled over a finite time, the plume center will then meander contributing to the width of the plume. The outline of the instantaneous and time-averaged plumes has been calculated by Sheih (1980) and their relative size has been compared.

2.2.2. Relative dispersion

A short review of some characteristic features of the instantaneous outline of a plume will be put forward; in the presentation intricate mathematical details are avoided in favour of final results. The first papers that formally treated the relative dispersion process were published by Brier (1950) and Batchelor (1952). Basically, a separated pair of simultaneously released particles is taken as representative of a group of such particles and the width of the cluster is represented by the variance of the distance between two particles. Let $Y_c(T)$ be the crosswind distance between a pair of particles at time T, and let $v_1(T)$, $v_2(T)$ be the lateral velocities of the two particles in question, then

$$\frac{d}{dt}\left[Y_c(T)-Y_o\right] = v_1(T) - v_2(T)$$

where Y_o is the initial separation of the particles. This equation can be rewritten to yield

$$\frac{d}{dt}\left[Y_c(T)-Y_o\right]^2 = 2\int_o^T \left[v_1(T)-v_2(T)\right]\cdot\left[v_1(\xi) - v_2(\xi)\right]d\xi$$

By assuming the turbulence to be homogeneous and stationary, the equation can be transformed to

$$\overline{Y_c(T)^2} = \overline{Y_o^2} + 2\int_o^T \int_o^t \overline{\delta v(t)\cdot\delta v(t+\xi)}\,d\xi\,dt \qquad (2.53)$$

where $\delta v(t) = v_1(t) - v_2(t)$ is the relative lateral velocity of the pair of particles. For a cluster of Gaussian shape, the mean-square separation between two particles, $\overline{Y_c^2}$, and the standard deviation of the cluster σ_y, are connected through $\overline{Y_c^2} = 2\sigma_y^2$. Equation (2.53) extended to dispersion in three dimensions was obtained originally by Batchelor (1952). The equation resembles Taylor's dispersion formula, but the fundamental difference lies in the meaning of the velocity, δv. The growth of the cluster is controlled by the velocity of the particles relative to each other. As the cluster grows, a larger part of the wind velocity spectrum will gradually influence the motion of the particles. This means that the growth is controlled only by a specific part of the wind velocity spectrum, and the part in question changes as the cluster grows. Roughly speaking, eddies from only half to about the double size of the cluster effectively take part in the growth of the cluster. Eddies smaller than the size of the cluster just mix the cluster internally, while eddies much greater than the cluster move it around; neither of these processes contributes to the growth of the cluster.

The growth of a cluster can be divided into 4 stages, namely,

a) the initial stage,
b) the inertial stage,
c) the central stage, and
d) the final stage.

For the initial stage it is characteristic that the dispersing particles have not appreciably changed their velocity relative to the velocity at T = 0. This implies that the initial stage predictions are applicable only very close to the source and are dependent on the initial separation, Y_o. Let the starting velocities of two particles be v_1 and v_2; then the relative velocity is $\delta v = v_1 - v_2$. By use of (2.53) this gives for the

mean-square separation

$$\overline{Y_c(T)^2} = \overline{Y_o^2} + 2 \int_0^T \int_0^t \overline{(v_1 - v_2)^2}\, d\xi dt$$

which can be integrated to yield

$$\overline{Y_c(T)^2} = \overline{Y_o^2} + \overline{(v_1 - v_2)^2}\, T^2$$

showing that the size of the cluster is a linear function of T.

As time progress, the assumptions for the initial stage are violated. If the separation of the particles are small compared with the height above the ground, then the movements of the particles will be controlled by the part of the wind velocity spectrum that is called the inertial subrange; here the crucial parameter is the rate of dissipation of the turbulent kinetic energy, ε. This is called the inertial stage of cluster growth. When expressing $\overline{Y_c(T)}$ in terms of ε and T dimensional analysis gives,

$$\overline{Y_c(T)^2} \propto \varepsilon\, T^3$$

which shows that the size of the cluster is proportional to $T^{3/2}$. The time, T_o, at which the transition between the initial and inertial stage takes place, can also be found by dimensional analysis. As T_o depends only on ε and the initial separation Y_o, the analysis gives

$$T_o = a\, Y_o^{2/3}\, \varepsilon^{-1/3}$$

where a is a constant.

The central stage is reached when eddies that are no part of the inertial subrange start to take part in the growth of the cluster. No easy way exists in which to establish the growth of a cluster in this stage, but successful attempts have been reported by Smith and Hay (1961). The analytical treatment is loaded by severe assumptions as, for example, Gaussian shape

of the cluster, isotropy of the turbulence (although the stage of inertial growth of the cluster is passed), similarity of Lagrangian and Eulerian covariances, and exponential form of the Eulerian correlogram. Smith and Hay (1961) came to an expression for the maximum growth rate of the cluster

$$\frac{d\,\sigma_y}{dt} \simeq 0.3\,\left(\overline{v'^2}\right)^{\frac{1}{2}} \tag{2.54}$$

written here as usual for the lateral component only. For the general mathematical analysis the original paper should be inspected. Integration of (2.54), paying no attention to the lower limit, gives

$$\sigma_y^2 = (0.3)^2\,\overline{v'^2}\,T^2 \tag{2.55}$$

which shows that the size of the cluster in the central stage is proportional to T. Equation (2.55) also shows that a cluster grows more slowly than a plume as described by Taylor's dispersion formula, (2.18).

When the cluster has reached a size where the velocity of the particles is uncorrelated, the particles move independently of each other so the mean separation reads

$$\overline{Y_c(T)^2} = \overline{(Y_1(T) - Y_2(T))^2}$$

or

$$\overline{Y_c(T)^2} = \overline{Y_1(T)^2} + \overline{Y_2(T)^2}$$

where the product term is excluded because Y_1 and Y_2 are uncorrelated. The individual particles move accordingly to a representation by Taylor's dispersion formula, which for large values of T reads

$$\overline{Y(T)^2} = 2\,\overline{v'^2}\,t_{L,v}\,T$$

But

$$\overline{Y_c(T)^2} = \overline{Y_1(T)^2} + \overline{Y_2(T)^2}$$

so

$$\overline{Y_c(T)^2} = 4\,\overline{v'^2}\,t_{L,v}\,T$$

Thus, for large values of T, called the final stage of cluster growth, the size of the cluster is proportional to $T^{1/2}$, and the relation between the mean-square separation of particles in the cluster and the mean-square displacement from the centerline of a single particle in a plume, is given by

$$\overline{Y_c(T)^2} = 2\,\overline{Y(T)^2}$$

This expression states that for large travel times the size of a cluster and the width of a Taylor plume are the same.

Figure 2.5 shows a schematic view of a Lagrangian velocity spectrum, nS(n), on a logarithmic frequency scale. As the expansion of the cluster is approximately carried out by eddies from about half to double the actual size of the cluster, the growth process, it is suggested, is illustrated by sweeping a band of constant width from right (high frequencies) to left (low frequencies) on the spectrum in Fig. 2.5. The expansion rate of the cluster at any time will then be proportional to the area under the spectrum that is enclosed by this band.

At very small values of T, the growth will be in the initial stage which depends on Y_o and cannot be exemplified by this simple model. As we sweep from the right, first the area included by the band increases, and so does the cluster growth-rate, well in accordance with the predictions for the inertial stage, where $\overline{Y_c(T)^2} \propto T^3$. Then the area remains constant for a while, which indicates that the cluster has reached the central stage, for which $\overline{Y_c(T)^2} \propto T^2$. Further sweeping to the left brings the cluster into the final stage, where the area and thus

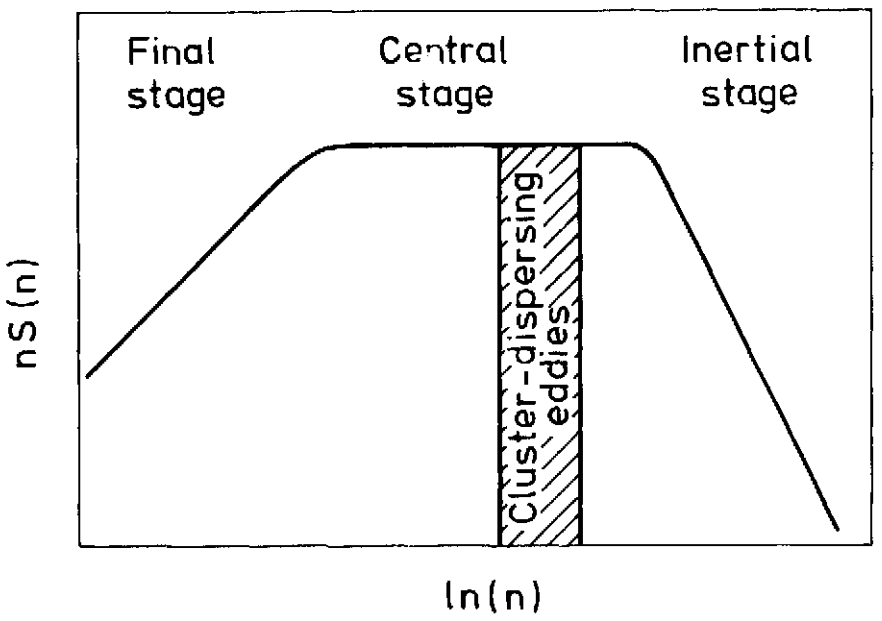

Fig. 2.5. Illustration of characteristic stages in the dispersion of a cluster. Shown is a schematic view of a Lagrangian velocity spectrum, n S(n), plotted on a logarithmic frequency scale, ln(n), where n is frequency. The expansion of a cluster is roughly illustrated by sweeping across the spectrum from right to left with a band of constant width. Then the enclosed area under the spectrum measures the cluster expansion rate at any time. The position in the spectrum of the characteristic stages of cluster dispersion is indicated.

the growth rate of the cluster decreases, which is in accordance with the prediction that $Y_c(T)^2 \propto T$.

2.3. Dependence on micrometeorological parameters

In a horizontally homogeneous atmosphere, turbulent kinetic energy is supplied partly from the horizontal shearing stress, and partly from the operation of buoyant forces, the latter only when the flow is thermally stratified. The variances of the wind velocity fluctuations, u'^2, v'^2, and w'^2, in the x-, y- and z-direction, respectively, can be taken as a measure of the ability of the atmosphere to disperse particulate and

gaseous matter. Main features of the mean turbulent energy, $\bar{E} = \frac{1}{2}(\overline{u'^2} + \overline{v'^2} + \overline{w'^2})$, are given briefly below.

1) Turbulent energy is extracted from the mean flow by the action of the horizontal shearing stress, and supplied to $\bar{E}$ mainly through $\overline{u'^2}$.
2) Turbulent energy is altered by the action of buoyant forces that convert potential into kinetic energy or vice versa. When the sensible heat flux is upwardly directed, energy is supplied to the turbulent fluctuations; when the flux is downward, turbulent energy is extracted from the flow. Turbulent energy is supplied or extracted to $\bar{E}$ mainly through $\overline{w'^2}$.
3) The fluctuating pressure and viscous forces transfer the turbulent energy among components, in an effort to make $\overline{u'^2} = \overline{v'^2} = \overline{w'^2}$. Large eddies are decomposed into smaller ones by vortex stretching, (Tennekes and Lumley, 1972).
4) Turbulent energy is continuously extracted from the flow by dissipation.

The complete expression for the turbulent energy balance, including divergence terms, can be found in Tennekes and Lumley (1972). The balance between production and dissipation of turbulent kinetic energy, including the variation in time of the mean total turbulent energy, $\partial\bar{E}/\partial t$, but excluding the divergence, can be written

$$\frac{\partial \bar{E}}{\partial t} = u_*^2 \frac{\partial \bar{u}}{\partial z} + \frac{g}{\bar{T}} (\overline{w'T'}) - \varepsilon \qquad (2.56)$$

The first term on the right-hand side is the production of turbulent energy due to horizontal shearing stress. The second term - in which T' is the fluctuating temperature and consequently $\overline{w'T'}$ is the upwardly directed temperature flux - is the production of turbulent energy by the action of buoyant forces. The rate of dissipation is denoted by ε.

2.3.1. Surface roughness

In stationary and purely mechanical turbulence, mechanical production of energy equals dissipation ($\frac{\partial \bar{E}}{\partial t} = 0$). Monin-Obukhov scaling gives

$$\varepsilon = \frac{u_*^3}{kz} \tag{2.57}$$

The actual values of the variances of the wind velocity fluctuations can also be found by means of Monin-Obukhov scaling

$$\begin{aligned} \sigma_u &\equiv \left(\overline{u'^2}\right)^{\frac{1}{2}} = A \cdot u_* \cdot \psi_u \left(\frac{z}{L}\right) \\ \sigma_v &\equiv \left(\overline{v'^2}\right)^{\frac{1}{2}} = D \cdot u_* \cdot \psi_v \left(\frac{z}{L}\right) \\ \sigma_w &\equiv \left(\overline{w'^2}\right)^{\frac{1}{2}} = C \cdot u_* \cdot \psi_w \left(\frac{z}{L}\right) \end{aligned} \tag{2.58}$$

where the influence of convection has been introduced through the dimensionless functions ψ_u, ψ_v, and ψ_w. A, D and C most likely are constants. In the absence of convection (2.58) can be written

$$\frac{\sigma_u}{\bar{u}} = \frac{k\,A}{\ln \frac{z}{z_o}} \tag{2.59a}$$

$$\sigma_\theta \simeq \frac{\sigma_v}{\bar{u}} = \frac{k\,D}{\ln \frac{z}{z_o}} \tag{2.59b}$$

$$\sigma_\phi \simeq \frac{\sigma_w}{\bar{u}} = \frac{k\,C}{\ln \frac{z}{z_o}} \tag{2.59c}$$

by use of the logarithmic wind profile, where σ_θ and σ_ϕ are the lateral and vertical wind direction fluctuations in radians. It is noted that σ_θ and σ_ϕ does not depend on the wind speed but only on the roughness of the area, z_o, and the height of the measurements, z. Equation (2.59c) is well established (Panofsky, 1973), whereas (2.59b) failed to be successfully verified. It has been suggested, (Kaimal et al., 1976) that for

unstable conditions, σ_v depends not only on z/L, but also on z_i/L, where z_i is the height of the lowest inversion.

The vertical wind velocity fluctuations in neutral conditions over an area called I with roughness length $(z_o)_I$ will be greater than that over an area called II, with roughness length $(z_o)_{II}$ by a factor of

$$\frac{(\sigma_w)_I}{(\sigma_w)_{II}} = \frac{\ln\left(\frac{z}{(z_o)_{II}}\right)}{\ln\left(\frac{z}{(z_o)_I}\right)}$$

For z = 115 m and with a hypothetical roughness length for a residential area of $(z_o)_I$ = 0.60 m, and a roughness length for a rural area of $(z_o)_{II}$ = 0.05 m, the vertical wind fluctuations over the residential area will be a factor of 1.5 greater than those over a rural area.

A similar argument cannot be used to evaluate the roughness effect on the lateral wind velocity fluctuations due to the dependence on σ_v of the two scaling parameters, z/L and z_i/L.

2.3.2. Thermal stability

The effect of thermal stability enters (2.56) through the second term on the right-hand side. The production of turbulent energy is proportional to the upwardly directed sensible heat flux $H = \rho\, c_p\, \overline{w'T'}$. The upwardly directed heat flux is driven by the temperature difference between the ground and the overlying air.

The radiation from the sun is the primary source of energy. On its way to the ground, the radiation may be reflected from cloud tops, scattered by air molecules and particles, and absorbed by gases present in the atmosphere. Part of the incoming radiation is reflected at the ground and the remainder absorbed by the soil surface, where it can cause water to evaporate or raise the soil temperature. The heating of the soil surface causes energy to be transmitted into the ground, and the induced

temperature difference between the soil surface and the adjacent air gives rise to upwardly directed sensible heat flux in the atmosphere. The controlling parameters of the heating of the ground are the thermal conductivity of the soil, which controls the rate of heat flow through the soil, and the specific heat of the soil, which controls the temperature rise for a given amount of heat. If both the thermal conductivity and specific heat are small, the energy will penetrate the soil only to a small depth, so the energy will be concentrated at the surface causing huge temperature fluctuations of the soil surface between night and day. Examples of this type of area are sand deserts, mountains of rocks, and rocks, bricks, concrete, and bitumen in cities. In the overall evaluation of the response of the surface to solar radiation both the albedo, moisture, and thermal properties of the ground must be taken into account, so that no simple connection exists between the incoming solar radiation and the upwardly directed sensible heat flux. In a city this is further complicated by the domestic heating that acts as an extra heat input entering the second term in (2.56).

The ratio between buoyant and mechanical turbulent energy production is known as the flux Richardson number, Ri_f, which from the terms in (2.56) can be estimated to

$$Ri_f = \frac{-\frac{g}{\bar{T}}\,(\overline{w'T'})}{u_*^2\,\frac{\partial \bar{u}}{\partial z}} \qquad (2.60)$$

In the surface layer, u_* and $\overline{w'T'}$ can be considered constant, whereas $\frac{\partial \bar{u}}{\partial z}$ decreases with increasing height, causing $|Ri_f|$ to also increase with height. For $Ri_f = -1$, buoyant and mechanical production of turbulent energy are equal; if $Ri_f = 1$, then buoyant forces remove energy as fast as it is produced by the horizontal shearing stress, and the turbulence no longer can maintain itself. It is pointed out in Lumley and Panofsky (1964) that the condition $Ri_f = 1$ is not a criterion for onset or disappearance of turbulence, and experimental evidence supports a value of $Ri_f \sim 0.25$ for the ultimate suppression or onset of turbulent fluctuations.

Practical use of Ri_f is troublesome because it is difficult to measure the covariances $\overline{w'T'}$ and u_*^2. In order to overcome this difficulty the flux terms for temperature and momentum in Ri_f have been expressed by use of K-theory

$$\overline{w'T'} = K_H\left(\frac{\partial \bar{T}}{\partial z} + \Gamma\right)$$

$$u_*^2 = K_M \frac{\partial \bar{u}}{\partial z}$$

which by substitution gives

$$Ri_f = \left(\frac{K_H}{K_M}\right) \cdot \left(\frac{g}{\bar{T}}\right) \cdot \left(\frac{\frac{\partial \bar{T}}{\partial z} + \Gamma}{(\frac{\partial \bar{u}}{\partial z})^2}\right)$$

where Γ is the dry adiabatic lapse rate. Assuming equality between the diffusion coefficients of heat and momentum, $K_H = K_M$, results in the definition of another dimensionless quantity

$$Ri = \frac{g}{\bar{T}} \frac{(\frac{\partial \bar{T}}{\partial z} + \Gamma)}{(\frac{\partial \bar{u}}{\partial z})^2}$$

known as the gradient Richardson number which often is used to characterize the atmospheric stability. Another fundamental dimensionless parameter that characterizes the atmospheric stability is the ratio of the height to the Monin-Obukhov length, L. The three stability parameters are related in the following way

$$Ri_f = \frac{K_H}{K_M} Ri = \frac{z}{L} \Phi^{-1} \left(\frac{z}{L}\right)$$

where $\Phi(\frac{z}{L})$ is a dimensionless function (Businger, 1973). Often z/L is the preferred stability parameter because L is height independent, but a practical evaluation of L still most often rests on empirical relations between Ri and z/L. Practical needs have provoked approximations to Ri ("poor man's Richardson numbers"), some of which will be discussed in Chapter 2.4.4.

2.3.3. Relation between dispersion characteristics over surfaces with dissimilar roughness and atmospheric stability, under near neutral and unstable conditions

When predictions of the concentrations in the air from an air pollution source are to be made, the necessary meteorological data for that specific area are often unavailable and cannot readily be established. In this case, computations must be based on meteorological data obtained at an area for which the surface roughness and atmospheric stability characteristics might differ from those actually controlling the dispersion. In statistical studies the effects of area dissimilarities often average out, rendering the final result reliable, but errors in the individual events that enter the statistics can be quite significant.

A simplified study has been undertaken which relates dispersion characteristics for two areas taking into account the dissimilarities in the surface roughness and atmospheric stability. Details of the study can be found in Gryning and Larsen (1981); here only the main results will be stated. We compared the crosswind-integrated concentration originating from dispersion over an area characterized with a roughness length $(z_o)_I$ and a Monin-Obukhov length $(L)_I$, with that for an area with surface roughness $(z_o)_{II}$ and Monin-Obukhov length $(L)_{II}$. It is assumed that the two areas are situated so closely to each other that the geostrophic winds are nearly equal; this assumption will be used to interrelate the wind conditions at the areas.

The ratio of the crosswind-integrated concentrations at a given downwind distance turned out to depend on only 4 dimensionless parameters, namely z_o/L and $\hat{z}/L$ for the two areas in question. Here $\hat{z}$ is the mean height of particles that have travelled a distance x; $\hat{z}/L$ can be found from (2.38) by an approximative method devised by van Ulden (1978), when z_o/L and x/z_o are known (Fig. 2.6). The model reduces the number of dimensionless parameters to three by merging $\hat{z}/L$ for the two areas into a composite parameter.

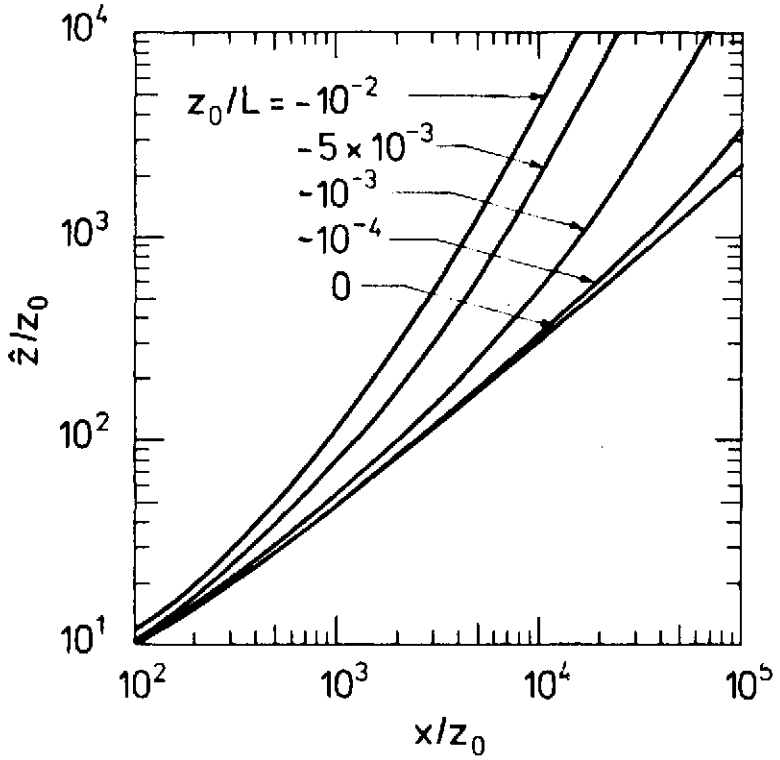

Fig. 2.6. Relation between $\hat{z}/z_o$ and x/z_o for discrete values of z_o/L. The curves are estimated from an approximative solution to (2.38) that was devised by van Ulden (1978).

The model. The model used is obtained by merging a resistance law model, relating the surface conditions at the two areas, with a dispersion model describing the crosswind-integrated surface concentration in terms of surface layer parameters.

By use of approximative expressions supplied by van Ulden (1978) for the vertical dispersion from sources near the ground, it turned out that the ratio of the crosswind-integrated concentration, $\bar{\chi}_{CWI}$, for two areas could be expressed as where

$$\frac{\left(\bar{\chi}_{CWI}\right)_I}{\left(\bar{\chi}_{CWI}\right)_{II}} = \frac{(u_*)_{II}}{(u_*)_I} \cdot \left[\frac{1-3.5\ (\frac{\hat{z}}{L})_{II}}{1-3.5\ (\frac{\hat{z}}{L})_I}\right]^{0.5} \qquad (2.61)$$

subscripts I and II refer to the areas in question. The parameter $\hat{z}/L$ is a function of downwind distance from the source x and L. The relation is illustrated in Fig. 2.6. The determination of the friction velocity u_* was accomplished by means of the resistance law as described by Zilitinkevich and Monin (1974) and Zilitinkevich (1975). In near neutral and unstable conditions it can be approximated by

$$u_* = \frac{kv_g}{\left\{\left(-\ln\left(\frac{z_o}{L}\right) + 1\right)^2 + 4.7^2\right\}^{0.5}}$$

where v_g is the geostrophic wind. This equation reveals the relation between the friction velocity, the geostrophic wind speed, and the dimensionless parameter z_o/L.

Assuming that the geostrophic wind speeds are equal at the two areas in question then the ratio of the friction velocities at the areas is a function of the dimensionless parameter z_o/L alone. By substituting the above expression for u_*, (2.61) now reads

$$\frac{\left(\bar{\chi}_{CWI}\right)_I}{\left(\bar{\chi}_{CWI}\right)_{II}} = \left[\frac{\left(-\ln\left(\frac{z_o}{L}\right)_I + 1\right)^2 + 4.7^2}{\left(-\ln\left(\frac{z_o}{L}\right)_{II} + 1\right)^2 + 4.7^2}\right]^{0.5} \cdot \left[\frac{1-3.5\left(\frac{\hat{z}}{L}\right)_{II}}{1-3.5\left(\frac{\hat{z}}{L}\right)_I}\right]^{0.5} \qquad (2.62)$$

This describes the ratio of the crosswind-integrated concentration as a function of only 4 dimensionless parameters namely z_o/L and $\hat{z}/L$ for the two areas in question.

Equation (2.62) can readily be computed for actual values of the 4 dimensionless parameters. However, without appreciable loss of accuracy, the last term can be Taylor expanded.

$$\left[\frac{1-3.5\left(\frac{\hat{z}}{L}\right)_{II}}{1-3.5\left(\frac{\hat{z}}{L}\right)_{I}}\right]^{0.5} = \left[\frac{1-\frac{3.5}{1-3.5a}\left[\left(\frac{\hat{z}}{L}\right)_{II}-a\right]}{1-\frac{3.5}{1-3.5a}\left[\left(\frac{\hat{z}}{L}\right)_{I}-a\right]}\right]^{0.5}$$

$$\simeq \left[1-\frac{3.5}{1-3.5a}\left\{\left(\frac{\hat{z}}{L}\right)_{II}-\left(\frac{\hat{z}}{L}\right)_{I}\right\}\right]^{0.5}$$

meaning that we have chosen an expansion point $(\hat{z}/L)_I = (\hat{z}/L)_{II} = a$. We elaborated on the quality of this expansion and ended up by setting $a = -1$. Then

$$\left[\frac{1-3.5\left(\frac{\hat{z}}{L}\right)_{II}}{1-3.5\left(\frac{\hat{z}}{L}\right)_{I}}\right]^{0.5} \simeq \left[1+\frac{7}{9}\left\{\left(\frac{\hat{z}}{L}\right)_{I}-\left(\frac{\hat{z}}{L}\right)_{II}\right\}\right]^{0.5}$$

which replaces the parameters $(\hat{z}/L)_I$ and $(\hat{z}/L)_{II}$ by the composite parameter $(\hat{z}/L)_I - (\hat{z}/L)_{II}$. Figure 2.7 illustrates the accuracy of this approximation; it can be seen that the overall best performance is obtained when $(\hat{z}/L)_I - (\hat{z}/L)_{II} \geq 0$. Use of this approximation reduces (2.62) to

$$\frac{\left(\bar{\chi}_{CWI}\right)_I}{\left(\bar{\chi}_{CWI}\right)_{II}} = \left[\frac{\left(-\ln\left(\frac{z_o}{-L}\right)_I+1\right)^2+4.7^2}{\left(-\ln\left(\frac{z_o}{-L}\right)_{II}+1\right)^2+4.7^2}\right]^{0.5} \cdot \left[1+\frac{7}{9}\left\{\left(\frac{\hat{z}}{L}\right)_I - \left(\frac{\hat{z}}{L}\right)_{II}\right\}\right]^{0.5} .$$

To illustrate the functional behaviour of this expression, Fig. 2.8 shows isolines for $(\bar{\chi}_{CWI})_I/(\bar{\chi}_{CWI})_{II}$ as a function of $(z_o/-L)_I$ and $(z_o/-L)_{II}$ for $[(\hat{z}/L)_I - (\hat{z}/L)_{II}]$ equal to 0, 0.5, 1, and 2.

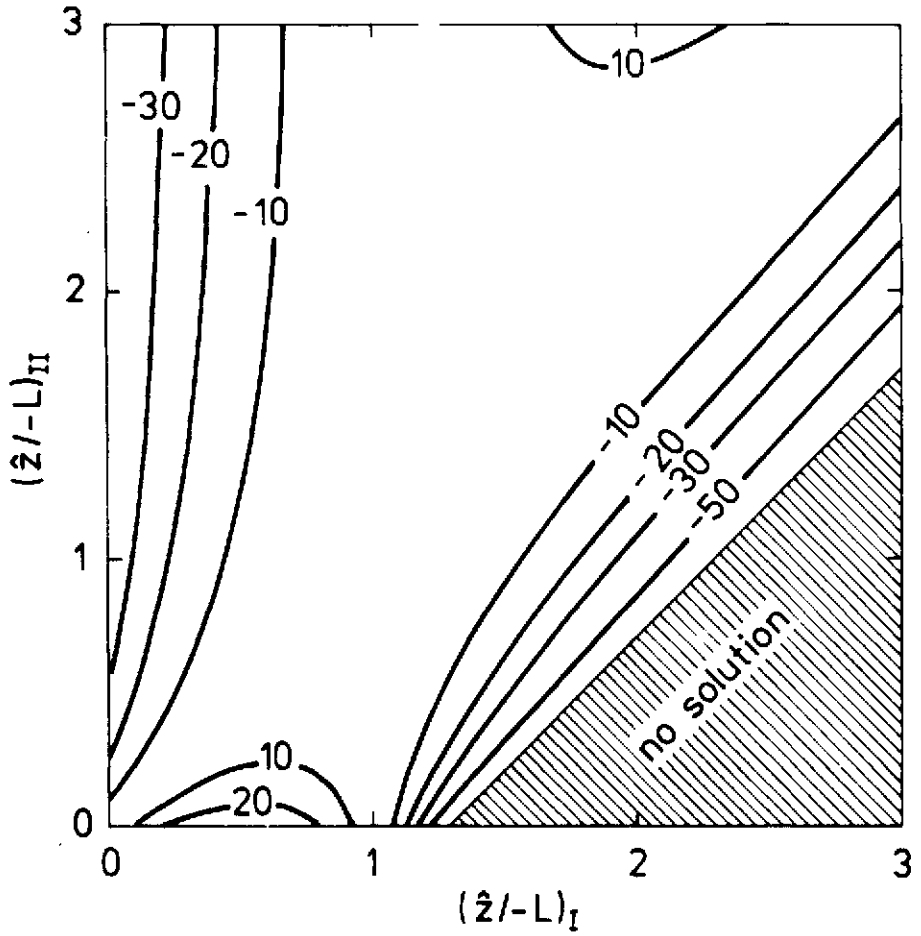

Fig. 2.7. Isolines of the percentage deviation between $\left[\frac{1-3.5\left(\frac{\hat{z}}{L}\right)_{II}}{1-3.5\left(\frac{\hat{z}}{L}\right)_I}\right]^{0.5}$ and its Taylor-expanded form $\left[1 + \frac{7}{9}\left\{\left(\frac{\hat{z}}{L}\right)_I - \left(\frac{\hat{z}}{L}\right)_{II}\right\}\right]^{\frac{1}{2}}$. The deviation is given as

$$\left[1 + \frac{7}{9}\left\{\left(\frac{\hat{z}}{L}\right)_I - \left(\frac{\hat{z}}{L}\right)_{II}\right\}\right]^{\frac{1}{2}} - \left[\frac{1-3.5\left(\frac{\hat{z}}{L}\right)_{II}}{1-3.5\left(\frac{\hat{z}}{L}\right)_I}\right]^{0.5} \Bigg/ \left[\frac{1-3.5\left(\frac{\hat{z}}{L}\right)_{II}}{1-3.5\left(\frac{\hat{z}}{L}\right)_I}\right]^{0.5}$$

Overall best performances are obtained when $\left(\frac{\hat{z}}{L}\right)_I - \left(\frac{\hat{z}}{L}\right)_{II}$ is positive.

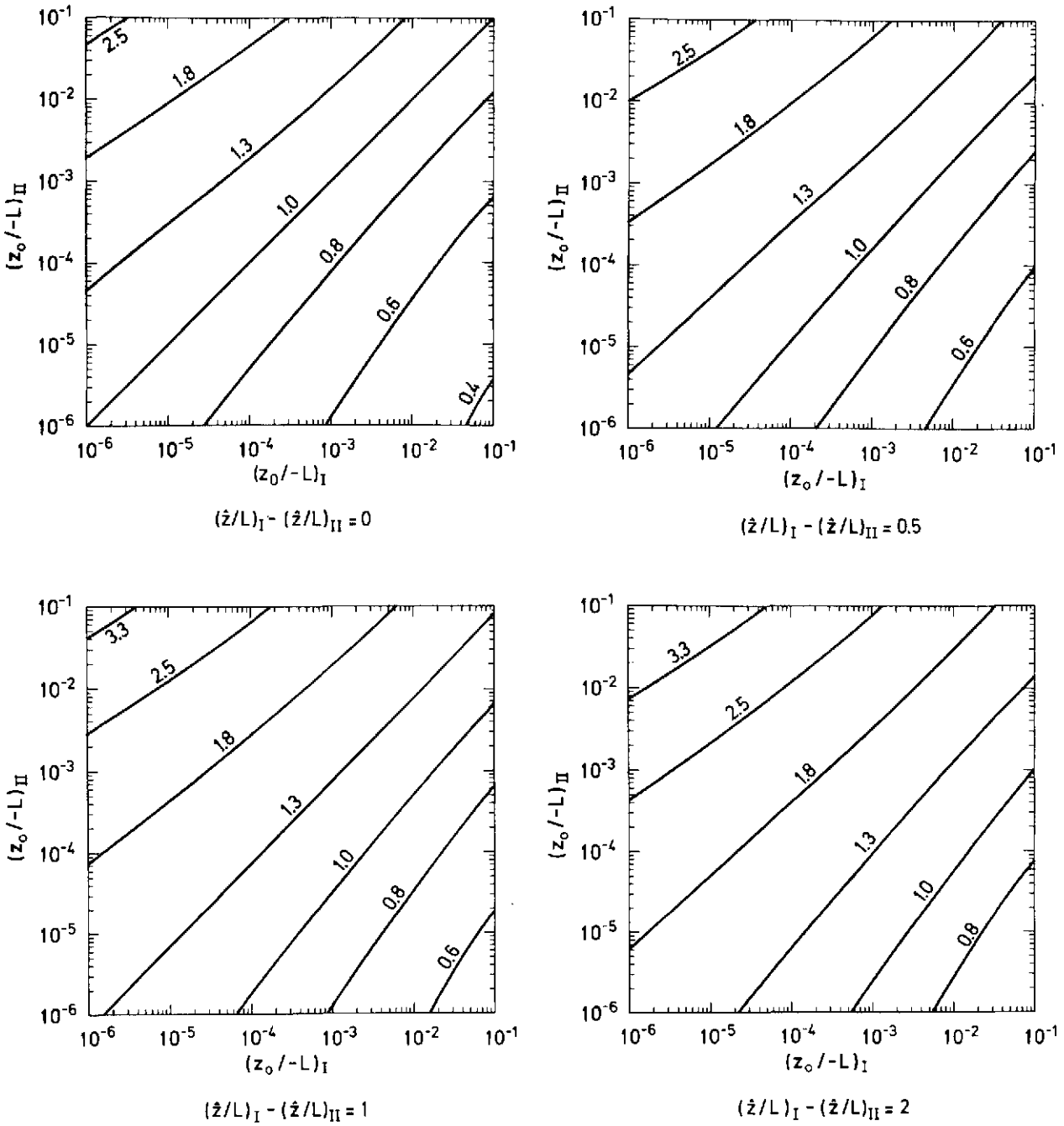

Fig. 2.8. Isolines of the ratio between the crosswind-integrated concentrations, $(\bar{\chi}_{CWI})_I/(\bar{\chi}_{CWI})_{II}$ plotted as function of $z_o/-L$ for the two areas, and for four values of the composite parameter, $(\hat{z}/L)_I - (\hat{z}/L)_{II}$.

Discussion. This simple model should be used in only near neutral to unstable conditions roughly corresponding to the Pasquill stability classes A-B to D. Also, the dispersion should be confined to the surface boundary layer for the similarity expressions to be applicable.

As an example of the use of the model, we shall consider the following situation: Assume that area I is rural, characterized by a roughness length $(z_o)_I$ = 0.01 m, and area II is urban with $(z_o)_{II}$ = 1 m. The atmosphere is moderately unstable at the two areas, corresponding to $(L)_I$ = -100 m, and $(L)_{II}$ = -200 m; the downwind distances will be set equal and 0.5 km. Then $(x/z_o)_I = 5 \cdot 10^4$ and $(z_o/L)_I = -10^{-4}$ which, by use of Fig. 2.6 is seen to correspond to $(\hat{z}/z_o)_I = 1.6 \cdot 10^3$ or $(\hat{z}/L)_I = -0.16$. Similarly, we find $(x/z_o)_{II} = 5 \cdot 10^2$, $(z_o/L)_{II} = -5 \cdot 10^{-3}$ and $(\hat{z}/L)_{II} = -0.19$; thus $(\hat{z}/L)_I - (\hat{z}/L)_{II} = 0.03$. The wind speed over the city differs from that over the rural area due to the variation in roughness and stability; furthermore, the enhanced roughness will increase the vertical dispersion of the plume. Both effects will influence $(\bar{\chi}_{CWI})_I$ compared to $(\bar{\chi}_{CWI})_{II}$. The combined effect can be resolved from Fig. 2.8, where for $(\hat{z}/L)_I - (\hat{z}/L)_{II} = 0$, we find that $(\bar{\chi}_{CWI})_I/(\bar{\chi}_{CWI})_{II}$ lies in the range 1.4-1.5. Actually $(\hat{z}/L)_I - (\hat{z}/L)_{II} = 0.03$. Direct substitution of the values for the 4 dimensionless parameters into (2.62) yields $(\bar{\chi}_{CWI})_I/(\bar{\chi}_{CWI})_{II} = 1.5$, in fine agreement with the previous result.

2.4. Practical methods for calculating dispersion

An expression for the concentration distribution of continuously released material from a point source must contain information about the shape of the distribution as well as the size of characteristic parameters in it. In Chapter 2.4.1, we shall discuss the shape being adopted for the concentration distribution. In Chapters 2.4.2, 2.4.3 and 2.4.4 various methods for calculating the size of the characteristic parameters will be presented.

2.4.1. On the shape of the concentration distribution

The crosswind concentration distribution is generally believed to be of Gaussian shape. Close to the source, the concentration distribution of the released material will be similar to the probability density distribution of the velocity fluctuations, which is observed experimentally to be approximately Gaussian. Far downwind from the source, the dispersing material has been influenced by a multiplicity of different processes, which, according to the "central limit theorem", will result in a Gaussian distribution of the material. Concerning the intermediate region there are no obvious reasons to expect, although it generally is believed, that the concentrations should be Gaussian distributed.

Concerning the vertical distribution of material, the situation is more complicated. For the description of the vertical concentration distribution of a plume released from ground-level, theoretical arguments favour the choice of an exponential function of the height raised to the power r. The value of the exponent, r, varies with the atmospheric stability, (Chapter 2.1.1, Table 2.1). The influence on the shape of the concentration distribution due to variations in r is illustrated in Fig. 2.9. It can be seen that the differences in the shape will be rather small for values of r deviating only slightly from 2, but for lower values of r this deviation may well be significant.

For elevated sources, the vertical concentration distribution seems to be well approximated by a Gaussian distribution as long as the plume is unaffected by the ground. Assuming a Gaussian distribution of material in the lateral and vertical direction, the expression for the concentration, $\bar{\chi}$, normalized with the windspeed and release rate, Q, reads

$$\frac{\bar{u}\,\bar{\chi}(x,y,z)}{Q} = \frac{1}{2\pi\sigma_y\sigma_z}\exp\left(-\frac{1}{2}\left(\frac{y}{\sigma_y}\right)^2\right)\exp\left(-\frac{1}{2}\left(\frac{z-h}{\sigma_z}\right)^2\right) \qquad (2.63)$$

where h is the height of release, and σ_y and σ_z are the second-order moments in the lateral and vertical concentration distribution at distance x, respectively.

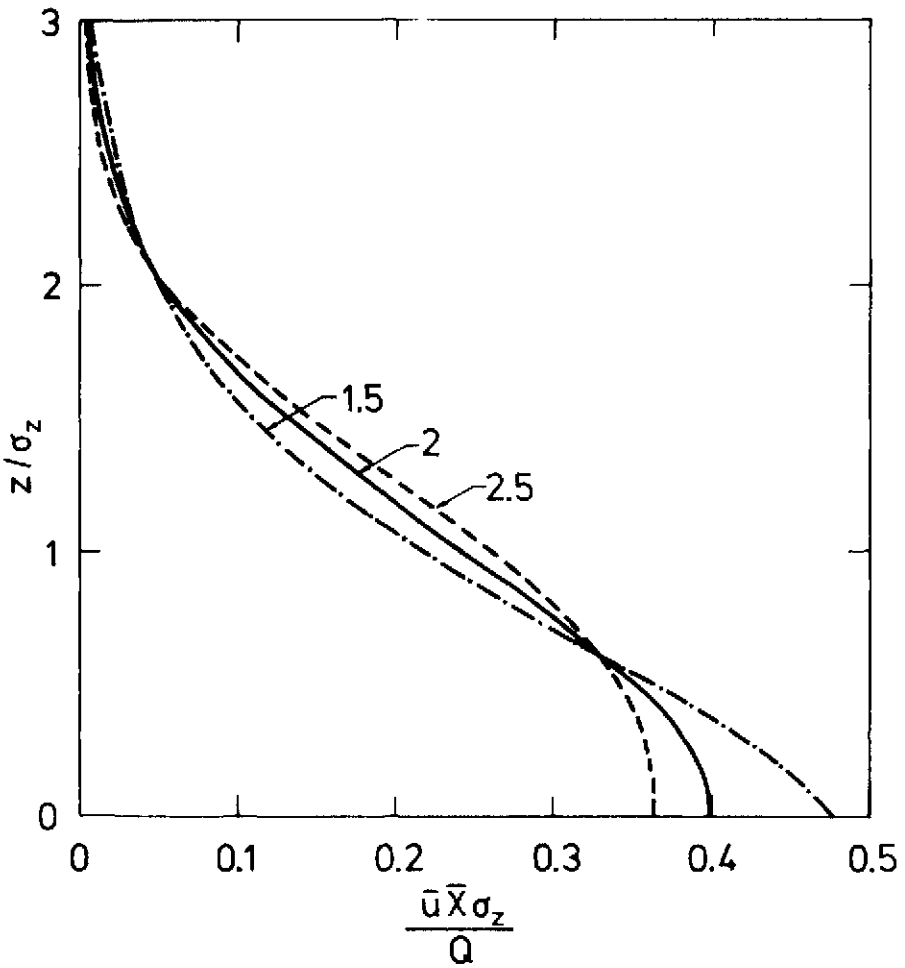

Fig. 2.9. Vertical normalized concentration profiles, plotted for various values of the power r. The curves illustrate the equation for the vertical concentration distribution for a continuous ground-level source

$$\frac{\sigma_z \bar{u}\bar{\chi}}{Q} = \Lambda(r,y)\ \exp\left[\left(\frac{\Gamma(3/r)}{\Gamma(1/r)}\right)^{r/2}\left(\frac{z}{\sigma_z}\right)^{r}\right]$$

where Λ is adjusted in order to take into account the actual lateral position with respect to the plume centerline, as well as to secure fulfilment of the continuity equation. The curves enclose equal areas. The equation can be found in Pasquill (1974) in an extended form.

Due to the presence of the ground, the plume cannot disperse infinitely downward. This is dealt with rather arbitrarily by assuming specular reflection of the plume at the ground. The plume will be reflected in a similar way if upwardly directed dispersion is limited by an overlying inversion. In an actual situation, the specular reflections at the ground and at the inversion should be repeated an infinite number of times. However, a good approximation for the ground-level concentration is

$$\frac{\bar{u}\,\bar{\chi}(x,y,o)}{Q} = \frac{1}{\pi\sigma_y\sigma_z}\exp\left(-\frac{1}{2}\left(\frac{y}{\sigma_y}\right)^2\right)\cdot\left\{\exp\left[-\frac{1}{2}\left(\frac{h}{\sigma_z}\right)^2\right]\right.$$

$$+\exp\left[-\frac{1}{2}\left(\frac{h}{\sigma_z}\right)^2\left(1-\frac{2z_i}{h}\right)^2\right]$$

$$\left.+\exp\left[-\frac{1}{2}\left(\frac{h}{\sigma_z}\right)^2\left(1+\frac{2z_i}{h}\right)^2\right]\right\} \qquad (2.64)$$

where z_i is the inversion height. Equation (2.64) contain three reflections at the ground and two in the inversion.

Gaussian concentration distributions suffer from a fundamental drawback. They extend to infinity and that is obviously unphysical. An alternative shape of the concentration distribution that avoids the difficulty of unlimited movements of material outwards from the source has been put forward by Monin (1959). The distribution resembles the Gaussian except at the fringes, where the Monin distribution goes sharply to zero.

Concerning the precise shape of the distribution of the plume material, fundamental problems still await further exploration, but for most practical applications these are of secondary importance as the Gaussian distribution seems to describe adequately most of the situations encountered. A crucial point, irrespective of any preferred shape of the concentration distribution, is the correct choice of the parameters that describe the actual size of the distribution. The uncertainty with which

these parameters can be determined is of far greater importance for the accuracy of the concentration calculations than is the uncertainty in the choice of the shape of the distribution. Further, the parameters often are estimated in a way that gives the best overall predictions when used in combination with a Gaussian-type model. In particular this is the case for the parameter that describes the vertical concentration distribution.

2.4.2. Hay and Pasquill's working approximation

So far the statistical dispersion theory has been described entirely in a Lagrangian framework. From a practical point of view this is inconvenient, because reliable Lagrangian statistics of a flow-field are difficult, if not impossible, to obtain. Hay and Pasquill (1959) proposed a working approximation to circumvent this difficulty by assuming that the Eulerian and Lagrangian autocorrelation functions are similar in shape, and that the ratio of the Lagrangian to the Eulerian time scales is the only parameter to be determined. Adoption of this simple theory was argued from the principle that in the absence of elaborate evidence, preference should be given to simplicity. Further, Hay and Pasquill argued that a substantial change in the shape of the autocorrelation function is less important than a substantial change in the time scale. Thus, the assumption of precise similarity between the Lagrangian and Eulerian autocorrelation functions is unlikely to produce substantial errors as long as the conditions of similarity in the shapes are roughly satisfied. The simple hypothesis is written

$$R_L(\beta t) = R_E(t) \tag{2.65}$$

where the subscripts L and E refer to Lagrangian and Eulerian quantities respectively and β is the ratio between the Lagrangian and the Eulerian time scales. The relation between the corresponding Lagrangian and Eulerian spectrum functions can easily be obtained by use of the definition of the Lagrangian and Eulerian spectra

$$F_L(n) = 4 \int_0^\infty R_L(\xi) \cos(2\pi n\xi) d\xi \tag{2.66}$$

Substitution of $\xi = \beta t$ implies that

$$F_L(n) = 4\beta \int_0^\infty R_E(t) \cos(2\pi n\beta t)dt$$

or that

$$nF_L(n) = \beta nF_E(\beta n) \qquad (2.67)$$

Hay and Pasquill's working approximation thus implies that when the wind velocity variance spectra are expressed in the form $nF(n)$, the value of the Lagrangian spectrum function at frequency n is equal to the Eulerian at frequency βn. Thus, the shapes of the Lagrangian and Eulerian spectra are equal, as illustrated in Fig. 2.10.

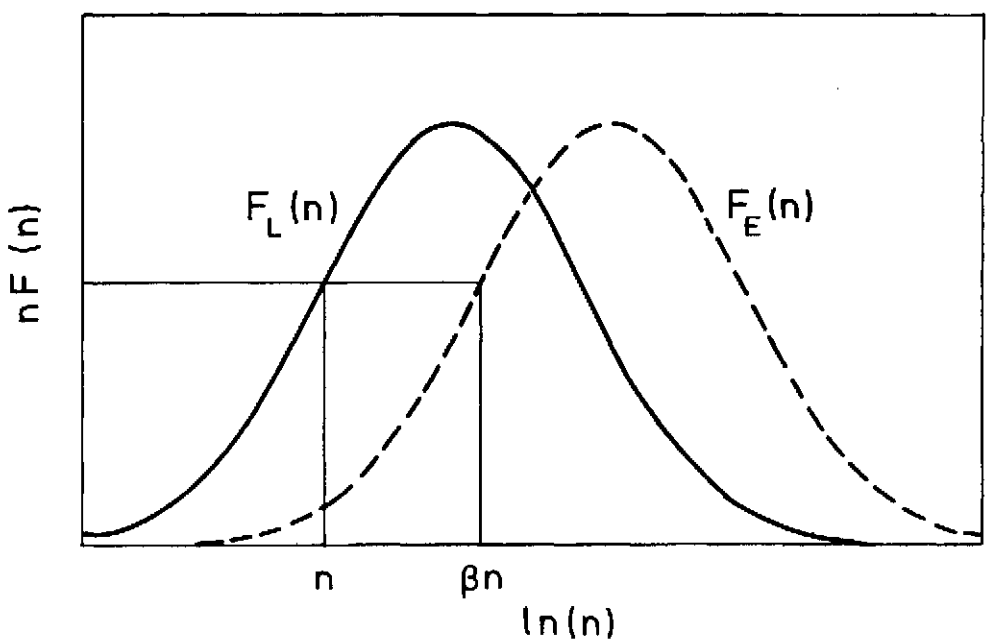

Fig. 2.10. The scale relation between Lagrangian and Eulerian spectra as proposed by Hay and Pasquill (1959).

Inserting (2.67) in Taylor's dispersion formula, (2.25), we obtain

$$\overline{Y(T)^2} = T^2 \overline{v'^2} \int_0^\infty \beta F_E(\beta n) \left(\frac{\sin \pi n T}{\pi n T}\right)^2 dn$$

or

$$\overline{Y(T)^2} = T^2 \overline{v'^2} \int_0^\infty F_E(n) \left(\frac{\sin \pi n \frac{T}{\beta}}{\pi n \frac{T}{\beta}}\right)^2 dn \qquad (2.68)$$

The effect of a finite averaging time, τ, might be achieved by introducing the Eulerian high-pass filter due to Ogura (1957), into (2.68)

$$\overline{Y(T)^2} = T^2 \overline{v'^2} \int_0^\infty F_E(n) \left\{1 - \left(\frac{\sin \pi n \tau}{\pi n \tau}\right)^2\right\} \left(\frac{\sin \pi n \frac{T}{\beta}}{\pi n \frac{T}{\beta}}\right)^2 dn \qquad (2.69)$$

Practical use of (2.69) is impeded because the formula requires knowledge of the variance spectrum, ideally extended over the entire range of frequencies. To get around this, Hay and Pasquill (1959) used in (2.68) the Eulerian spectrum measured over the duration of release or duration of sampling. When calculating $\overline{Y(T)^2}$ from the experimental results reported herein, we chose to use $F_E(n)$ and $\overline{v'^2}$ in (2.68) measured over the actual averaging time. Practical use does not necessarily require computations of the Eulerian spectrum, as the type of low-pass filter in (2.68) allows the formula to be written as

$$\overline{Y(T)^2} = T^2 \overline{v'^2}_{\tau, T/\beta} \qquad (2.70)$$

where the double subscript, $\tau, T/\beta$, indicates that the wind-velocity record measured over the period, τ, has been block-averaged over intervals of T/β prior to the calculation of the variance. This formulation of Taylor's dispersion formula will be heavily used in this report in combination with an expression for the Lagrangian-Eulerian time-scale ratio, β, that is due to Wandel and Kofoed-Hansen (1962)

$$\beta = \frac{\sqrt{\pi}}{4} i^{-1} \qquad (2.71)$$

where i is the intensity of turbulence for the direction in question. Details of (2.71) will be discussed in the following chapter.

On the relation between Eulerian and Lagrangian properties

Attempts to obtain relations between Eulerian and Lagrangian statistics from theoretical considerations, especially with reference to the ratio of the Lagrangian and Eulerian integral time scales, the so-called "Pasquill-β", has been reviewed by Pasquill (1974). Theory tends to give $t_L/t_E \propto i^{-1}$, where t_L and t_E are the Lagrangian and Eulerian time scales, respectively, with the constant of proportionality falling in the range 0.35-0.80.

Corrsin (1963) derived an expression for the ratio between the Lagrangian and the Eulerian time scales using an approach in which the Eulerian and Lagrangian spectra were completely represented by their form in the inertial subrange. In this chapter, the relationship will be rederived by a method that is based on Corrsin's (1963) approach, but with a more realistic description of the spectra. The low frequency part of the Lagrangian and Eulerian spectra will be approximated by a constant value for all frequencies below some limiting frequency that will be denoted n_E for the Eulerian and n_L for the Lagrangian spectrum. At frequencies higher than n_E and n_L respectively the spectra will be represented entirely by their forms in the inertial subrange.

The shape of the Eulerian spectrum in the inertial subrange is essentially dependent only on the wavenumber, κ, and the flow of energy which is equal to the dissipation, ε. Dimensional analysis leads us directly to the so-called -5/3 law, which, by use of Taylors hypothesis, $n = \bar{u}\,\kappa$, can be stated as

$$S_E(n) = A\ \bar{u}^{2/3}\ \varepsilon^{2/3}\ n^{-5/3}\ ,$$

where A is a constant and $\int_0^\infty S_E(n)dn = \sigma_E^2$ the Eulerian variance of the wind velocity fluctuations. The connection between the

dimensionless spectrum function, F(n), and S(n) reads $S_E(n) = \sigma_E^2 F_E(n)$. The complete Eulerian spectrum will then be represented as

$$S_E(n) = A \bar{u}^{2/3} \varepsilon^{2/3} n_E^{-5/3} \qquad 0 \leq n < n_E$$

$$S_E(n) = A \bar{u}^{2/3} \varepsilon^{2/3} n^{-5/3} \qquad n_E \leq n$$

The shape of the Lagrangian spectrum in the inertial subrange can be found by a similar analysis, but Lagrangian scaling must be formed with ε and the frequency n (Tennekes and Lumley, 1972). This leads to

$$S_L(n) = C \varepsilon n^{-2}$$

where C is a constant and $\int_0^\infty S_L(n)dn = \sigma_L^2$ the Lagrangian variance of the wind velocity fluctuations. The complete Lagrangian spectrum then reads

$$S_L(n) = C \varepsilon n_L^{-2} \qquad 0 \leq n < n_L$$

$$S_L(n) = C \varepsilon n^{-2} \qquad n_L \leq n$$

The characteristic Eulerian and Lagrangian integral time scales, t_E and t_L, respectively, can be found from (2.66) which can be formulated as

$$F_E(0) = 4 t_E$$

for n = 0. Similarly we can write

$$F_L(0) = 4 t_L$$

From these the Eulerian time scale can be found

$$F_E(0) = A \bar{u}^{2/3} \varepsilon^{2/3} n_E^{-5/3} \sigma_E^{-2} \qquad \text{or}$$

$$t_E = 0.25 \; A \bar{u}^{2/3} \varepsilon^{2/3} n_E^{-5/3} \sigma_E^{-2}$$

and similarly for the Lagrangian time scale

$$F_L(0) = C\ \varepsilon\ n_L^{-2}\ \sigma_L^{-2} \qquad \text{or}$$

$$t_L = 0.25\ C\ \varepsilon\ n_L^{-2}\ \sigma_L^{-2}$$

Integration of the spectra with subsequent elimination of n_E and n_L, respectively, yields

$$\sigma_E^2 = \int_0^\infty S_E(n)\,dn \qquad \text{or}$$

$$\sigma_E^2 = \frac{5}{2} \cdot 10^{2/3} \cdot A \cdot \bar{u}^{-2/3} \cdot \varepsilon^{2/3} \cdot t_E^{2/3}$$

$$\sigma_L^2 = \int_0^\infty S_L(n)\,dn \qquad \text{or}$$

$$\sigma_L^2 = 16\ C\ \varepsilon\ t_L$$

An assumption about equality between the Eulerian and Lagrangian wind velocity variances and finally elimination of ε leads to

$$\frac{t_L}{t_E} = D \cdot \frac{\bar{u}}{\sigma_E}$$

where D is a constant of proportionality and $\sigma_E/\bar{u}$ the intensity of the turbulence, i. Recalling the definition of "Pasquill's β" we have

$$\beta = D\ i^{-1}$$

as stated in (2.71). The estimates reported in the literature for the value of D display a large scatter. In Pasquill (1962) it was argued that Taylor's dispersion formula as given in (2.70) was insensitive to the value of β, and it was recommended that β be set equal to 4. Later, Pasquill (1974) refined the estimate taking into account the inverse proportionality with i, and a value of D = 0.44 was adopted. It is interesting to note that $D = \sqrt{\pi}/4$ was advocated by Wandel and Kofoed-Hansen

(1962) in perfect agreement with the much later adopted value of Pasquill (1974).

2.4.3. Semiempirical methods

The use of the Hay and Pasquill's (1959) working approximation requires thorough measurements of the turbulent wind velocity fluctuations, as well as computational facilities to accomplish the required low-pass filtering. It would be worthwhile to have methods that were easier to apply but still consistent with Taylor's dispersion formula. Such methods have been suggested by Draxler (1976) and Pasquill (1976). They are based on a rewriting of Taylor's dispersion formula in terms of dimensionless quantities as proposed by Pasquill (1975b). First we introduce the Lagrangian autocorrelation functions of dimensionless time lag $R^*_{L,i}(t/t_{L,j})$, $(i,j) = (v,y)$, (w,z), where the time lag, t, has been normalized with the Lagrangian integral time scales. Assuming that all autocorrelation functions to be encountered will coincide with $R^*_{L,i}(t/t_{L,j})$ when t is normalized with the actual time scale, we can write $nt_{L,j} F^*_{L,i}(nt_{L,j}) = nF_{L,i}(n)$, $(i,j) = (v,y)$, (w,z). Here $F^*_{L,i}(nt_{L,j})$ is a dimensionless spectrum function and $F_{L,i}(n)$ carries the unit of time. In reality, autocorrelation functions from actual measurements are unlikely to be of equal shape, but as mentioned in Chapter 2.4.2, substantial dissimilarities in the actual shapes of the autocorrelation functions are less important than substantial differences in the time scales. To follow common practice, we will denote $\sigma_v = (\overline{v'^2})^{0.5}$ and $\sigma_w = (\overline{w'^2})^{0.5}$. By defining the dimensionless spread S_j as

$$S_j = \frac{\sigma_j}{\sigma_i T} \qquad (i,j) = (v,y),\ (w,z)$$

or

$$S_j \simeq \frac{\sigma_j}{\sigma_k x} \qquad (k,j) = (\theta,y),\ (\phi,z)$$

Taylor's dispersion formula, (2.25), can be written

$$S_j^2 = \int_0^\infty F^*_{L,i}(nt_{L,j}) \left[\frac{\sin(\pi (nt_{L,j}) \frac{T}{t_{L,j}})}{\pi (nt_{L,j}) \frac{T}{t_{L,j}}} \right]^2 d(nt_{L,j}) \qquad (2.72)$$

$$(i,j) = (v,y),(w,z)$$

In this way the dimensionless frequencies $(nt_{L,j})$ and the dimensionless spectrum functions $F^*_{L,i}(nt_{L,j})$ are introduced. Equation (2.72) is a function only of $T/t_{L,j}$ and the dimensionless spreads therefore can be written

$$S_j = f_j\left(\frac{T}{t_{L,j}}\right) \qquad j = y,z$$

The limits of the f_j-functions for small as well as large values of T can easily be found when recalling the behaviour of Taylor's dispersion formula in the limits. From (2.18) it follows immediately that

$$\lim_{T \to 0} f_j\left(\frac{T}{t_{L,j}}\right) = 1$$

and (2.20) gives the limit for large T

$$\lim_{T \to \infty} f_j\left(\frac{T}{t_{L,j}}\right) = \left(2\ t_{L,j}/T\right)^{0.5}$$

The behaviour of the f_j-function at intermediate values of T is determined entirely by the shape of the spectrum function.

Equation (2.72) generally can be written

$$\sigma_j = \sigma_i\ T\ f_j(T/t_{L,j}) \qquad (i,j) = (v,y),\ (w,z) \qquad (2.73)$$

and this form is the starting point in the methods, proposed by Pasquill (1976) and Draxler (1976), for estimating σ_y and σ_z from the variance of the wind fluctuations.

Pasquill (1976) argues that for the lateral spread of the plume, (2.73) follows the relation

$$\sigma_y = \sigma_\theta \times f_y(x)$$

within fairly close limits. In other words, the f_y-function is assumed to depend primarily on the downwind distance, x. The Lagrangian time scale, $t_{L,y}$, can be written as $t_{L,y} = \ell/\sigma_v$, where ℓ is a characteristic lateral length scale. Consequently, $T/t_{L,y}$ can be set equal to $x\,\sigma_v/\bar{u}\ell$, (Gryning and Lyck, 1980a). Pasquill (1976) assumes that $\sigma_v/\bar{u}\ell$ varies only slightly and lists a number of discrete values of $f_y(x)$ for x less than 10 km; for x larger than 10 km, a formula has been suggested, Table 2.3. For the determination of σ_z, Pasquill recommends use of the

Table 2.3. Pasquill's (1976) method for calculating σ_y.

x(km)	0.1	0.2	0.4	1	2	4	10	>10
$f_y(x)$	0.8	0.7	0.65	0.6	0.5	0.4	0.33	$0.33(10/x)^{\frac{1}{2}}$

$\sigma_y = \sigma_\theta \cdot x \cdot f_y(x)$ with σ_θ in radians.

workbook curves, e.g. Turner (1970), which are based on the Pasquill (1961) stability classification. For dispersion over a city Pasquill (1976) suggests that the enhancement in the dispersion due to the heat output from a city, the so-called "heat island effect", can be taken into account by changing the estimated stability class one half class towards more unstable conditions. The roughness at the area is taken into account directly by enhancement of the σ_z-values by a factor which has been estimated by Smith (1972).

In contrast to Pasquill (1976), Draxler (1976) assumes that the f_j-functions depends on the travel time T, i.e. (2.73) is

rearranged in the form

$$\sigma_y = \sigma_\theta \times f_y(T/T_y)$$

$$\sigma_z = \sigma_\phi \times f_z(T/T_z)$$

where T is normalized by T_j, (j = y,z), a quantity proportional to the Lagrangian time scale. Values of T_j are given in Draxler as a function of the stratification. Table 2.4 shows the functions.

Table 2.4. Summary of T_y, T_z and equations for f_y and f_z, after Draxler (1976).

	Horizontal diffusion		Vertical diffusion	
	Stable	Unstable	Stable	Unstable
Ground sources	T_y=300s ($T < 550s$) f_y=1) ($T > 550s$) f_y=2)	T_y=300s f_y=1)	T_z= 50s f_z=1)	T_z=100s f_z=3)
Elevated sources	T_y=1000s f_y=1)	T_y=1000s f_y=1)	T_z=100s f_z=4)	T_z=500s f_z=1)

1) $$f_{y,z} = \frac{1}{1+0.90(T/T_{y,z})^{0.5}}$$

2) $$f_y = \frac{1}{1+28T^{-0.5}}$$

3) $$f_z = \frac{0.3(T/T_z-0.4)^2}{0.16} + 0.7$$

4) $$f_z = \frac{1}{1+0.945(T/T_z)^{0.806}}$$

The values of f_j by Pasquill (1976) and Draxler (1976) are suggested to be independent of terrain roughness and averaging times up to 1 hour. However, there is some evidence that the f_y-function depends on the sampling time (averaging time) and also on the wind velocity when f_y is expressed as function of distance, (Doran et al., 1978). This can be seen, when by use of (2.69) S_y is expressed as

$$S_y^2 = \frac{\int_0^\infty S_{E,v}(n)\left\{1 - \left(\frac{\sin\pi n\tau}{\pi n\tau}\right)^2\right\}\left(\frac{\sin\pi n \frac{T}{\beta_y}}{\pi n \frac{T}{\beta_y}}\right)^2 dn}{\int_0^\infty S_{E,v}(n)\left\{1 - \left(\frac{\sin\pi n\tau}{\pi n\tau}\right)^2\right\}\left(\frac{\sin\pi n t_i}{\pi n t_i}\right)^2 dn} \qquad (2.74)$$

where the low-pass filter in the denominator is due to instrument response-time, which ideally should be negligible.

Before discussing (2.74) further, it seems reasonable to present a few details regarding to v-spectra. Figure 2.11, taken from Kaimal (1978), shows the form of a v-spectrum for unstable meteorological conditions as a function of the dimensionless frequency $f = \frac{nz}{\bar{u}}$. Kaimal (1978) divides the spectrum into three regions, each of which is described by

$$\frac{n\, S_{E,v}(n)}{u_*^2\ \phi_\varepsilon^{2/3}} = \begin{cases} 0.4\ f^{-2/3} & \lambda \leq z \\ 0.4\ f^{-p} & 0.25\ z_i \geq \lambda \geq z \\ A^*B^*f/[1 + 3.1(B^*f)^{5/3}] & \lambda \geq 0.25\ z_i \end{cases}$$

where λ is wavelength, $\lambda = \frac{\bar{u}}{n}$, $A^* = \frac{1}{2}(\sigma_u^2 + \sigma_v^2)/(u_*^2 \cdot \phi_\varepsilon^{2/3})$, ϕ_ε is the dimensionless dissipation, $B^* = z/z_i$, and $p = (\ell n\ 0.44A^*/\ell n\ 0.33B^*)$. In Region 1, the spectrum obeys surface layer scaling; thus it is described as a function of f. In Region 3, the spectrum is described completely in terms of mixed-layer scaling. Thus it is described as a function of $\frac{nz_i}{\bar{u}} = B^*f$. Region 2 that constitutes the transition from surface layer to mixed layer co-ordinates, has simply been achieved by Kaimal (1978) by assuming a power law for the

spectrum satisfying the requirements for continuity at the end points.

The characteristic cut-off frequencies for the filter functions in (2.74) are also illustrated in Fig. 2.11. The filter due to the sampling time τ, has a characteristic dimensionless high-pass

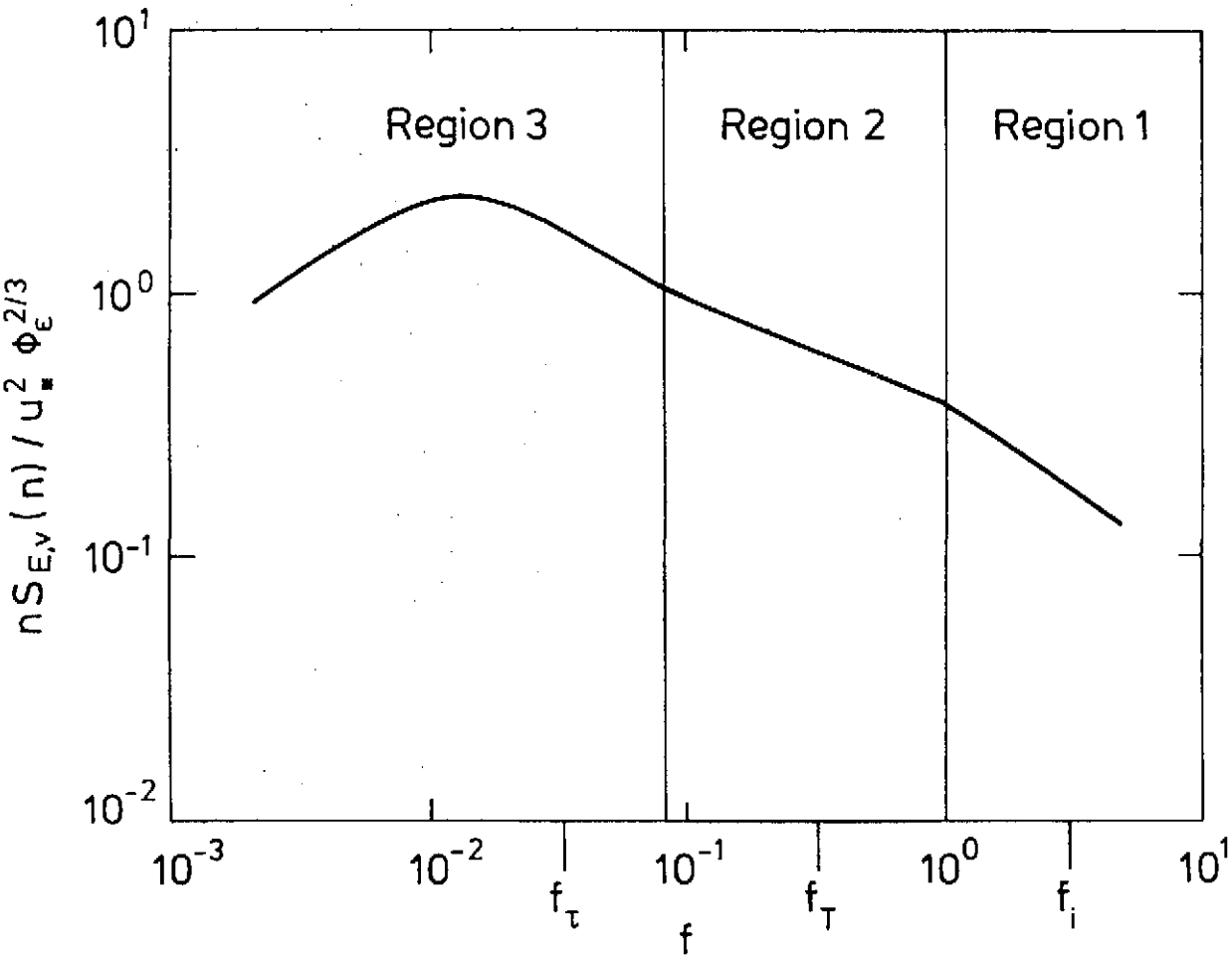

Fig. 2.11. Dimensionless v-spectrum for unstable meteorological conditions (Kaimal, 1978), plotted as a function of the dimensionless frequency f, illustrating the characteristic frequencies of the filter functions in (2.74).

filtering frequency of $f_\tau = \frac{z}{\tau \cdot \bar{u}}$, the travel time filter has a characteristic dimensionless low-pass filtering frequency of $f_T = \frac{\beta_y z}{T \bar{u}}$ or $f_T = \frac{\beta_y z}{x}$ using Taylor's hypothesis, and the charac-

teristic dimensionless low-pass filtering frequency due to instrument response reads $f_{t_i} = \frac{z}{t_i \bar{u}}$. If the instrument response is described by a distance constant $l = t_i \bar{u}$, where l is independent of $\bar{u}$, f_{t_i} can be expressed as $f_{t_i} = z/l$. Note that f_T, for a given downwind distance, and f_{t_i} is roughly independent of the wind velocity in contrast to f_τ. The numerator in (2.74) is approximately proportional to the area enclosed by f_τ and f_T, and the denominator is nearly proportional to the area enclosed by f_τ and f_{t_i}. Consider the situation for a given downwind distance and instrument distance constant. An increase of $(\tau\bar{u})$ moves f_τ to the left, which increases the numerator in (2.74) relatively more than the denominator, resulting in an increase of the value of S_y. The value of $(\tau\bar{u})$ can be increased by an increase either of τ or $\bar{u}$; thus for fixed τ, S_y can be expected to vary in dependence of $\bar{u}$ in a way such that high values of S_y are associated with high wind speed conditions, and vice versa.

It is tempting to evaluate the $\bar{u}$ and τ dependence on the S_y-function by integrating of (2.74), but as the error introduced by use of the Eulerian Kaimal-spectrum as a substitute for a Lagrangian spectrum is unknown it will be a pointless exercise that should be omitted. Therefore, rather than carry out the integration, the S_y-function should be experimentally determined.

A third wind-variance-based method to evaluate σ_y and σ_z is reported by Smith (1973) in the ASME-guide. The dispersion parameters simply are approximated by power laws as

$$\begin{aligned} \sigma_y &= 0.045\ \sigma_\theta\ x^{0.86} \\ \sigma_z &= 0.045\ \sigma_\phi\ x^{0.86} \end{aligned} \qquad \text{unstable conditions}$$

$$\begin{aligned} \sigma_y &= 0.15\ \sigma_\theta\ x^{0.71} \\ \sigma_z &= 0.15\ \sigma_\phi\ x^{0.71} \end{aligned} \qquad \text{stable conditions} \qquad (2.75)$$

where σ_θ and σ_ϕ here are in degrees. Use of empirical power laws in x to describe the downwind evolution of the dispersion parameters dates back to dispersion experiments at Brookhaven National Laboratory in the fifties. The determination of the constants in these expressions is often the main result from dispersion experiments. Thus, in spite of the empirical nature of (2.75), a huge number of power law constants with amazingly small deviations can be found in the literature.

2.4.4. Empirical methods

Application of the methods in the foregoing chapter assumes knowledge of the wind variances. This requires a rather complex on-line computerized data handling system to obtain a routine basis. Methods of estimating the dispersion characteristics, based on the use of more easily available meteorological data was suggested some twenty years ago.

Basically, the atmospheric stability is separated according to a stability classification. The dispersion parameters are then given as functions of downwind distance, represented by curves that are characteristic for the stability classes in question. Pasquill (1961) suggested a classification of the atmospheric stability into the classes A to F, where A corresponds to the most unstable, D to neutral, and F to the most stable atmospheric condition. This classification has received much appreciation and is extensively used, but the ways in which the class for a given meteorological situation are estimated vary. Pasquill (1961) suggested the scheme in Table 2.5, which is based on insolation and windspeed at a 10 m height. It is characteristic for Pasquill's scheme that unstable conditions can occur only in the daytime, and stable conditions during the night. The most unstable situations are associated with low windspeed and strong insolation, neutral situations are characterized by higher windspeed and less insolation, and strongly stable situations occur at night, when the wind speed is low and when there is no cloud cover. Nighttime conditions with wind speeds lower than 2 m/s is not assigned any stability class, in this situation meandering is likely to occur.

Table 2.5. Classification of the atmospheric stability according to Pasquill (1961).

Surface wind speed (m/sec)	Insolation			Night	
	Strong	Moderate	Slight	Thinly overcast or ≥ 4/8 low cloud	≤ 3/8 cloud
< 2	A	A-B	B	-	-
2-3	A-B	B	C	E	F
3-5	B	B-C	C	D	E
5-6	C	C-D	D	D	D
> 6	C	D	D	D	D

(for A-B take average of values for A and B etc.)

Strong insolation corresponds to sunny midday in midsummer in England, slight insolation to similar conditions in midwinter. Night refers to the period from 1 hr before sunset to 1 hr after dawn. The neutral category D should also be used, regardless of wind speed, for overcast conditions during day or night, and for any sky conditions during the hour preceding or following night as defined above.

The connection between Pasquill's scheme and the Ri-number

$$Ri = \left(\frac{g}{\bar{T}}\right) \frac{\frac{\partial \bar{T}}{\partial z} + \Gamma}{\left(\frac{\partial \bar{u}}{\partial z}\right)^2}$$

can be illustrated by the bulk Richardson number B which serves as an approximation for the Ri-number

$$B = \left(\frac{g}{\bar{T}}\right) \frac{\frac{\partial \bar{T}}{\partial z} + \Gamma}{\left(\frac{\bar{u}}{z}\right)^2} \quad .$$

The wind speed should be measured at the height $z = \left(z_1 \cdot z_2\right)^{0.5}$, where z_1 and z_2 are the height of the temperature measurements that goes into the temperature gradient. For conditions of strong insolation, the vertical gradient of the potential temperature will be large and negative. For small wind speeds B will become large and negative, which indicates that convective turbulence is dominant relative to shear-stress-produced turbulence, a situation characteristic for strongly unstable conditions. For increasing wind speeds, B will approach zero, which indicates that a higher part of the turbulence is produced by shear stresses. Neutral conditions occur when all turbulence is produced by shear stresses. Thus, the basic parameters in the Ri-number are closely connected to the parameters that go into Pasquill's scheme.

Pasquill (1961) does not give much guidance for the proper discrimination between the insolation categories, but leaves it to the subjective evaluation of the user. This led Turner (1970) to propose a connection between cloud cover and insolation in the Pasquill (1961) sense. An even more refined method, Klug (1969), also includes the elevation of the sun.

A somewhat different approach to the problem of stability classification was contrived in the United States some 20 years ago. This stability classification system, of which the origin is uncertain, is entirely in terms of the temperature gradient, leaving out the wind speed (see Table 2.6). The system avoids the subjective element in Pasquill's (1961) stability classification, and can be used in situations where profile measurements of standard meteorological data are available.

Having determined the proper atmospheric stability class, a number of curves exists, separated according to stability classes that gives dispersion parameters as function of distance.

Table 2.6. Classification of the atmospheric stability based on the temperature gradient from the ground to a height of 100 m., here taken from NRC Regulatory Guide (1972). Pasquill category G does not form part of the original stability classes in Pasquill (1961), but is added later.

Pasquill category	Temperature gradient (°C/100 m)
A	< -1.9
B	-1.9 to -1.7
C	-1.7 to -1.5
D	-1.5 to -0.5
E	-0.5 to 1.5
F	1.5 to 4.0
G	> 4.0

The most popular set of curves, heavily used (and misused) also in Denmark, was originally proposed by Pasquill (1961). The curves were reformulated by Gifford (1962) and obtained their final very popular and easy form in Turner (1970) (Fig. 2.12). They are reported to be characteristic for an averaging time of about 10 min. The curves rests on the Porton and Cardington tracer experiments that were carried out in the twenties and thirties in England, and the American Prairie Grass experiments from the fifties, all of which have typical averaging times of 3-15 min. In all experiments the tracer was released close to the ground and sampled up to 1-km downwind over a smooth area with roughness lengths of the order of 1 cm. The curves are extrapolated for downwind distances beyond 1 km.

An alternative set of curves is suggested in the ASME-guide by Smith (1973) (Fig. 2.13). These curves are based on dispersion

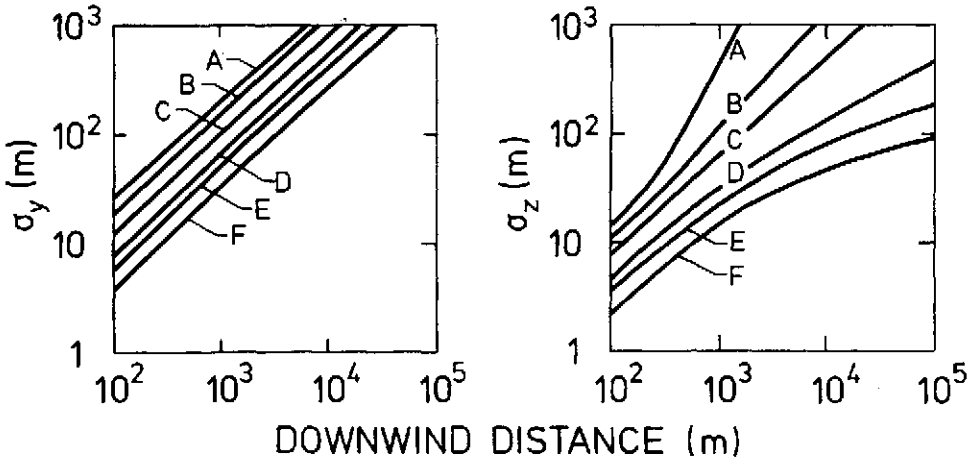

Fig. 2.12. Dispersion parameters as functions of downwind distance from the source, according to Turner (1970). The curves are separated according to the Pasquill stability classification.

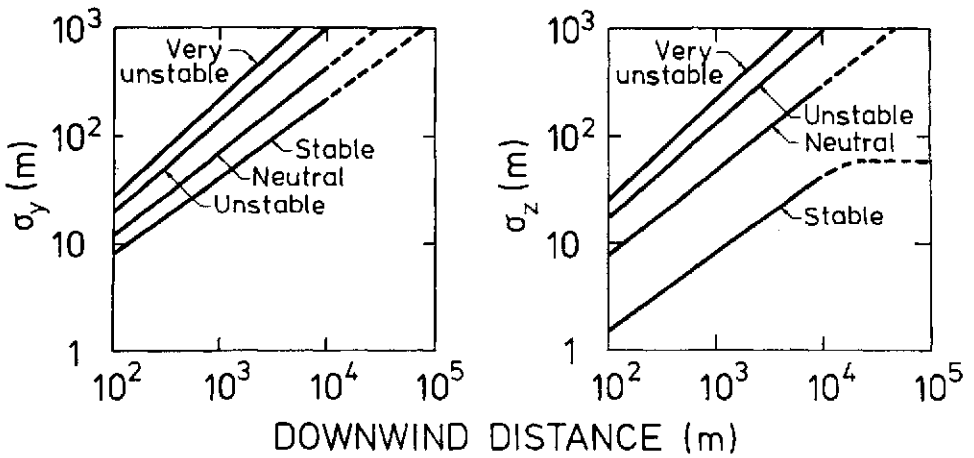

Fig. 2.13. Dispersion parameters as functions of downwind distance from the source, as proposed in the ASME-guide by Smith (1973). The curves are separated according to atmospheric stability. The dashed lines indicate that beyond 10 km the curves are tentative and unrealistic.

experiments carried out at Brookhaven National Laboratory in the fifties. The tracer was released at a height of about 100 m at a rather rough area that can be characterized by a roughness length of about 1-2 m. The tracer sampling time was 1 hour. Atmospheric stability was classified as stable, neutral, unstable and very unstable, and curves are given for each class, but Smith (1973) does not advise any scheme or method that can be used to classify atmospheric stability conditions into these four classes.

3. FULL-SCALE TRACER EXPERIMENTS

All the more-or-less empirical methods that are in use in order to predict the dispersion parameters rest on a mixture of theoretical considerations and result from tracer experiments. A very large number of experiments have been carried out; here the more significant experiments will be briefly described as well as the main results they supplied.

3.1. The Porton, Cardington, and Prairie Grass experiments

The first atmospheric dispersion experiments ever performed by means of a tracer technique were carried out in 1923 at Porton, England. A harmless smoke formed by burning candles of pitch was released and the concentration of smoke in the air was measured by a stain-meter technique. A hand pump was used to draw smoke-laden air through a filter. By comparing the resultant stain on the filter with calibrated standard stains, the smoke concentration could be estimated. The crosswind distribution of smoke then could be determined from the samples, taken by a team of observers downwind of the smoke source. In later works, the vertical concentration distribution was measured as well.

The experiments were carried out under near neutral conditions over open gently rolling downland. Smoke was released during a period of 4 min in each experiment and sampled up to 1 km downwind from the source.

Rather similar experiments were carried out in 1931 at Cardington, England, and again in 1934. This area was locally even more homogeneous than that around Porton. For these experiments, smoke was sampled over a period of 3-6 min.

The main conclusion that was drawn from these early ground-level source experiments, for which the data remained virtually un-

resolved until Pasquill's discussion (Pasquill, 1962) has been stated by Pasquill (1974) as:

(a) The width of cloud under neutral conditions at 100 m downwind, as defined by one-tenth axial or peak concentration, has an average value in the region of 40 m, but with individual variations of up to perhaps ±15 m from his figure.
(b) In the range 100-1000 m, again under neutral conditions, cloudwidth increases with distance raised to a power of approximately 0.8.
(c) As the atmospheric stability changes from near-neutral to moderately stable there is a systematic decrease of cloudwidth, and a close correlation between cloudwidth and the lateral component of the intensity of turbulence.

A substantial extension of the data on crosswind spread of continuous plumes was supplied by the American Prairie Grass experiments in 1956 that were carried out over a large flat field with a reported roughness length of less than 1 cm. The experimental results have been presented in Barad (1958).

These dispersion experiments were carried out by the use of sulphur dioxide as a tracer gas, released approximately 0.5 m above the surface and then sampled up to 800 m downwind from the source. Also, the vertical tracer concentration distribution was measured in some of the experiments. All the data from these experiments refer to a sampling time of 10 min. The experiments included measurements of the lateral and vertical wind fluctuations by use of fast responding instruments.

The data from the Prairie Grass experiments led to a number of publications, focusing on different aspects of the experiment and the data are still used in model validations; e.g. Nieuwstadt (1980), Briggs and McDonald (1978). Cramer (1959) focused on the empirical relation between the lateral wind fluctuations and the lateral spread of the tracer plume, and found a close dependence for a downwind distance of 100 m. Also, the dependence on σ_y of the downwind distance was investigated, giving values of the

exponent q in

$$\sigma_y \propto \sigma_\theta \, x^q$$

Cramer et al. (1958) concluded that the exponent q tends to be invariant with distance, and depends on stability as

unstable conditions	0.8-0.9
near-neutral conditions	0.8
stable conditions	0.6

Elliott (1961) investigated the shape of the vertical distribution of tracer concentrations. The distribution was approximated by

$$\bar{\chi}(z) = \bar{\chi}(z=o) \cdot \exp\,(-z^r/B_r)$$

and were examined for values of B_r and r. The data indicated that a value of $r \approx 1.5$ seems appropriate for near-neutral conditions and a somewhat smaller value should be used under unstable conditions. A Gaussian distribution requires $r = 2$.

The main reason that these old experiments still are of interest rests also on their constituting the experimental basis for Pasquill's relations (Pasquill, 1961) between the spread of a plume and the downwind distance. They are presented as curves separated according to a classification of the atmospheric stability. A slightly revised, more easily applicable version of Pasquill's relations are given in Turner's workbook (Turner, 1970), Fig. 2.12.

3.2. The St. Louis dispersion study

In the period 1963-65, low-level tracer experiments were carried out over a metropolitan area of St. Louis in U.S.A. (McElroy, 1969; McElroy and Pooler, 1968), a relatively flat, midwestern city. The tracer used was fluorescent particles (zinc cadmium sulfide) that were released near ground-level

over a one hour period. Measurements of total dosage near the surface were obtained in circular arcs up to 16 km from the source.

The results were presented as families of curves in terms of downwind distance as well as travel time. It turned out that the dispersion in the crosswind direction was more accurately described as a function of downwind distance; concerning the vertical dispersion, descriptions in terms of distance or travel time were equally good. The urban area affected the crosswind dispersion from the low-level point source primarily by increasing the size of the plume close to the source. As the plume became substantially larger than the size of eddies created by the local obstructions, the crosswind dispersion converged to that of a rural area. For the vertical dispersion, enhanced dispersion and enlarged initial cloud spread were observed when compared with dispersion over a rural area. The enhancement in the vertical dispersion appeared to be somewhat greater for stable than unstable meteorological conditions.

3.3. The early experiments at Brookhaven National Laboratory

Atmospheric dispersion experiments have been conducted since the beginning of the fifties at Brookhaven National Laboratory in U.S.A. The purposes of these experiments have been varied and in this context only a series of elevated-source dispersion experiments will be reviewed.

Oil fog was released at a height of 110 m at Brookhaven National Laboratory, a region that can be characterized by alternating open fields and areas of mature pines. The roughness length was approximately 1-2 m. The experiments are discussed in Smith (1956) and serves as the experimental basis for the curves and formulas describing the atmospheric spread that was published in the ASME-guide by Smith (1973). Comparisons of the results from this series of experiments, with the results for the low-source, rural area experiments (Porton, Cardington, Prairie Grass), reported in Turner (1970), shows that the two sets of curves are, as expected, significantly different.

3.4. Experiments at Jülich and Karlsruhe

Field experiments to investigate the atmospheric dispersion of plumes from elevated sources have been carried out at Kernforschungsanlage Jülich and Kernforschungszentrum Karlsruhe, both in Germany.

The experiments at Jülich (Vogt and Geiss, 1974) were carried out at a site with large surface roughness. The results from more than 40 tracer experiments with a tracer release height of 50 or 100 m showed that the distance from the source to the ground-level maximum concentration was a factor of 2 to 5 smaller than could be predicted by the use of the curves in Turner (1970). This effect was ascribed to the difference in surface roughness that is characteristic for the curves given by Turner (1970), compared with the surface roughness for the Jülich site. It was concluded that the use of stability classification systems that do not include the influence of the surface roughness, as e.g. the Pasquill stability classification scheme, in combination with the workbook curves by e.g. Turner (1970), will be justified in dispersion calculations only if a correction with regard to the surface roughness is introduced. It was also stated by Vogt and Geiss (1974) that typical site conditions in central Europe generally are characterized by a higher surface roughness than the characteristic surface roughness for the curves given by Turner (1970).

Results from ongoing tracer experiments at Karlsruhe are described by Thomas and Nester (1976). The tracer is released through a 100-m high reactor stack and sampled up to ~ 5 km downwind. The roughness length for this site is reported to be 1.1 m. The distance dependence of the dispersion parameters, σ_y and σ_z, is described by power laws for which the characteristic parameters were assessed by a rather complex statistical technique. The dispersion parameters determined in this way have been compared with the curves given by Turner (1970). The experimentally determined σ_z-curves for the Karlsruhe site turned out to be displaced towards unstable conditions relative to those reported by Turner. The shift is most pronounced in

neutral conditions and lesser for the unstable categories, A and B. This result was expected, as the mechanically produced part of the turbulence is greatest in the neutral category. Also, the measured σ_y-values for the Karlsruhe site turned out to be higher than Turner's.

3.5. Dispersion experiments under low wind speed conditions in a stable atmosphere

Pasquill's scheme, Table 2.5, for the classification of the atmospheric stability, does not assign any stability class to nighttime conditions for wind speeds lower than 2 m/s. Under these circumstances, the air is very stable and to a very high degree the vertical dispersion process is suppressed and horizontal dispersion is very slow. Large horizontal eddies, moved forward by the mean wind, seem to be responsible for the plume behaviour, termed meandering. Under these circumstances a plume will be spread over a large angular sector, so the use of the curves for stable conditions in Turner (1970) is completely inappropriate for the lateral component.

Sagendorf and Dickson (1974) describe a series of dispersion experiments, carried out under stable conditions at wind speeds less than 2 m/s. Ground-level releases of the tracer SF_6 were performed and the tracer-sampling units were placed up to 400 m from the source. The averaging time of the measured tracer concentrations was 1 hour. Normalized concentrations, $(\bar{\chi}U/Q)$, were derived from the measured tracer concentrations and were compared with normalised concentrations, calculated by assuming a Gaussian tracer distribution in the vertical and lateral direction, with total reflection of the tracer at the ground.

In the first approach, the Pasquill stability class was determined from the measurements of the vertical temperature gradient. Both σ_y and σ_z were then determined from the curves in Turner (1970). Using this approach, the calculated plume was consistently narrower than the measured one, and the calculated maximum concentrations were higher. In a second approach, σ_y was based

on a stability class, determined from the measurements of σ_θ (Sagendorf and Dickson, 1974), and σ_z was based on a stability class that was determined from the vertical temperature gradient. This is the so-called "split-sigma" method. Significant improvements were found relative to the first approach. The calculated maximum concentrations were much closer to the measured concentrations, and the calculated plume width more closely approximated the measured plume width, although they still were too narrow. A third approach consisted in deriving σ_y and σ_z from Markee's curves (Yanskey et al., 1966), which are shown on Fig. 3.1. The curves are based on experiments in which effluents were released over a period of 15 min to 1 hour. It should be

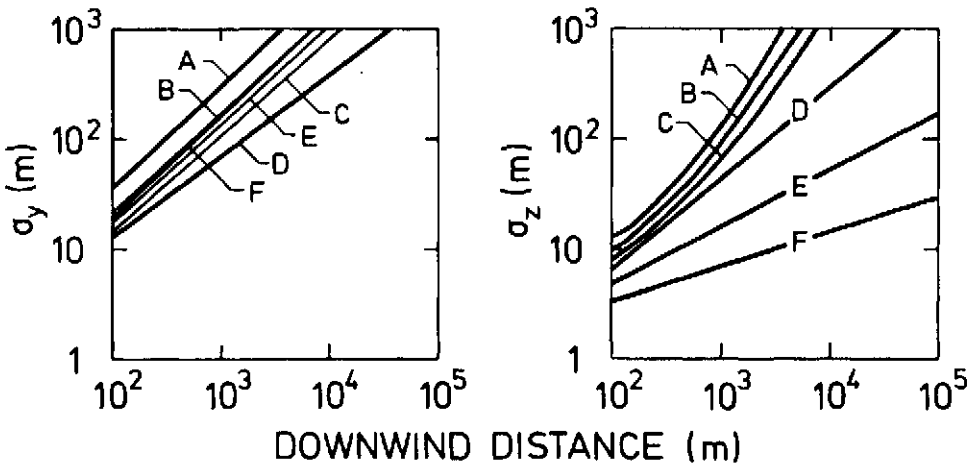

Fig. 3.1. Markee's dispersion parameters as function of downwind distance from the source, separated according to the Pasquill stability classification; from Sagendorf and Dickson (1974).

noted that the value of σ_y in the stable categories increases as the conditions becomes more stable. This represents the contribution of horizontal plume meander to the lateral spread. Use of the Markee-curves gave results that were quite comparable with the results based on the split-sigma method.

3.6. Dispersion experiments over inhomogeneous terrain

Only a few tracer experiments concentrate on the dispersion process over inhomogeneous surfaces. Among those are a measuring programme that was initiated at Brookhaven National Laboratory in order to evaluate the effect on the atmospheric dispersion that would originate from nuclear power plants sited on floating platforms moored at offshore locations. A small island, 800 m long and 175 m across at its widest, was selected as an appropriate substitute. The experiments are described by Raynor et al. (1975) and by Raynor et al. (1978).

Oil-fog plumes were simultaneously released from both the island and a small boat, anchored nearby in a position where the flow is undisturbed by the island. The concentration distribution of the plumes were measured at one or more distances downwind by traversing the plume with a boat that was equipped with a photometric densitometer. Also, extensive series of photographs were taken. Three measures of the standard deviation of the plumes were calculated. The mean of the standard deviations in the measured concentration distributions, computed from successive traverses across the plume at a given downwind distance were denoted σ_y; thus, it is the mean of several short period (4-8 min) measurements. The standard deviation in the concentration distribution that results from the summation of all the individual traverses, including meander of the plume as well as dispersion is represented by $\Sigma\sigma_y$, which thus represents a sampling period of 30-60 min. The standard deviation in the distribution of the locations of the plume centerlines is represented by $M\sigma_y$, and describes the effect of meander on the plume.

The experiments were separated with respect to atmospheric stability. The lateral spread, σ_y, of the island plumes were found generally to be greater than the same quantity of the plume from the boat. For unstable conditions, the ratio (island σ_y)/(boat σ_y) at a downwind distance of 100 m was 2.5, and at 1 km it was 1.3. Under neutral conditions, the corresponding ratios were 1.8 and 1.9; for the experiments in stable conditions, the ratios turned out to be 1.3 and 2.2. Thus, the ratio as a function of distance seems to converge to 1 under unstable conditions, re-

mains about constant under neutral conditions and seems to increase with increasing downwind distance under stable conditions. The ratio $\Sigma\sigma_y/\sigma_y$ for the boat plumes varied in the range 1.3 to 4.3 and the mean was 2.3. For the island plume, the range covered 1.2-7.8 with a mean value also of 2.3. The ratio $M\sigma_y/\sigma_y$ of the boat plume ranged from 0.8 to 4.1, the average value was 2.0. The equivalent ratios for the island plume covered a range of 0.7-7.7 with an average value of 2.0.

No significant separation between unstable and stable conditions was apparent in the values of the ratio $M\sigma_y/\sigma_y$, indicating that low frequency wind direction fluctuations were present in both regimes. Also, it was shown from the data that over a sufficiently long period of time meander may contribute more to the lateral spread of the plume than does the dispersion, even under unstable conditions. It also was observed that the island plume sometimes meandered less than the boat plume, and so under certain conditions the island appeared to damp some of the low frequency fluctuations in the wind direction. The investigation is not yet finished.

4. AIM AND SCOPE OF THE PROJECT

It is evident from the foregoing chapter that there has been a considerable effort made by many groups towards relating dispersive characteristics of the atmosphere to relatively easily obtainable meteorological parameters, but it is also evident that no unique description exists that covers all types of dispersion processes. Also, no dispersion experiments were reported from elevated sources situated in an urban area, although a considerable amount of the industry that uses the atmosphere as a pollutant depository, is situated in or in the immediate surroundings of cities. To elucidate the special features of atmospheric dispersion in that specific type of environment, a three part study was undertaken, the purpose of which was to

a) develop a cheap and easy-to-use technique for directly measuring the dispersion of a passive tracer, released from a point source,
b) determine the relationship between releases of air polluting material from elevated sources in an urban area, and the air quality, and
c) evaluate the methods used to calculate the dispersion of material released to the atmosphere and, if they are found justified, to suggest improvements in the methods.

The implementation of the project demanded development of a tracer technique that possessed a high degree of mobility combined with low staff requirements. Because of the use in urban areas, the tracer to be used should be without health effects when dispersed. Besides, it would be desirable that the tracer be nonreactive in order to diminish the potential problem of deposition or even chemical reactions in the tracer plume. Furthermore the tracer should be easy to release in the required quantities.

It was decided to base the development of the technique on the use of sulphur hexafluoride, SF_6, as a tracer. It is a nontoxic,

chemically stable gas, delivered in cylinders from which it can easily be released with the required flowrate. Chemical analysis of air with content of SF_6 is performed with a gas chromatograph equipped with an electron capture detector. This enables the detection of tracer concentrations down to about 10^{-12}ppp (parts SF_6 per parts of air).

Knowledge of the governing meteorological conditions during the dispersion experiments is crucial for a more thorough understanding of the way the tracer-plumes actually spread, and the meteorological measurements provides input for parameterizations of the dispersion process. But the requirements of mobility and low-staff demands, which are so crucial for the success of the experiments, excluded meteorological measurements that needed several hours calibration work on the day of the experiment. As a compromise, the tracer releases were carried out from a mast equipped with standard meteorological instruments for determining 10 min averages of wind speed and direction as well as temperature. Further, the three-dimensional wind-velocity fluctuations were measured continuously during the experiments.

The site for this kind of dispersion experiment may not contain, either upwind or downwind from the tracer release point, any pronounced shifts in surface roughness or topography, such as, e.g. high buildings. Also, it should include a pattern of roads, suitable for positioning the network of tracer-sampling units. These requirements are almost fulfilled when the TV-tower in Gladsaxe is used as the point of tracer release. The TV-tower is situated in the northern part of the Greater Copenhagen area, in a mixed residential, small industry area. Half a kilometer to the south stands a group of houses of 7 stories, but excluding these from the experimental sector revealed a 110° sector suitable for the experiments.

The tracer was released at a height of 115 m from the TV-tower and sampled at positions along near-concentric arcs centered at the tower, approximately 2, 4, and 6 km downwind. The tracer concentration measurements allowed for determining the lateral tracer-concentration distribution at ground level. The vertical

distribution was not directly measured. The measured tracer concentrations were then referred to the meteorological measurements through the use of models.

In order to test the developed tracer technique prior to the start of the experiments in Copenhagen, a number of dispersion experiments were carried out at Risø, using a rather small number of tracer-sampling units. In these experiments, the influence on the atmospheric dispersion process that arises from the inhomogeneity between the Roskilde Fjord water surface and the Risø peninsula was investigated (Gryning et al., 1978; Gryning and Lyck, 1980a). These experiments provided an estimate of the number of tracer sampling units necessary in each cross-wind series. The tracer sampling units ought to be positioned closely in order to obtain the fine structure of the plume, and far enough apart to secure that the plume will fall inside the sector covered by the sampling-units, even when shifts in wind direction occur. The Risø experiments showed that 20 tracer-sampling units, positioned with an angular separation of about 2^{o} constitute a reasonable compromise. These preliminary experiments were carried out with a maximum of 22 units, each equipped with a system for preset starting of the sampling. It was evident from these experiments that additional sampling-units for use in urban area experiments necessarily had to be radio controlled.

5. MEASURING AND SAMPLING TECHNIQUES

This chapter deals with the instrumentation and the operational procedures of the dispersion experiments.

Some of the instruments used were well established and readily available, some were commercially available but were modified to meet the requirements of this project, and some were developed especially for these experiments.

5.1. Implementation of the dispersion experiments

The experiments that were performed in Copenhagen will be described here; the pilot experiments at Risø discussed by Gryning et al. (1978) and by Gryning and Lyck (1980a) are reviewed briefly in the appendix.

5.1.1. Preparatory work

A boom designed for this project was mounted at a height of 115 m at the TV-tower in Gladsàxe. This boom was equipped with an instrument package for measuring the three-dimensional wind velocity and the turbulent sensible heat flux. Unfortunately, a cable to the temperature sensor failed during the experimental period.

A system for releasing SF_6 was built. This tracer was released at rates ranging from 1.9 to 4.7 g/sec in the various experiments. A constant flow rate was assured by observing a flowmeter. The tracer was discharged from cylinders placed in a building near the TV-tower and piped through a nylon pipe to the 115-m high point of release next to the experimental boom. The tracer release rate was estimated from the weight of the cylinders before and after an experiment and from the time of release.

In order to facilitate a rapid experimental procedure, positions separated by approximately 2° were marked out at lampposts along selected roads running approximately circular about the TV-tower at radial distances of 2, 4, and 6 km. Each position was plotted on a large-scale map on which distance and a characteristic angle between adjoining positions could then be determined. A chart of the experimental area with all the possible sampling-positions is shown in Fig. 5.1. The sector chosen for the experiments (220-330°) was determined by the possibility of finding suitable roads and of avoiding special topographical features that could influence the dispersion process.

A total number of 62 tracer-sampling units were available for these experiments; 40 of the units were equipped with radio to control the start of the sampling and the rest were those with a preselected sampling and preprogrammed starting time that had been used in the Risø pilot experiments.

5.1.2. Experimental procedure

In choosing a day to carry out an experiment, two requirements had to be taken into account: the weather forecast and the availability of the necessary laboratory staff members. Stationary meteorological conditions during the time duration of an experiment (approximately 3 hours) were required. Forecasts one day in advance were supplied by the Danish Meteorological Institute. When the required meteorological conditions could be foreseen, the final decision of the initiation of an experiment was taken on the basis of a renewed forecast on the morning of the measurements.

Having decided to proceed with the experiment, the tracer sampling units were loaded in cars, approximately 20 units per car and in addition to other necessary equipment transported to Gladsaxe. At the TV-tower, preparations were started to record the signals from the turbulence sensors at the 115-m level. The recordings were made on an analog tape recorder (AMPEX Model FR-1300) and this technique requires the recording of calibration voltages prior to each experiment. The proper

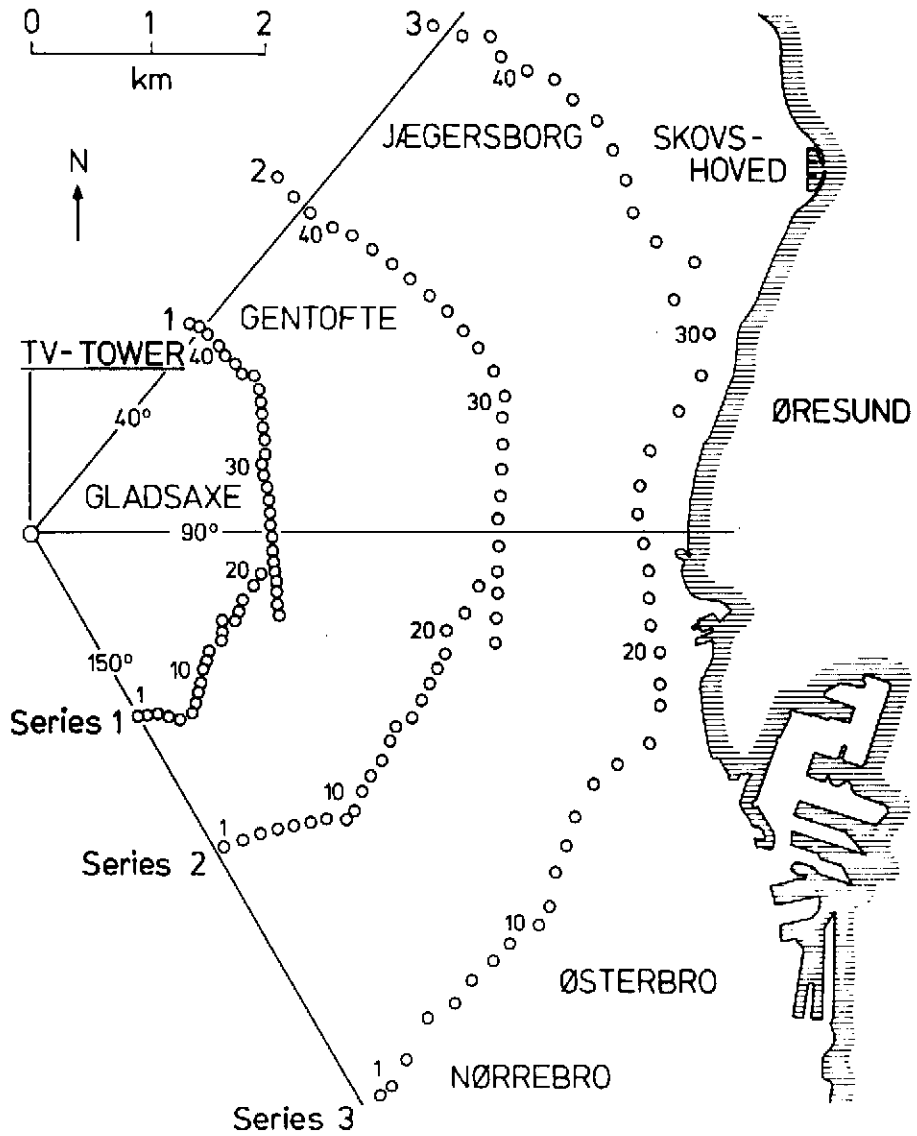

Fig. 5.1. The experimental site. Sampling unit positions used at the experiments are indicated by o; also shown is the numbering of the positions in the individual series. In siting these positrons it was intended that equal numbers in the three series be situated approximately on a straight line through the TV-tower. Due to the lack of suitable positions for mounting of tracer sampling-units in the southern part of series 3, position 9 in this series has been left out. In each experiment normally 20 sampling-units were used per series.

part of the experimental sector for placement of the tracer sampling units was determined by observing the direction of the wind at the height of release over a suitable period. In most experiments, 20 sampling units were used in the individual crosswind series, thus covering an angular sector of approximately 40°. Having decided upon the proper experimental sector, the positioning of sampling units was started. The units with a preselected sampling time were initiated for the start of sampling one hour later, and from then on, the experiment was completely fixed in time.

Tracer release began between 1/2 to 1 hour prior to the start of operation of the tracer sampling units. In all experiments, the time between start of tracer release and start of tracer sampling units was at least $2x/\bar{u}$ where $\bar{u}$ is the mean wind speed at the release height and x the distance to the most distant series. The continuous recording of the signals from the meteorological instruments at the release height began approximately 15 min before the start of the sampling units. Upon the start of the units at a preselected starting time, a radio signal initiated the radio-controlled units. Full radio contact between the persons in the field and the meteorologist at the TV-tower was accomplished by means of walkie-talkies. This allowed last-minute changes in the tracer sampling unit set-up.

Upon termination of the tracer sampling, the sampling units were collected and transported to Risø for subsequent chemical analysis. The time involved in the practical execution of a single experiment was typically 8 hours and it involved 6-7 staff members. The subsequent chemical analysis occupied one person for about 2 days.

5.2. Site description

The TV-tower at Gladsaxe that is being used for tracer release, is situated in an area with small-scale industry, one-family houses, and apartment buildings. The upwind experimental sector (220-330°) includes industrial areas at Herlev to the southwest

and Bagsværd to the northwest, both approximately 3 km from the mast. Except for a small unused area situated 4 km to the west and a complex of forests and lakes approximately 6 km to the northwest, the upwind area can be characterized as residential. The downwind sector (40-150°) is purely residential except for a mixed park-forest complex to the northeast 7 km from the mast. In the southeasterly direction the area changes character approximately 5 km downwind; initially it is residential and then becomes heavily built-up. The experimental site is limited by the Øresund approximately 7 km east of the TV-tower.

5.3. Meteorological instrumentation

The TV-mast is instrumented for routine measurements of wind speed (10, 60, 120, 200 m; 10 min averages), direction (10, 120, 200 m; 10 min averages) and temperature (2, 40, 80, 120, 160, 200 m; 10 seconds every 10 minutes). These instruments belong to the Danish Meteorological Institute. Wind speed and direction are obtained from cup anemometers and wind vanes, and temperature is measured by quartz thermometers.

These instruments are well suited for determining mean values of the meteorological parameters over typically 10 min periods, but they respond too slowly for measuring turbulent wind fluctuations. To measure these an instrument package consisting of a fast response, lightweight cup anemometer, wind vane, and vertical propeller was mounted at the boom at 115 m. Temperature fluctuations were derived using a uniquely referenced thermocouple pair. The signals (analog or pulsed) from these instruments were recorded continuously during the experiments and were later digitized with the sampling frequency of 1 or 2 Hz. A short description of the lightweight instruments is given below.

5.3.1. Cup anemometer

A Risø model 70 cup anemometer was used as a wind speed sensor. It is a lightweight, strong instrument with cups made of carbon-reinforced plastic. The distance constant is about 1.5 m. The version of the Risø 70 anemometer used here is a light-chopper type, producing 30 pulses per rotation. The number of pulses can be counted and converted to wind speed. An empirical, slightly nonlinear relationship is used for converting the pulse frequency to windspeed.

Cup anemometers respond more quickly to an increase in wind speed than to a decrease of equal magnitude; this effect is called overspeeding. The mean wind speed in turbulent flow will be overestimated if the cup anemometer has been calibrated in laminar flow. This problem has been discussed by Busch and Kristensen (1976) and Busch et al. (1979). It was shown that a fast-responding anemometer, as used here, is less influenced by overspeeding than a slowly responding one, and that the overspeeding is equal to or less than $\sigma_u^2/\bar{u}^2$, which typically is about 1%.

Ideally the angular response of a cup anemometer is the so-called cosine response. For a cup anemometer with this response, the angular velocity will be independent of the wind velocity component parallel to the axis. The angular response of the Risø-70 cup anemometer is, like that of most cup anemometers, nonsymmetrical with respect to a horizontal plane. Due to the anemometer shaft, the angular response for subhorizontal wind attack angles measurably departs from a cosine function. For superhorizontal attack angles up to ~ 20° the angular response is well approximated by a cosine. The angular response of the cup anemometer used is shown in Fig. 5.2. Corrections have been applied in the analysis of the data for the lack of cosine response. The correction is especially important for light wind, strong surface heating conditions.

Notwithstanding the problem of overspeeding (and angular response), the Risø-70 cup anemometer is accurate to within ± 1% of the actual wind speed reading above 5 m/s, and to ± 5 cm/sec below (Busch et al., 1979).

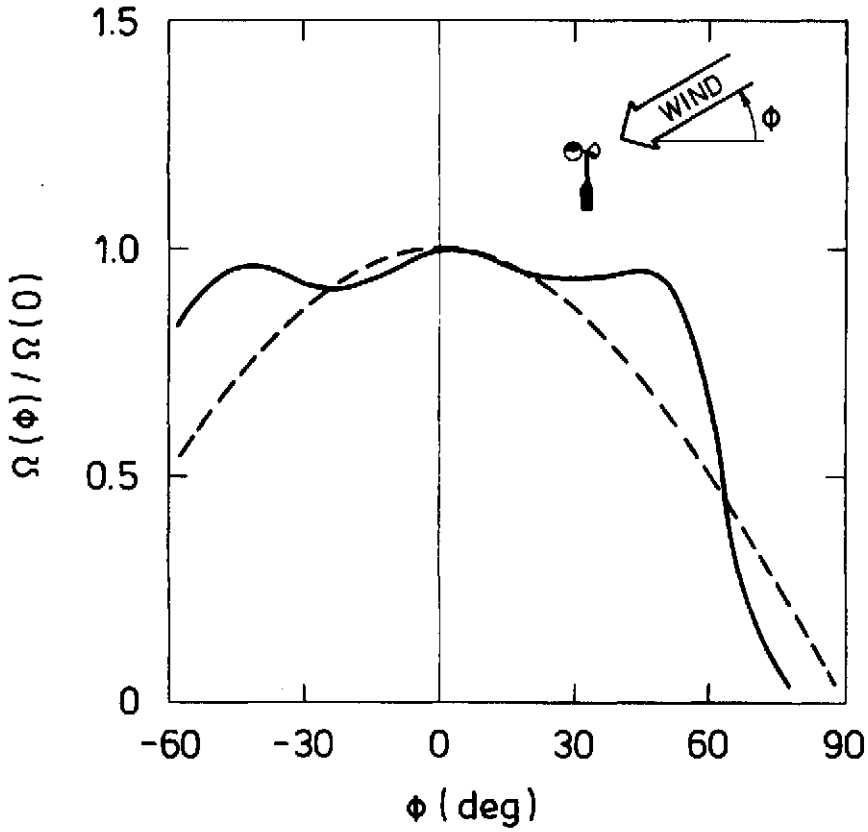

Fig. 5.2. Angular responses of the Risø 70 cup anemometer. Positive angles indicate that the wind attacks from above. The full line is the directly measured angular response; the dashed line is the ideal, cosine response (from Busch et al., 1979). The ordinate shows the angular response, $\Omega(\phi)/\Omega(0)$, where $\Omega(\phi)$ is the angular velocity of the cup anemometer for an angle of attack ϕ, and $\Omega(0)$ is the angular velocity for horizontal flow of an equal speed.

5.3.2. Wind vane

The horizontal wind direction was sensed using a lightweight vane, also developed at Risø and described in detail by Larsen and Busch (1974). In the vane design much attention was paid to the proper response characteristic at relatively high frequencies. The vane was designed with minimal weight and friction; a rough, flat, lightweight plate made of expanded polystyrene was used for vane material. From the approximate, theoretical relation between the wind vane deflection to the true wind direction (Larsen and Busch, 1974) it can be seen

that a wind vane acts as a second-order filter with the transfer function $H_V(\omega)$:

$$H_V(\omega) = \left[1 - \left(\frac{\omega}{\omega_e}\right)^2 - 2i\zeta\left(\frac{\omega}{\omega_e}\right)\right]^{-1}$$

where ω_e is a characteristic frequency (rad/s), ζ the damping ratio and ω the frequency (rad/s). The amplitude transfer function $H_V(\omega)$ as well as phase lag for different values of ζ are shown in Fig. 5.3, taken from MacCready (1965). It can be seen that the overall best performance of the amplitude transfer function is obtained for $\zeta \approx 0.6$. The characteristic frequency ω_e is related to a basic characteristic length scale λ_V, associated with the design of the wind vane; λ_V is approximately independent of the wind velocity. This is not the case for ω_e. Fast-response vanes require that ω_e be large. This is equivalent to stating that λ_V is small. The wind vane used in these experiments is characterized by $\zeta \approx 0.6$ and $\lambda_V \approx 1.5$ m.

The Risø vane output is two analog signals proportional to the cosine and sine of the wind direction. The signals are recorded directly on the FM-Ampex recorder.

5.3.3. Vertical propeller anemometer

The vertical wind velocity component is measured with a vertically mounted Gill propeller anemometer with four helicord-shaped polystyrene blades. The propeller diameter is 23 cm. A 10-cm shaft extender was employed to improve the response in the stall region. For along-axis winds the propeller anemometer in this configuration is reported to have a distance constant of approximately 1 m. The distance constant for the propeller, λ_p is usually measured by releasing a propeller from rest in a steady wind (wind tunnel) and observing the time necessary for the change towards stable rotation to reach 63%. The distance constant is a function of the angle of attack of the wind vector (the angle between the wind vector and the propeller axis), γ, which is given by

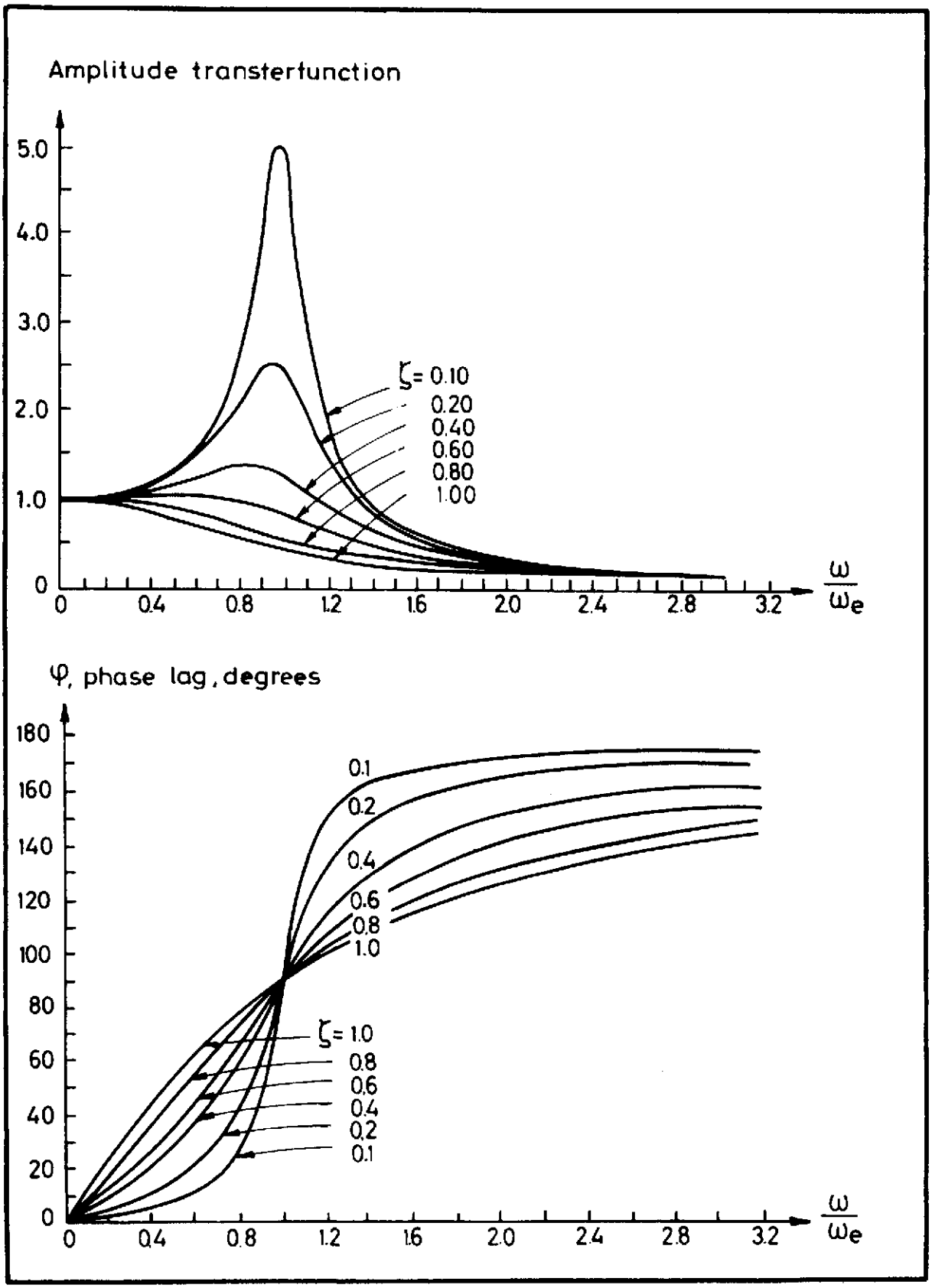

Fig. 5.3. Amplitude transfer function and phase lag for a number of values of the damping ratio, ζ, (Busch et al., 1979).

$$\gamma = \cos^{-1} \left(- w/(u^2 + v^2 + w^2)^{\frac{1}{2}}\right)$$

and λ_p is fairly well approximated by (Brook, 1977)

$$\lambda_p(\gamma) = \lambda_p(o) \cos^{\frac{1}{2}} \gamma$$

As a consequence, as γ approaches 90^o the distance constant becomes infinitisimal and the time constant $\lambda_p(\gamma)/w$ becomes infinite. Thus, the frequency response of the propeller anemometer depends on the instantaneous vertical wind speed and γ, so the response time will always be changing. Francey and Sahashi (1979) suggested a transfer function for the propeller anemometer that could account for the unsteadiness in the response time. The transfer function $H_p(n)$ was derived from the ratio between the spectra of the vertical wind velocity fluctuations as measured by a sonic anemometer and a Gill vertical propeller anemometer. This ratio became

$$|H_p(n)|^2 = (1 + (2\pi\lambda_p n/\bar{u})^p)^{-1}$$

where $2\pi\lambda_p \simeq 2$ m, $p \simeq 2.5$, and n is frequency in Hz.

Like the cup anemometer, the propeller anemometer does not have an ideal angular cosine response. Thus, the output signal is not a simple linear function of the vertical velocity component. The steady state angular response of the propeller anemometer used here was measured in a wind tunnel and is shown in Fig. 5.4. The response deviates significantly from the ideal cosine response; also it is markedly different for a downwardly ($0 \leqslant \gamma \leqslant 90^o$) and upwardly directed ($90 \leqslant \gamma \leqslant 180^o$) vertical wind component. The propeller will stall in a region of about $\pm 1^o$ around $\gamma = 90^o$. Measurements shows that the angular response function of the propeller anemometer is approximately independent of the wind velocity.

The Gill propeller anemometer output is a voltage proportional to the angular velocity of the propeller. Each propeller has been individually calibrated. The calibration for axial flow is given by

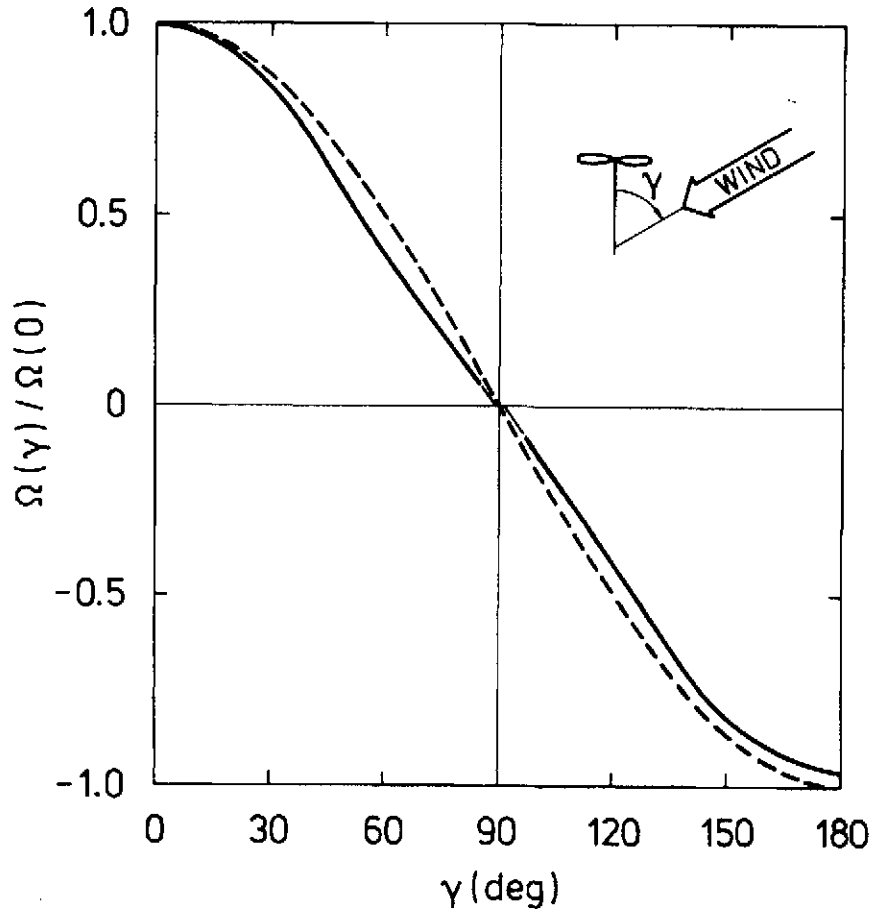

Fig. 5.4. Steady-state angular response for the Gill-propeller. For $0 < \gamma < 90^{o}$, the wind attacks from above; for $90 < \gamma < 180^{o}$, the wind attacks from below. The full line is the directly measured angular response, the dashed line the ideal cosine response. The ordinate shows the angular response $\Omega(\gamma)/\Omega(0)$, where $\Omega(\gamma)$ is the angular velocity of the propeller anemometer for an angle of attack γ, and $\Omega(0)$ is the angular velocity for axial flow of an equal speed.

$$w = \Delta w + K \cdot V$$

where $\Delta w \sim 0.2$ m/s and $K \sim 3.8$ m/(s·volt); V is the output voltage from the propeller.

5.3.4. Temperature sensor

An instrument to measure the fluctuating temperature was developed. Air temperature fluctuations are derived from the in-

stantaneous temperature difference between a thermocouple junction extending 5 mm into the airstream and a reference junction imbedded in the center of a acrylic sphere with a diameter of 10 cm. The low-level voltage produced by the thermocouple pair is amplified before the electric signal is transmitted through a cable to the recording instruments. The result of this design is that the air-temperature fluctuation measurements are effectively band-pass filtered with an upper frequency characterized by a time constant of ~ 1 s., owing to the size of the thermocouple wires, and a lower frequency corresponding to a time constant of ~ 75 min that is controlled primarily by the diameter of the acrylic sphere. A thorough description of this instrument is given by Gryning and Thomson (1979).

The temperature sensor was mounted at 115 m at the TV-tower and successfully tested. Unfortunately, it was not in working order during the period of the experiments and it could not be serviced. The TV-tower is not equipped with a personnel elevator, and having this is of crucial importance in facilitating the servicing of such micrometeorological instrumentation.

5.3.5. Radiosonde launches

Mixing heights were estimated from the routine radiosonde launch, performed routinely at Jægersborg only 5 km NE of the TV-tower. The synoptic time for the daytime launches is 1 p.m., which is quite close to that of the experiments.

5.4. Three-dimensional wind velocity sensing by means of the instrument system (cup and propeller anemometer, wind vane)

The continuous signals from the instruments are used for computating the fluctuating, three-dimensional wind velocity vector. For the propeller, the calibration function for axial flow is given by

$$w = V \cdot K + \Delta w$$

For nonaxial flow, the measured wind component along the propeller axis, $V \cdot k + \Delta w$, is not the projection of the actual wind speed on the propeller axis, but is given by

$$V \cdot k + \Delta w = S(\gamma) \cdot (u^2 + v^2 + w^2)^{0.5}$$

where $S(\gamma)$ is the angular response function, which can be measured. The wind attack angle, γ, is 0° for along axis flow, and 90° for flow perpendicular to the axis.

In the following an outline of the method that was used to take the angular response function into consideration when calculating the wind velocity vector, will be given. The response function $S(\gamma)$ was approximated by a finite Fourier series

$$S(\gamma) = \sum_{n=o}^{m} \{a_n \cos n\gamma + b_n \sin n\gamma\} \qquad (5.1)$$

where m is a positive integer, and a_n and b_n are the usual constants in a Fourier expansion. The Fourier decomposition of $S(\gamma)$ was carried out following a method originally proposed and described in detail by Christensen (1971). We will here restrict the derivation to the sector $0^\circ \leq \gamma \leq 90^\circ$, where it is assumed that $S(\gamma)$ has been measured at N equispaced angles between 0 and 90 degrees. A finite Fourier series of N terms of the form

$$S(\gamma) = \sum_{m=1}^{N} a_{2m-1} \cos(2m-1)\gamma$$

can then be determined so that the measured values of $S(\gamma)$ is exactly reproduced. Christensen (1971) devised a method to determine the Fourier coefficients. Having computed a_n, $S(\gamma)$ will be approximated in further calculations by

$$S(\gamma) = \sum_{m=1}^{N_1} a_{2m-1} \cos(2m-1)\gamma \qquad (5.2)$$

which will be used to relate nonmeasured values of $S(\gamma)$ to the measured ones. Keeping $N_1 < N$, (5.2) cannot reproduce the measured values of $S(\gamma)$ exactly, but produces approximations only; the accuracy of these approximations increases for increasing values of N_1, and when $N_1 = N$, (5.2) reproduced all measured values of $S(\gamma)$ exactly.

Computing $S(\gamma)$ by means of this formula requires that the cosine function be calculated N times, and that is very time consuming.

To reduce computer time, the formula has been expressed as a polynomial series in $\cos(\gamma)$

$$S(\gamma) = \cos(\gamma) \sum_{m=1}^{N_1} b_{2m-2} \cos^{2m-2}(\gamma) \qquad (5.3)$$

By tedious and extremely laborious reductions, the relations between a_{2m-1} and b_{2m-2} have been derived up to $N_1 = 12$.

$$b_0 = 2^0\{a_1 - 3a_3 + 5a_5 - 7a_7 + 9a_9 - 11a_{11} + 13a_{13} - 15a_{15} + 17a_{17} - 19a_{19} + 21a_{21} - 23a_{23}\}$$

$$b_2 = 2^2\{a_3 - 5a_5 + 14a_7 - 30a_9 + 55a_{11} - 91a_{13} + 140a_{15} - 204_{17} + 285a_{19} - 385a_{21} + 506a_{23}\}$$

$$b_4 = 2^4\{a_5 - 7a_7 + 27a_9 - 77a_{11} + 182a_{13} - 378a_{15} + 714a_{17} - 1254a_{19} + 2079a_{21} - 3289a_{23}\}$$

$$b_6 = 2^6\{a_7 - 9a_9 + 44a_{11} - 156a_{13} + 450a_{15} - 1122a_{17} + 2508a_{19} - 5148a_{21} + 9867a_{23}\}$$

$$b_8 = 2^8\{a_9 - 11a_{11} + 65a_{13} - 275a_{15} + 935a_{17} - 2717a_{19} + 7007a_{21} - 16445a_{23}\}$$

$$b_{10} = 2^{10}\{a_{11} - 13a_{13} + 90a_{15} - 442a_{17} + 1729a_{19} - 5733a_{21} + 16744a_{23}\}$$

$$b_{12} = 2^{12}\{a_{13} - 15a_{15} + 119a_{17} - 665a_{19} + 2940a_{21} - 10948a_{23}\}$$

$$b_{14} = 2^{14}\{a_{15} - 17a_{17} + 152a_{19} - 952a_{21} + 4692a_{23}\}$$

$$b_{16} = 2^{16}\{a_{17} - 19a_{19} + 189a_{21} - 1311a_{23}\}$$

$$b_{18} = 2^{18}\{a_{19} - 21a_{21} + 230a_{23}\}$$

$$b_{20} = 2^{20}\{a_{21} - 23a_{23}\}$$

$$b_{22} = 2^{22}\, a_{23}$$

The value of N_1 was chosen by performing the Fourier expansion with increasing values of N_1 until the deviation between measured and predicted values of $S(\gamma)$ were found to be less than 5% at all measuring angles. For both the vertical propeller and the cup anemometer, N = 18. For the $S(\gamma)$ function of the vertical propeller, a value of $N_1 = 12$ was necessary, while for the cupanemometer response function, $N_1 = 9$ fulfilled this requirement.

A separate Fourier expansion of $S(\gamma)$ for the vertical propeller was performed for $0 \leq \gamma \leq 90^{o}$ (downwind-directed flow) and for $90 \leq \gamma \leq 180^{o}$ (upwardly directed flow). The Fourier expansion coefficients for the propeller are given in Table 5.1. Also, the response function for the cup anemometer was approximated by the Fourier expansion, but as a function of ϕ, the angle between the wind vector and a horizontal plane. The Fourier expansion coefficients for downwind ($\phi > 0^{o}$) and upwardly ($\phi < 0^{o}$) directed flow are shown in Table 5.2.

Table 5.1. Fourier expansion coefficients for the angular response function of the propeller-anemometer.

	$0 \leq \gamma \leq 90^{o}$	$90 < \gamma \leq 180^{o}$
b_o	0.806466802	0.908712582
b_2	-3.795520500	-7.044744516
b_4	54.97795978	130.6937190
b_6	-353.2345701	-1249.194742
b_8	1226.149286	7062.533548
b_{10}	-2782.710363	-25051.27001
b_{12}	4168.858214	57717.54140
b_{14}	-5003.308335	-87528.21515
b_{16}	5385.296347	86550.16591
b_{18}	-4591.891775	-53599.76841
b_{20}	2401.507475	18831.31347
b_{22}	-541.6566129	-2856.715289

Table 5.2. Fourier expansion coefficients for the angular response function of the cup anemometer.

	$\phi > 0^o$	$\phi < 0^o$
b_o	0.890156023	2.135892638
b_2	7.633982644	-9.963957960
b_4	-95.13121280	92.32332186
b_6	617.1309676	-481.4282778
b_8	-2049.978027	1435.814281
b_{10}	3735.467129	-2538.148253
b_{12}	-3815.934775	2619.656987
b_{14}	2058.175578	-1456.058122
b_{16}	-457.2545024	336.6655099

Using the Fourier expansion representation of the angular response functions, and the instantaneous cup anemometer and propeller outputs, an iterative procedure was worked out to calculate both the horizontal wind speed, $\sqrt{u^2+v^2}$, and the vertical velocity, w, taking into account the lack of the ideal cosine-response function for both the propeller and cup anemometer. Figure 5.5 shows a combination of w, $\sqrt{u^2+v^2}$ and the length of the wind vector $\sqrt{u^2+v^2+w^2}$.

$$w = \sqrt{u^2+v^2+w^2}\ \cos(\alpha)$$

$$\sqrt{u^2+v^2} = \sqrt{u^2+v^2+w^2}\ \sin(\alpha)$$

$$\Omega^+ = \sqrt{u^2+v^2+w^2}\ S_{prop}(\alpha)$$

$$\beta^+ = \sqrt{u^2+v^2+w^2}\ S_{cup}(\alpha)$$

where S_{prop} and S_{cup} are the appropriate angular response functions for the propeller and cup anemometer with respect to this definition of α; Ω^+ and β^+ are estimates of the vertical and

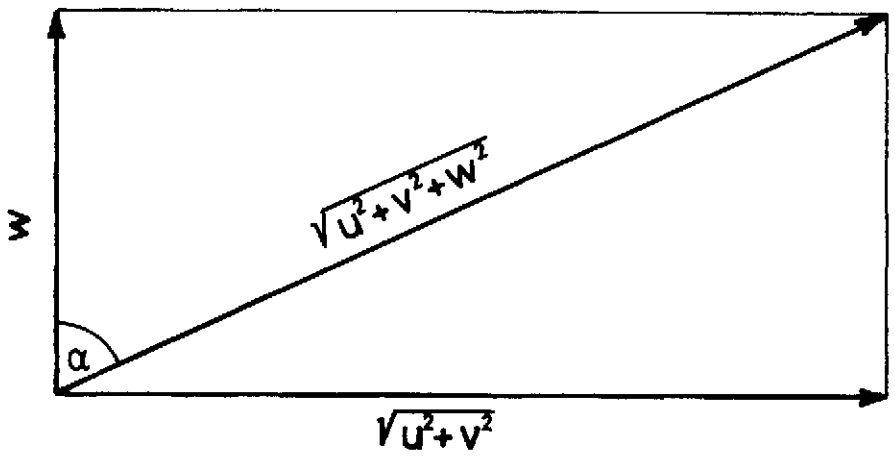

Fig. 5.5. Illustration of the vertical velocity w, the horizontal speed $\sqrt{u^2+v^2}$, and the length of the wind vector, $\sqrt{u^2+v^2+w^2}$.

horizontal wind components derived from the propeller and cup anemometer output by use of calibration curves for axial flow (propeller) and horizontal flow for the cup anemometer; there is no compensation for the lack of ideal cosine response functions.

The iterative procedure that was used for deriving values of w and $\sqrt{u^2+v^2}$ corrected for the effect of the lack of the ideal cosine function for the propeller and cup anemometer starts by computing a first estimate of the attack angle, α

$$\alpha = \tan^{-1}\left(\frac{\beta^+}{\Omega^+}\right)$$

This value of α is used to derive a revised value of w and $\sqrt{u^2+v^2}$

$$w = \frac{\Omega^+}{S_{prop}(\alpha)} \cos\alpha \quad ,$$

$$\sqrt{u^2+v^2} = \frac{\beta^+}{S_{cup}(\alpha)} \sin\alpha$$

and then a revised estimate of α is calculated

$$\alpha = \tan^{-1}\left(\frac{\sqrt{u^2+v^2}}{w}\right)$$

With this new value of α, estimates of w and $\sqrt{u^2+v^2}$ are recalculated. This iteration continues until the difference between two successive values of α is less than a specified limit.

Finally, from the entire time record of w, $\sqrt{u^2+v^2}$ and the wind direction θ, the longitudinal, u, lateral, v, and vertical, w, wind velocity components are extracted.

5.5. Tracer sampling units

Prior to the decision on the tracer sampling technique that was to be used in these experiments, several techniques were investigated.

Tracer sampling in evacuated steel containers, filled at a constant flow rate through critical orifices, as adopted by Raynor (1978), was investigated but given up due to the size, weight and foreseen handling problems of these sampling units. Tracer sampling in glass vessels initially filled with water, which during the sampling period is let out through a capillary, was also given up because of inconvenient handling of the glass vessels; the technique is described in Nieuwstadt and Duuren (1979). Finally, a technique using plastic bags was selected for these experiments, primarily because of the possibility of obtaining easy handling of the sampling unit.

Plastic bags made of Saranex film were filled with a dilute concentration of SF_6 in the range of about 10^{-9}ppp (parts SF_6 per parts of air) and stored for one week. No measurable losses of SF_6 were detected. Saranex film has a laminated structure and the surface consists of polyethylene surrounding a Saran (PVCD) layer. The polyethylene surface makes the film easy to weld and the Saran makes it effectively airtight.

An automatic air-sampling unit, based on sampling in plastic bags, was developed in two steps. For testing and subsequent use in a series of pilot experiments carried out at Risø, a low cost unit was developed. Air was sucked in through an intake tube by a small diaphragm pump and let to one of three plastic bags which are inflated with a flow rate of about 300 ml/min; the inflation of the bags is regulated by magnetic valves. The sampling procedure is controlled by an electronic timer; pulses from a quartz 100 kHz oscillator are counted and the sampling period (time for each air sample) can be preselected as 2^{26}, 2^{27} or 2^{28} pulses, corresponding to approximately 11, 22, or 45 min, respectively. The timer circuit can be triggered by an electric pulse; the time from the initial triggering to the start of the pump can be selected as a multiple of 1 to 9 of the sampling period of each bag. Prior to an experiment all sampling units are connected to a central box, which by pressing a button produces a pulse that simultaneously triggers the timers in the sampling units. Then, the sampling units are disconnected from the central box and brought out in the field. Power for the units is supplied by rechargeable NiCd batteries, making the units completely self-contained. Figure 5.6 shows the interior of one unit. On fig. 5.7 a unit with plastic bags put on, mounted on a portable rack is shown. During operation the plastic bags were protected by a large paper bag which was pulled down over the entire unit.

The sampling unit was found to work well at Risø, but the pilot experiments indicated that the technique based on the timer is convenient only when the number of units is relatively low (10-20). As it was required to use 60 sampling units in the experiments at Copenhagen, remote control of the sampling start would be required. Therefore, the 40 extra sampling units that were built for use in the Copenhagen experiments, were basically identical to the original units, but the timer was replaced by a radio receiver for the start of sampling. Figure 5.6 shows the interior of one radio-controlled unit. When started, the units inflate the three plastic bags in sequence, each having a sampling time of 20 min. To secure proper transmission of the coded signal from the 5 watt transmitter to all radio-controlled sampling units when used

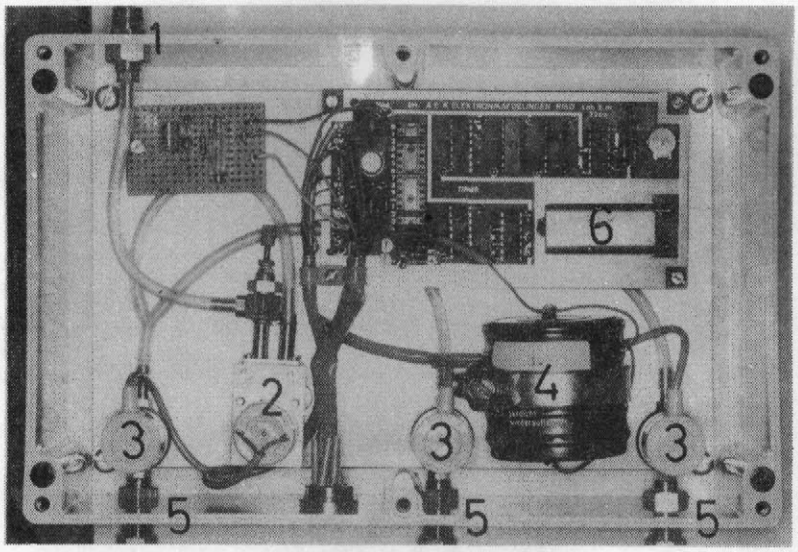

(a)

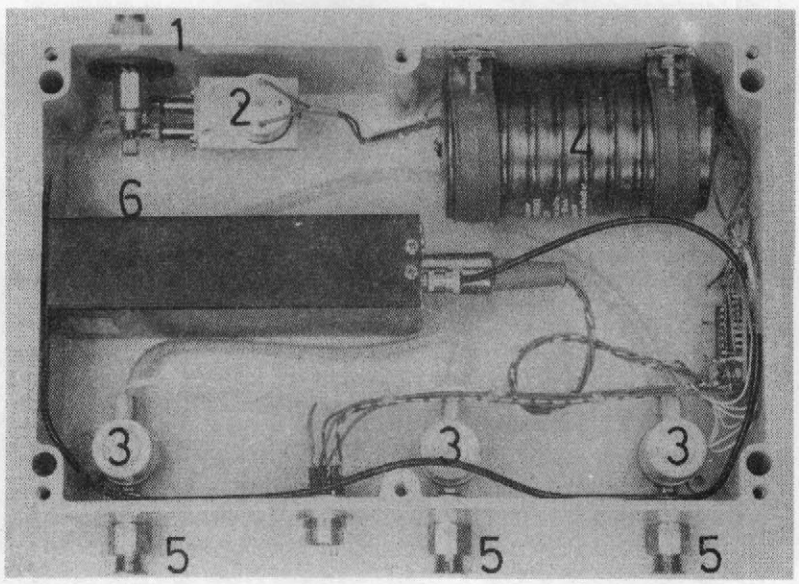

(b)

Fig. 5.6. Interior of a) timer-controlled and b) radio-controlled SF_6 tracer sampling unit. 1) fitting for mounting of the intake tube, 2) diaphragm pump, 3) magnetic valves, 4) NiCd battery, 5) fittings at which the plastic bags can be mounted. In figure a 6) shows the timer for control of the sampling, and in figure b 6) shows the radio receiver for the start of the sampling.

Fig. 5.7. Sampling unit mounted with plastic bags and placed on a portable rack.

in an urban environment, it was chosen to use a UHF radio system. This makes the transmitter and receivers rather expensive, but secures effective transmission of the radio signals. Our radios were operated at the government-assigned frequency of 447.150 MHz, and the signals were emitted from an antenna placed at a height of 160 m at the TV-tower. The signals were always properly received at the sampling units, even when placed in the street canyons of Copenhagen.

For use in Copenhagen, also the quartz oscillators in the original sampling units were replaced, allowing for a sampling time of 20 min.

During the experiments in Copenhagen, the units were mounted in plastic baskets that prior to each experiment were placed on lampposts secured by rubber bands (Fig. 5.8).

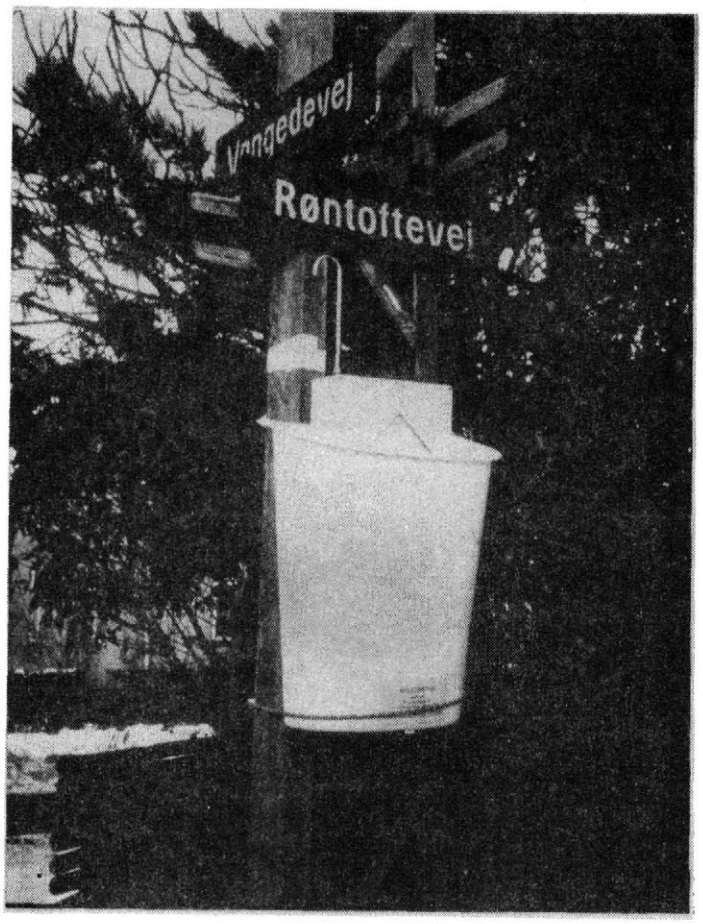

Fig. 5.8. Sampling unit mounted in lamppost in Copenhagen, ready for an experiment. The basket protects the Saran bags.

5.6. Tracer analysis and calibration

All air samples were brought to the laboratory immediately after each experiment and analyzed for their content of SF_6. The SF_6 concentrations were measured by means of a pulsed electron capture detector gas chromatograph equipped with a molecular sieve column and operated at room temperature.

In the calibration procedure, use is made of the high ionization factor (about 95%) which can be achieved by SF_6 molecules. This factor is the percentage of the SF_6 molecules let through the electron capture detector being ionized. The calibration is performed as follows: A test dilution having a SF_6 concentration of $0.5 \cdot 10^{-9}$ ppp was produced by injecting 25-µℓ SF_6 gas into a room of 50 m^3 volume. Use of test dilutions below about $0.5 \cdot 10^{-9}$ ppp in the calibration procedure was avoided due to severe difficulties connected with the preparation of such low concentrations. With this test dilution the ionization factor was measured by comparing the signals from two identical electron capture detectors connected in series. The ionization factor is taken as the signal from the first detector divided by the sum of the signals.

For the system used, the ionization factor turned out to be about 95%, so apparently the detector is almost coulometric (meaning that the ionization factor is 100%). For lower concentrations the ionization factor will increase by about 1-2%. This was seen by measuring the ionization factor of SF_6 concentrations prepared by further dilution of the original test dilution of $0.5 \cdot 10^{-9}$ ppp. Thus, the electron capture detector is linear to within 1-2% in the concentration range from about $0.5 \cdot 10^{-9}$ ppp and below.

Knowing the ionization factor and the concentration of the test dilution, the signal from the electron capture detector assuming single ionization of the SF_6 molecules can be calculated. Good agreement was found between measured and calculated signals so it was concluded that the measured ionization factor represents single ionization of the SF_6-molecules. Accordingly, it is possible to determine the SF_6 concentration of an air-sample by

using the measured ionization factor and the integrated gas-chromatographic signal.

The accuracy of this calibration approach is estimated to about 20%, and with better facilities for preparing the test dilution it can probably be improved to about 10%. The short term precision, that is the reproducibility within the time necessary for the analysis of all air samples from a dispersion experiment, is about 2%. The calibration results showed that SF_6 concentrations could be detected down to about $2 \cdot 10^{-12}$ ppp with a signal-to-noise ratio of 4.

6. DESCRIPTION OF THE TRACER EXPERIMENTS IN COPENHAGEN

Ten out of a total number of 13 tracer experiments, carried out in the Copenhagen area in the period September 12, 1978 to July 19, 1979, were found suitable for analysis. Because of wind direction shifts the others were discarded. All the dispersion experiments were carried out in neutral and unstable conditions.

6.1. Meteorological conditions

In Table 6.1 important parameters for the 10 experiments are shown. Three experiments are performed under near neutral conditions (Pasquill stability class D), 5 experiments under slightly unstable conditions (Pasquill C), and 2 under slightly unstable to unstable conditions (Pasquill B-C). The stability classification is based on both the mean wind speed at 10 m and the insolation. For the vertical dispersion over a city Pasquill (1976) suggests that the heat island should be taken into account by changing the estimated stability class one half class towards more unstable conditions (Table 6.1).

We note from Table 6.1 that whereas those experiments assigned Pasquill class D are associated with large negative values of the Monin-Obukhov length, L, as expected (-382 to -569 m), and those assigned Pasquill class B-C are associated with small, negative values of L (-136 and -72 m), the range of values of L in Pasquill stability class C (-46 to -577 m) covers completely the values of L in Pasquill stability class B-C as well as those of class D. Thus,the separation of the experiment in stability classes D,C and B-C is not coincident with a classification according to the Monin-Obukhov length. In the various experiments, the mean wind velocity (one hour average) at the height of release varied from 3.4 to 13.2 m/s, and the stability, expressed through the Monin-Obukhov length, varied from -46 to -577 m.

Table 6.1. Meteorological conditions during the experiments. All parameters are one hour averages except for the experiment of April 30 in which 40 min averages have been used. The symbol "-" indicates that the parameter was impossible to determine.

Experiment 1978/1979	Mean wind speed 115 m (m/s)	Mean wind speed 10 m (m/s)	Friction velocity $\sqrt{-\overline{uw}}$ at 115 m (m/s)	Friction velocity from mean wind profile (m/s)	Standard deviation 115 m height Wind velocity lateral σ_v(m/s)	Wind velocity vertical σ_w(m/s)	Wind fluctuations lateral σ_θ(°)	Wind fluctuations vert. σ_ϕ(°)	$\Delta\overline{T}/\Delta z$ (2-40m) (°C/100m)	Monin-Obukhov length (m)	Pasquill stability class. Heat island effect not incl.	Pasquill stability class. Heat island effect incl.	Inversion height z_i(m)
Sep. 14	8.9	-	0.50	-	1.14	0.68	7.5	4.5	-0.97	-	D	C-D	-
Sep. 20	3.4	2.1	0.38	0.37	0.98	0.83	16.0	14.7	-3.33	-46	C	B-C	1980
Sep. 26	10.6	4.9	0.76	0.74	1.39	1.07	7.7	6.2	-3.07	-384	C	B-C	1920
Oct. 19	5.0	2.4	0.36	0.39	0.85	0.68	9.6	8.4	-2.52	-108	C	B-C	1120
Nov. 3	4.6	2.5	0.20	0.39	0.47	0.47	6.0	6.3	-2.06	-173	C	B-C	390
Nov. 9	6.7	3.1	0.49	0.46	0.77	0.71	6.9	6.4	-1.54	-577	C	B-C	820
Apr. 30	13.2	7.2	1.15	1.07	2.26	1.33	9.8	6.6	-3.99	-569	D	C-D	1300
Jun. 27	7.6	4.1	0.48	0.65	1.61	0.87	11.8	7.0	-4.65	-136	B-C	B	1850
Jul. 6	9.4	4.2	0.42	0.70	1.35	0.72	8.8	4.7	-7.63	-72	B-C	B	810
Jul. 19	10.5	5.1	1.00	0.77	1.71	0.98	9.7	5.8	-3.25	-382	D	C-D	2090

Table 6.1 also shows the height of the lowest inversion estimated from the routine radiosonde launches, which are performed only 5 km from the TV-tower. The synoptic times are quite close to that of the experiments. Except for the November 3 experiment where z_i = 390 m, the height of the lowest inversion is seen to be more than 6 times the height of tracer release. The variance of the wind fluctuations are shown in Table 6.1 also.

The Monin-Obukhov stability length was determined following a method that was devised by Golder (1972). First, a bulk Richardson number, B, is calculated by means of the formula

$$B = \frac{g \cdot \partial \bar{\theta}/\partial z}{\bar{T}\ \bar{u}^2}\ z^2 \qquad (6.1)$$

Here, an appropriate value of the potential temperature gradient, $\partial \bar{\theta}/\partial z$, is found from the mean temperature at 2 and 40 meters height

$$\frac{\partial \bar{\theta}}{\partial z} = \frac{\bar{T}(40\ m) - \bar{T}(2\ m)}{38} + \Gamma$$

with Γ, the dry adiabatic lapse rate, set equal to $\Gamma = -0.98 \cdot 10^{-2}$ (^{o}C/m). The average wind velocity that enters (6.1) should preferably be measured at the height

$$z_m = \sqrt{z_1 \cdot z_2}$$

where z_1 and z_2 are the measuring heights for the temperatures. The bulk Richardson number is related to the Richardson number through

$$Ri = \frac{B\ \bar{u}^2}{[\partial \bar{u}/\partial(\ln z)]^2} \qquad (6.2)$$

Inserting the wind shear

$$\frac{\partial \bar{u}}{\partial z} = \phi_m(Ri)\frac{u_*}{kz}$$

as well as the integrated wind profile

$$\bar{u} = \frac{u_*}{k} \left[\ln\left(\frac{z}{z_o}\right) - \psi(Ri) \right] \tag{6.3}$$

in (6.2), we get the relationship between B and Ri

$$Ri = B \left\{ \frac{\ln\frac{z}{z_o} - \psi(Ri)}{\phi_m(Ri)} \right\}^2 \tag{6.4}$$

Under unstable conditions, the ψ and ϕ_m-functions are quite well established. Paulson (1970) recommends use of

$$\phi_m(Ri) = (1 - 16\ Ri)^{-0.25}$$

and

$$\psi(Ri) = 2 \ln\left[(1 + x)/2\right] + \ln\left[(1 + x^2)/2\right] - 2 \tan^{-1}(x) + \pi/2$$

where

$$x = \phi_m(Ri)^{-1}$$

Knowing Ri, the Monin-Obukhov length can be found from $L^{-1} = Ri/z$. Golder (1972) constructed a nomogram for B as functions of Ri and $\ln(z/z_o)$, (Fig. 6.1).

In the present experiments, the temperature measurements at 2 and 40 m were used for the calculation of Ri; we have z_m = 8.9 m, so it seemed reasonable to use the wind speed, measured at a 10-m height in (6.1). Having determined Ri, L was estimated using L = 10/Ri (m). The use of (6.4) requires knowledge of the surface roughness length z_o. We shall see in the next subsection how this quantity is determined. The value z_o = 0.6 m is used.

The friction velocity, u_*, was estimated from (6.3), von Kármán's constant, k, was set equal to k = 0.4, and, for the mean wind speed, the measured value at 10 m was used. The friction velocity was also calculated from the measurements of the turbulent wind fluctuations at a 115-m height, as $u_* = \sqrt{-\overline{u'w'}}$. The friction

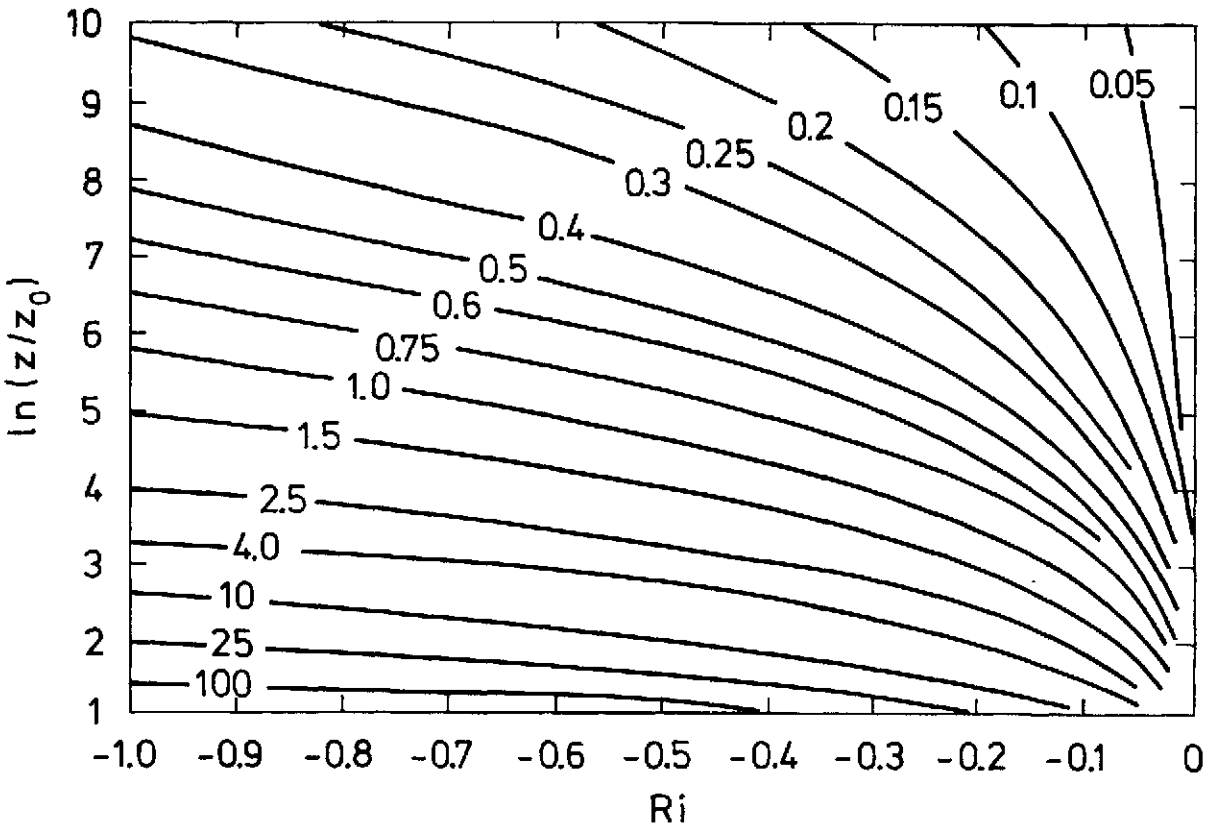

Fig. 6.1. The bulk Richardson number, B, in unstable conditions as functions of the Richardson number, Ri, and $\ln(z/z_0)$ (Golder, 1972). Having estimated Ri, the Monin-Obukhov length can be found as L = z/Ri. Isopleths of B have been multiplied by -100.

velocity, derived by this method, compares rather favorably with the estimates of u_* based on the wind speed at 10 m (Table 6.1). This is noteworthy, as the instruments at 115 m were never intended for measurements of covariances. Values of the cloud cover that were used in the determination of the Pasquill stability class for the individual experiments, were obtained from observations, performed at 1 p.m. at the airports at Værløse and Kastrup, both of which are situated in the Copenhagen area.

6.2. Roughness length for the site

The roughness length, z_o, was determined to be 0.6 m on the basis of two independent methods, which turned out to give approximately equal estimates of z_o.

Use of the expression for the neutral wind profile

$$\bar{u}(z) = \frac{u_*}{k} \ln\frac{z}{z_o}$$

where $\bar{u}(z)$ is the mean wind speed at height z, gives

$$\frac{\bar{u}(120\ m)}{\bar{u}(10\ m)} = \frac{\ln(120/z_o)}{\ln(10/z_o)} \qquad (6.5)$$

Values of the ratio $\bar{u}(120\ m)/\bar{u}(10\ m)$ estimated from data measured during the experiments are given in Table 6.2 and are also shown in Fig. 6.2 plotted as a function of $-L^{-1}$. The cross-over point between the y-axis and the curve that subjectively best approximates the points indicates the ratio of $\bar{u}(120\ m)/\bar{u}(10\ m)$ under neutral conditions. We find for $L^{-1} = 0$ that $\bar{u}(120\ m)/\bar{u}(10\ m) = 1.86$ and from (6.5) z_o can be estimated as 0.6 m.

Alternatively, the roughness length can be estimated on the basis of the measurements at 115 m of the vertical wind variance, σ_w^2, that were performed during the experiments. Under neutral conditions σ_w scales with u_* (Panofsky, 1973) as

$$\sigma_w = A \cdot u_* \qquad (6.6)$$

where the variation of A is reported to fall within the range 1.2–1.35, with a value of 1.3 usually recommended. Elimination of u_* in (6.6) by use of the neutral wind profile gives

$$\frac{\sigma_w}{\bar{u}(z)} = \frac{A\ k}{\ln(\frac{z}{z_o})} \qquad (6.7)$$

Table 6.2. Meteorological parameters used in the determination of the roughness length. The symbol "-" indicates that the parameter was impossible to determine.

Experiment 1978/1979	$\frac{\bar{u}(120\ m)}{\bar{u}(10\ m)}$	Corrected σ_w 67 min. (m/s)	*) u_* (m/s)	$\frac{\sigma_w}{u_*}$	$\bar{u}$(115 m) 67 min (m/s)	$\frac{\sigma_w}{\bar{u}(115\ m)}$	$-L^{-1}$ ($10^{-2}m^{-1}$)
Sep. 14	-	0.71	-	-	8.9	0.080	-
Sep. 20	1.81	0.84	0.37	2.27	3.4	0.247	2.17
Sep. 26	1.92	1.09	0.74	1.47	10.5	0.104	0.26
Oct. 19	2.04	0.70	0.39	1.79	5.0	0.140	0.93
Nov. 3	1.52	0.50	0.39	1.28	4.6	0.109	0.58
Nov. 9	1.87	0.75	0.46	1.63	6.7	0.112	0.17
Apr. 30	1.79	1.39	1.07	1.30	13.3	0.105	0.18
Jun. 27	1.78	0.92	0.65	1.42	7.5	0.123	0.74
Jul. 6	2.26	0.79	0.70	1.13	9.4	0.084	1.39
Jul. 19	1.92	0.99	0.77	1.29	10.4	0.095	0.26

*) from mean wind profile.

The characteristic value of the constant A for the Copenhagen site was found by plotting σ_w/u_* as a function of $-L^{-1}$ (Fig. 6.3). The values of σ_w that were used in this context were corrected for the unsteadiness of the response time of the vertical propeller, by applying the transfer function given in Chapter 5 in the discussion of the w-spectrum. As the w-spectrum is based on a 67-min record, all averaging times in this analysis will be 67 min. Corrected values of σ_w, the friction velocities and the the 67 min averaged values of $\bar{u}$(115 m) are given in Table 6.2. The points in Fig. 6.3 reveal a large scatter. A value of A = 1.3 was subjectively adopted for the value of A under neutral conditions ($L^{-1} = 0$). Then $\sigma_w/\bar{u}$(115 m) was plotted as a function of $-L^{-1}$ (Fig. 6.4). Following the same procedure as in Fig. 6.3, the neutral value of $\sigma_w/\bar{u}$(115 m) was found to be 0.10. By means

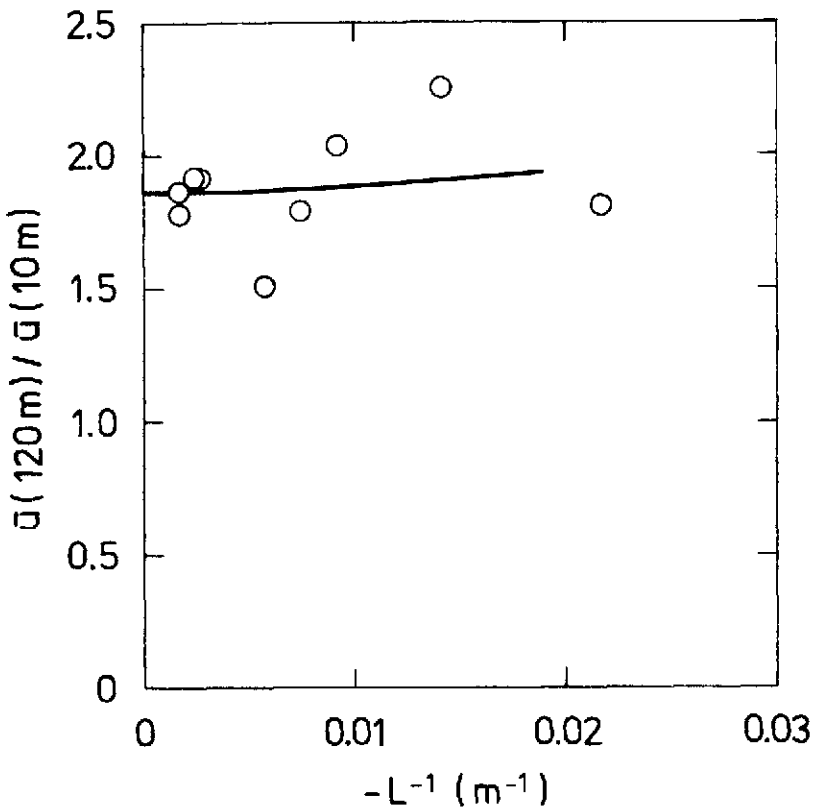

Fig. 6.2. The ratio $\bar{u}(120\ m)/\bar{u}(10\ m)$ plotted as a function of $-L^{-1}$. The value of $\bar{u}(120\ m)/\bar{u}(10\ m)$ for neutral conditions ($-L^{-1} = 0$) is subjectively determined as 1.86.

of (6.7), with A = 1.3, the roughness length is estimated as z_o = 0.6 m.

This roughness length is actually characteristic for that part of the upwind area that influences the dispersion of the tracer just after release. The downwind area, over which the dispersion process actually takes place, is rather similar to the upwind area, and no significant changes in the roughness length are likely to be present.

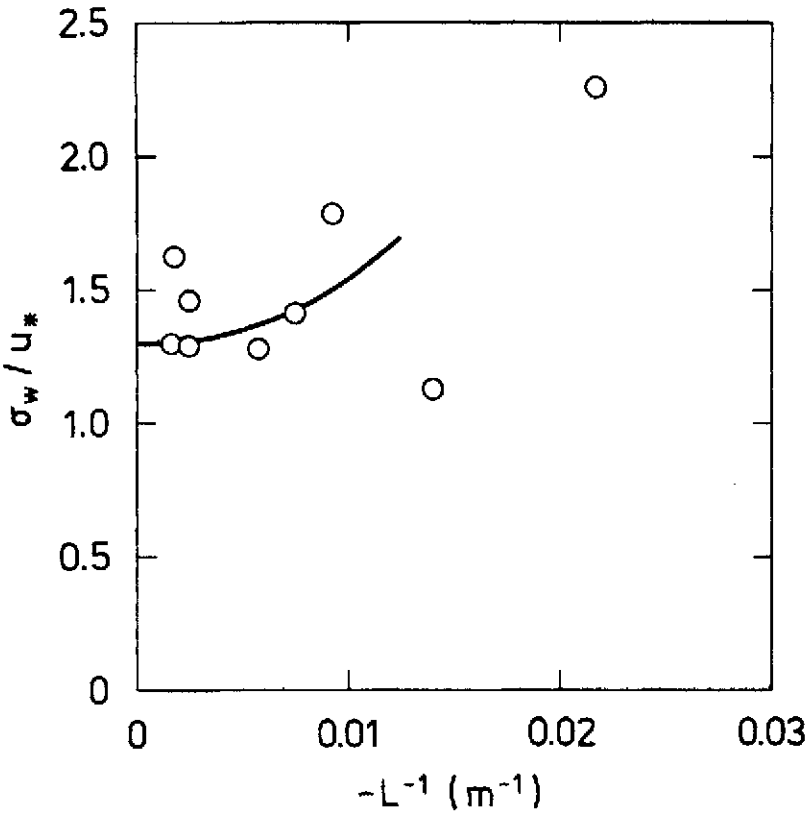

Fig. 6.3. The ratio σ_w/u_* plotted as a function of $-L^{-1}$. The value of σ_w/u_* for neutral conditions is subjectively determined as 1.3.

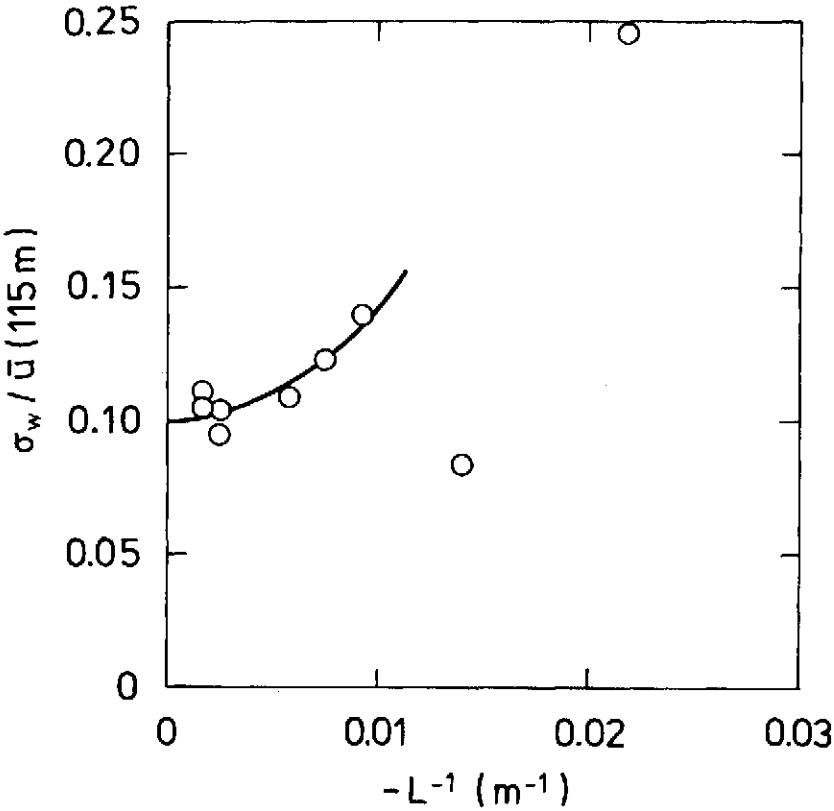

Fig. 6.4. The ratio $\sigma_w/\bar{u}$(115 m) plotted as function of $-L^{-1}$. The value of $\sigma_w/\bar{u}$(115 m) for neutral conditions is subjectively determined as 0.10.

6.3. Description of the experiments

A short description of each experiment with special regard to the meteorological conditions is given below.

6.3.1. Experiment of September 14, 1978

This experiment was performed during a period that was strongly influenced by passing lows with associated fronts. A cold front passage was forecast to take place around noon, and the sampling units were positioned in consideration of the wind direction shift, following the front passage. The front passed between 1445 and 1455 at Gladsaxe (indicated by a wind direction shift from 240° to 290°). The experiment was carried out during the period 1523-1623. The first part of the experiment took place under rainfall, and the sky was completely covered by clouds throughout

the experiment. The Pasquill stability class was determined as D. Tracer sampling units were positioned only in the 4-km series from the TV tower. The measured 1-hour averaged tracer concentration distribution is shown in Fig. 6.5.

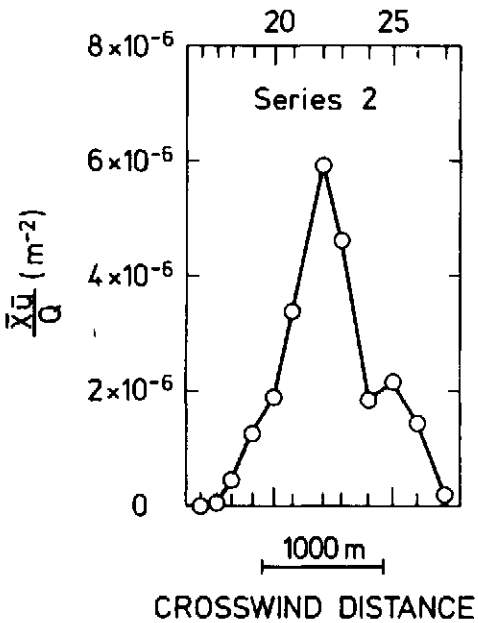

Fig. 6.5. Measured normalized tracer concentrations, o, averaged over 60 min for the experiment of September 14, 1978. The positions of the sampling units are indicated on the abscissa; two positions in each crosswind series are numbered according to the numeration in Fig. 5.1.

6.3.2. Experiment of September 20, 1978

Between a high over the English Channel and a low over Finland, rather dry air was advected over Denmark from the northwest. The sky was partly sunny before noon with increasing cloud cover in the afternoon. The experiment was carried out in the period 1317-1417. Observations made at 1300 at Kastrup and Værløse reported 7/8 cloud cover composed of mainly cirrus and cirrostratus clouds. On the Campbell-Stokes sunshine recorder at the TV mast, no sunshine was registered during the experiment. The Pasquill stability class was determined as C.

Tracer sampling units were positioned in the series that were 2 and 4 km from the TV tower. The 1-hour averaged tracer distributions are shown in Fig. 6.6.

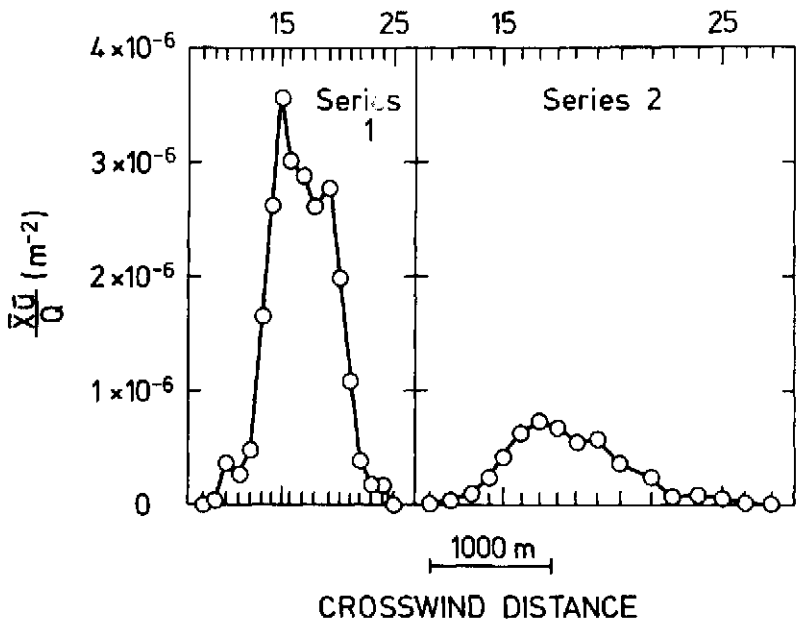

Fig. 6.6. Measured normalized tracer concentrations, o, averaged over 60 min for the experiment of September 20, 1978. The positions of the sampling units are indicated on the abscissa; two positions in each crosswind series are numbered according to the numeration in Fig. 5.1.

6.3.3. Experiment of September 26, 1978

This experiment was carried out in a westerly flow of humid, unstable air. The experimental period was 1140 to 1240. The routine meteorological observations at 1300 at Kastrup reported a cloud cover of 5/8 and at Værløse of 7/8 in which cumulus clouds were dominant. The Pasquill stability class was determined as C.

Tracer sampling units were positioned in the series that were 2 and 4 km from the TV tower. The tracer concentration distributions are shown in Fig. 6.7.

6.3.4. Experiment of October 19, 1978

During the night of the 18-19th of October, a warm, followed by a cold front passed over Copenhagen. Thus, the experiment that was performed during the period 1213-1313, was carried out in cool air of maritime origin. At Værløse the cloud cover was reported

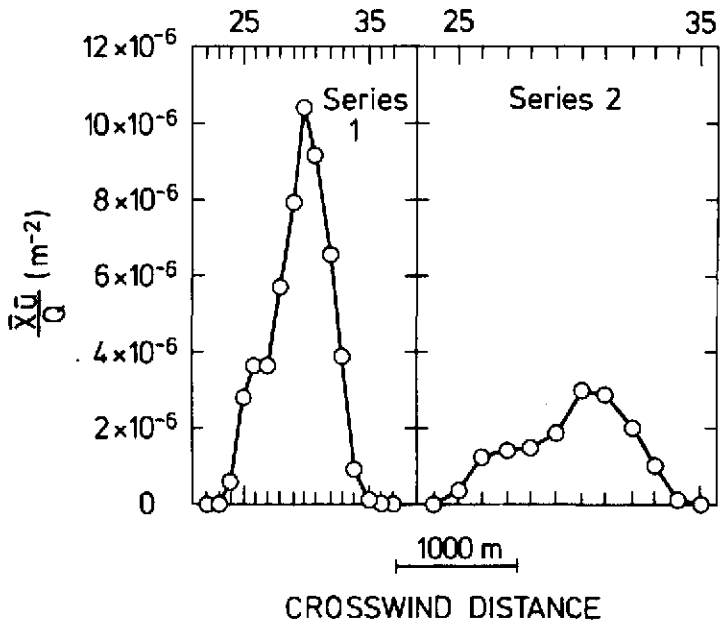

Fig. 6.7. Measured normalized tracer concentrations, o, averaged over 60 min for the experiment of September 26, 1978. The positions of the sampling units are indicated on the abscissa; two positions in each crosswind series are numbered according to the numeration in Fig. 5.1.

to 5/8 and at Kastrup 6/8, both mainly composed of cumulus and altocumulus clouds. The Campbell-Stokes sunshine recorder at the TV tower registered sunshine during approximately 5% of the experimental period. The Pasquill stability class was determined as C. Tracer sampling units were positioned in all three series; Fig. 6.8 shows the one hour averaged tracer concentration distributions.

6.3.5. Experiment of November 3, 1978

Between a high pressure area over the Central Europe and a low over Iceland, air of maritime origin flowed over Denmark. On the experimental day, a warm front passed over Copenhagen during the morning, and the experiment was carried out during the period 1320-1420, only a few hours after the front passage. The cloud cover at Værløse was 3/8 and at Kastrup 5/8, consisting mainly of cirrus. The experiment was assigned Pasquill stability class C.

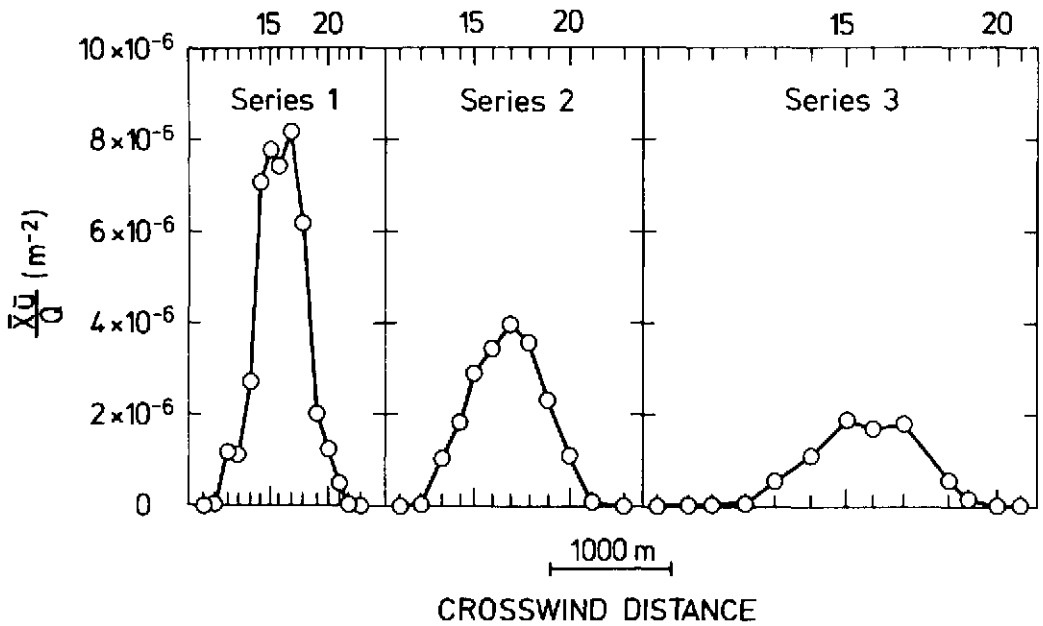

Fig. 6.8. Measured normalized tracer concentrations, o, averaged over 60 min for the experiment of October 19, 1978. The positions of the sampling units are indicated on the abscissa; two positions in each crosswind series are numbered according to the numeration in Fig. 5.1.

Tracer sampling units were positioned in the series that was 4 km from the TV tower; the concentration distribution is shown in Fig. 6.9.

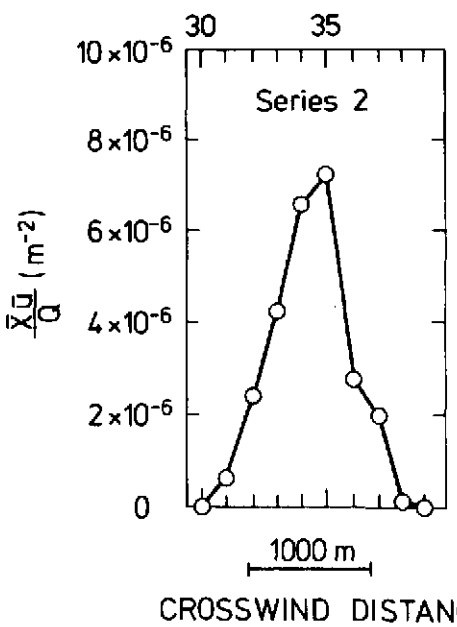

Fig. 6.9. Measured normalized tracer concentrations, o, averaged over 60 min for the experiment of November 3, 1978. The positions of the sampling units are indicated on the abscissa; two positions in each crosswind series are numbered according to the numeration in Fig. 5.1.

6.3.6. Experiment of November 9, 1978

The meteorological situation resembled that of the foregoing experiment, characterized by a high pressure area over the Central Europe and a low over Iceland. The experiment was performed in a mild, humid air current from west- southwest. No rain was observed in the experimental period, 1330-1430, and no sunshine was registered at the sunshine recorder. Cloud cover was 7/8 at Værløse and 6/8 at Kastrup, mainly consisting of stratocumulus. The Pasquill stability was estimated as class C. Tracer sampling was carried out in all three series, the one-hour averaged tracer concentration distributions are illustrated in Fig. 6.10.

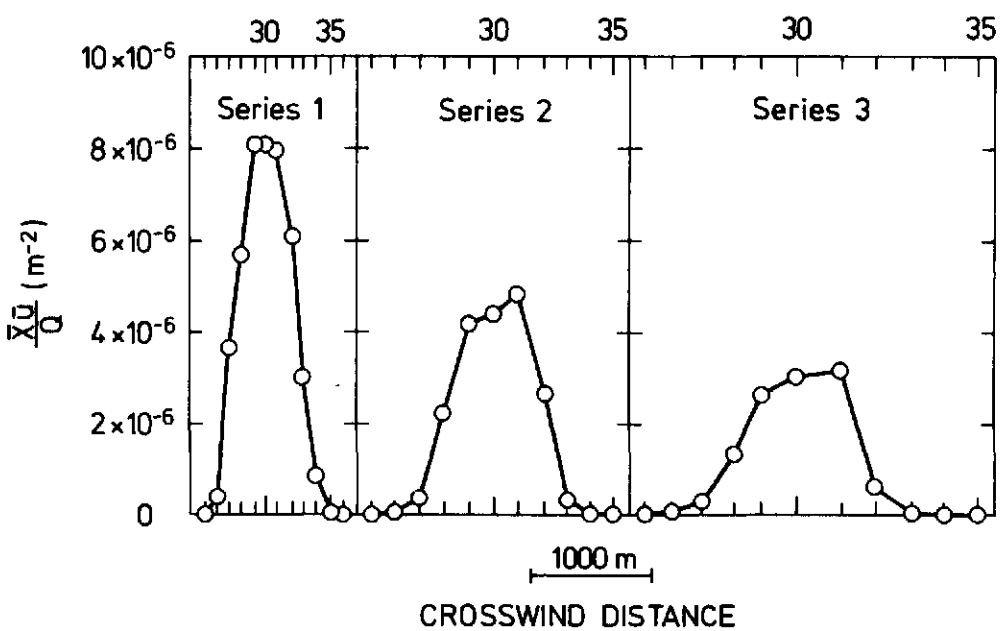

Fig. 6.10. Measured normalized tracer concentrations, o, averaged over 60 min for the experiment of November 9, 1978. The positions of the sampling units are indicated on the abscissa; two positions in each crosswind series are numbered according to the numeration in Fig. 5.1.

6.3.7. Experiment of April 30, 1979

The wind pattern over Denmark was governed by a low pressure area situated over the central part of Scandinavia. A front system passed over Copenhagen during the night of 29-30 April. Thereafter, the wind turned west and the front-associated rain ceased. Then the experiment was carried out during the period 1302-1402. Cloud cover at both Værløse and Kastrup was reported at 5/8, mainly consisting of cumulus and stratus, and with a few cumulonimbus clouds. The sunshine recorder registered sunshine during approximately 50% of the experimental period. The Pasquill stability class was determined to D.

Tracer sampling units were positioned in all three series. The tracer concentration distributions are shown in fig. 6.11.

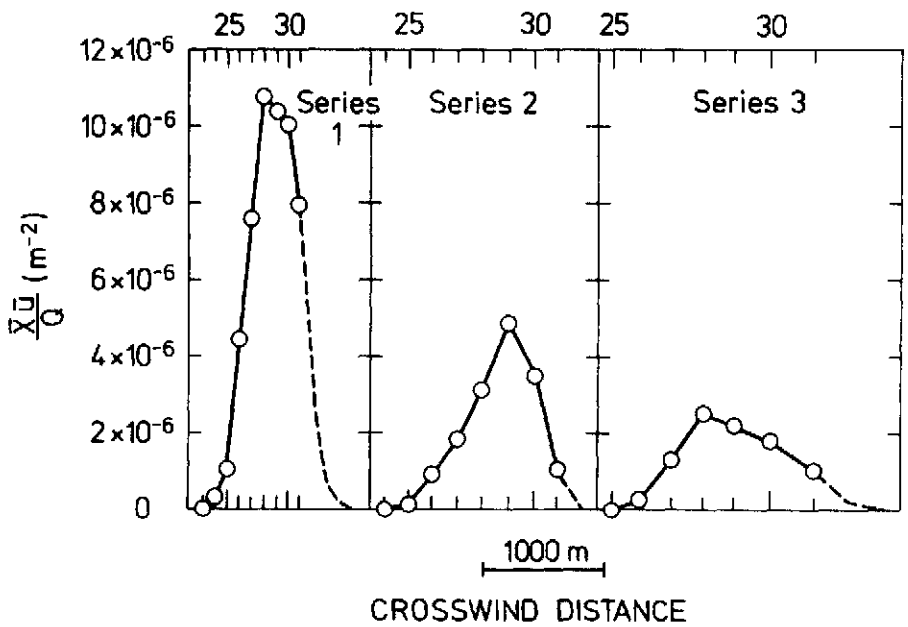

Fig. 6.11. Measured normalized tracer concentrations, o, averaged over 40 min for the experiment of April 30, 1979. The positions of the sampling units are indicated on the abscissa; two positions in each crosswind series are numbered according to the numeration in Fig. 5.1. Extrapolated parts of the concentration distributions are shown by the dashed lines.

6.3.8. Experiment of June 27, 1979

The weather in Denmark was influenced mainly by a low pressure area over the northern part of Scandinavia, causing a westerly flow of unstable air over Copenhagen. The cloud cover at both Værløse and Kastrup was reported to 6/8, largely consisting of cumulus and altocumulus clouds. Sunshine was registered on the sunshine recorder during approximately 50% of the experimental period, 1245-1345. The experiment was assigned Pasquill stability class B-C. Tracer sampling was carried out in all three series. Figure 6.12 shows the one-hour averaged tracer concentration distributions.

6.3.9. Experiment of July 6, 1979

A low pressure area situated over the Eastern part of the Baltic States and a high over the western part of Europe gave rise to a westerly flow of maritime air over Denmark. The cloud cover at 1300 at Værløse was reported at 5/8 and at Kastrup 6/8, consisting of cumulus, altocumulus, and cirrus clouds. Sunshine was reported during 30% of the experimental period, 1250-1350. The Pasquill stability class was determined as B-C. The tracer concentration distribution from the three series are shown in Fig. 6.13.

6.3.10. Experiment of July 19, 1980

Between a widespread low pressure area over Iceland and Scandinavia, and a high over the southern part of Europe, unstable, cool air flowed from the northwest over Denmark. Most of the sky was cloud covered during the experimental period, 1215-1318. Værløse reported a cloud cover of 6/8 and Kastrup 7/8. The clouds were mainly of cumulus and altocumulus type, but a few nimbocumulus clouds were also reported. The sunshine recorder registered some sunshine. The experiment was assigned Pasquill stability class D. Tracer sampling units were positioned in all three series. Figure 6.14 shows the one-hour averaged tracer concentrations.

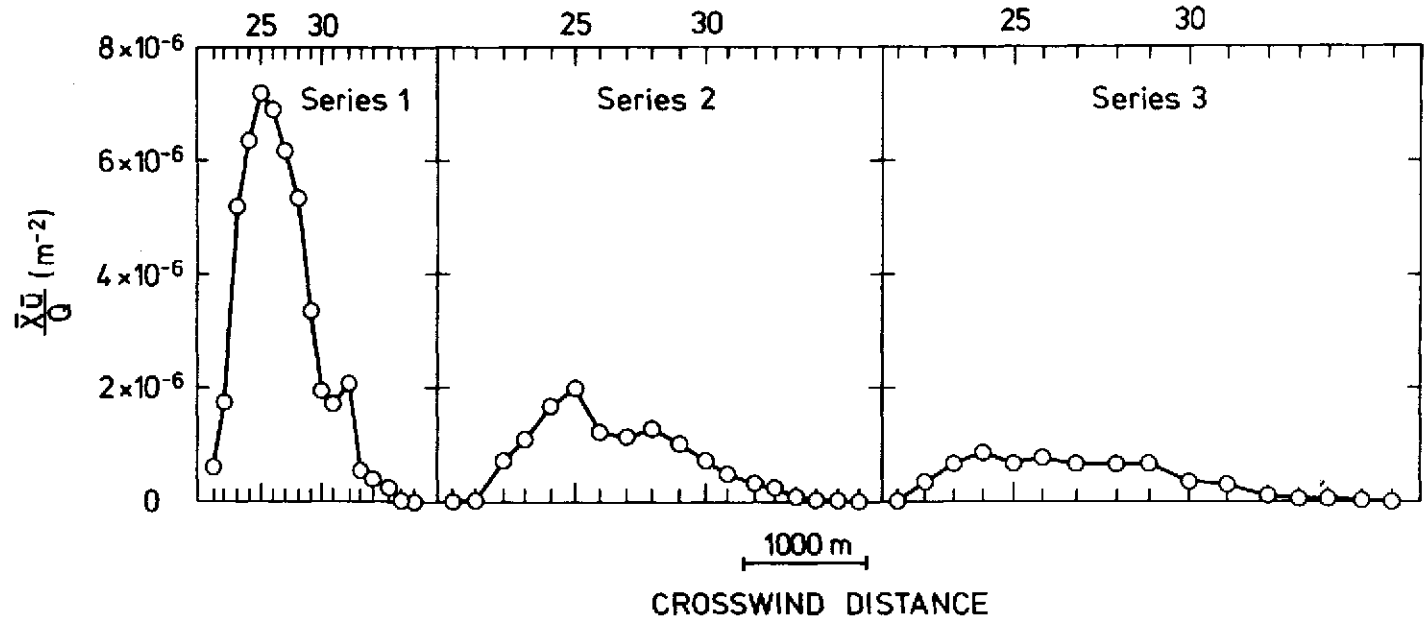

Fig. 6.12. Measured normalized tracer concentrations, o, averaged over 60 min for the experiment of June 27, 1979. The positions of the sampling units are indicated on the abscissa; two positions in each crosswind series are numbered according to the numeration in Fig. 5.1.

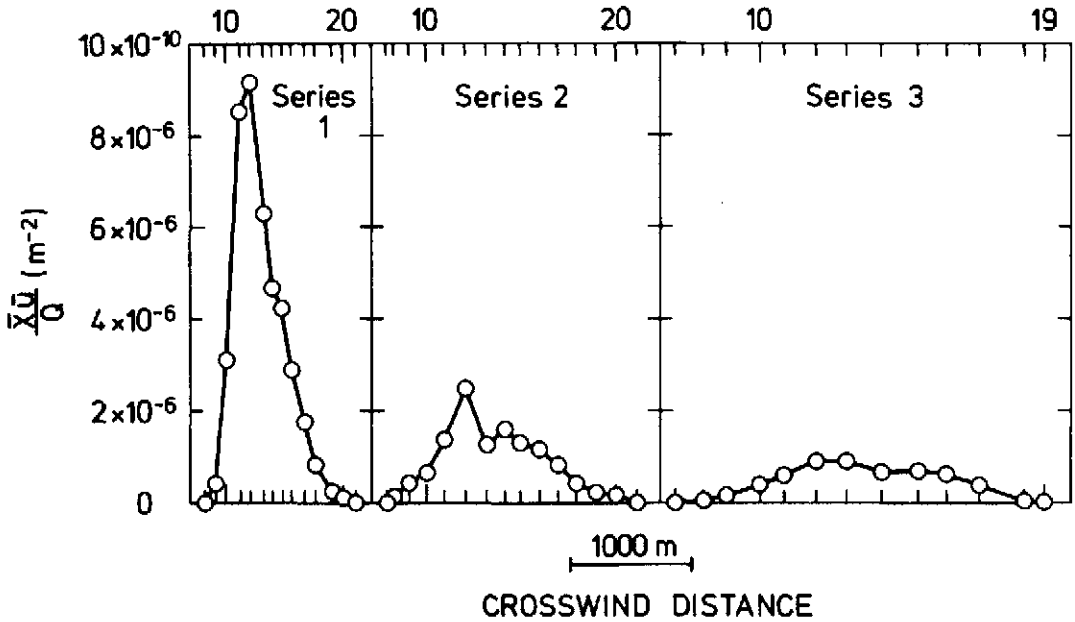

Fig. 6.13. Measured normalized tracer concentrations, o, averaged over 60 min for the experiment of July 6, 1979. The positions of the sampling units are indicated on the abscissa; two positions in each crosswind series are numbered according to the numeration in Fig. 5.1.

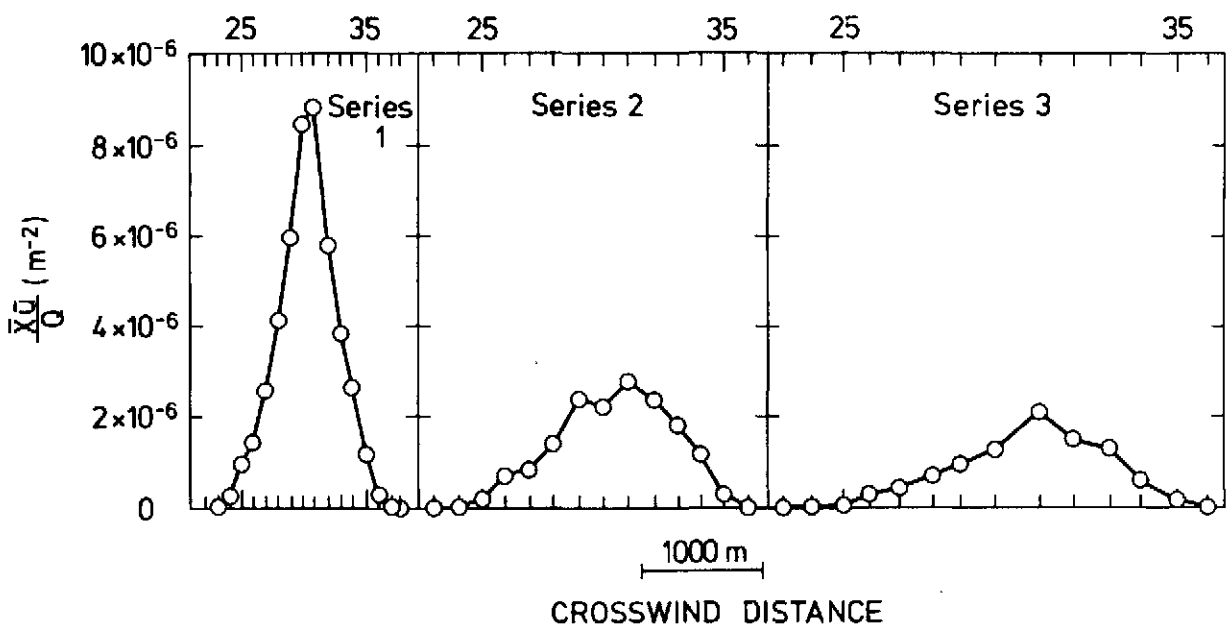

Fig. 6.14. Measured normalized tracer concentrations, o, averaged over 60 min for the experiment of July 19, 1979. The positions of the sampling units are indicated on the abscissa; two positions in each crosswind series are numbered according to the numeration in Fig. 5.1.

7. DATA-ANALYSIS

In all experiments but one, the 60-min averaged tracer plume was well covered by the sampling-units and Gaussian in appearance. Except for the one experiment, the data-analysis will be based on the 60-min averaged tracer concentration distribution, deduced from the three 20-min sampled tracer concentrations.

In the experiment on April 30, only runs 1 and 2 (averaging time 40-min) were well covered due to wind direction shift in run 3. This experiment was excluded from the analysis of the lateral dispersion parameter because of the instationarity. However, the 40-min averaged tracer distribution was used in the analysis of the crosswind-integrated tracer concentration distribution, as these are less sensitive to instationarities.

7.1. Analysis of measured tracer concentrations

As the tracer sampling units during the experiments were placed near ground level at preselected positions along roads, the measured tracer concentrations primarily allowed for an estimate of the lateral standard deviation of the tracer concentration distribution, $(\sigma_y)_{mea}$. It was derived as the square root of the second moment of the tracer concentration distribution, projected on the crosswind line through the position of the center of the tracer concentration distribution. It was calculated by means of the standard formula

$$(\sigma_y)^2_{mea} = \frac{\Sigma(\bar{\chi}_i \cdot y_i^2)}{\Sigma\bar{\chi}_i} - \left(\frac{\Sigma(\bar{\chi}_i \cdot y_i)}{\Sigma\bar{\chi}_i}\right)^2 \qquad (7.1)$$

where $\bar{\chi}_i$ is the measured tracer concentration and y_i the corresponding crosswind distance. The crosswind-integrated concentration distribution, $(\bar{\chi}_{CWI})_{mea}$, was approximated by

$$(\bar{\chi}_{CWI})_{mea} = \frac{1}{2} \Sigma(\bar{\chi}_{i-1} + \bar{\chi}_i)\Delta y_i \qquad (7.2)$$

where Δy_i is the crosswind distance between positions i-1 and i.

As the vertical distribution of the tracer was not measured in these experiments, the standard deviation of the vertical tracer concentration distribution, $(\sigma_z)_{est}$, could be infered only indirectly from continuity considerations, assuming a certain shape of the vertical tracer concentration distribution. One of the most widely used mathematical models of dispersion from a continuous point source contains the assumption that the crosswind and vertical distribution are of a Gaussian shape. Assuming this, the crosswind-integrated tracer concentration at ground level can be expressed in terms of the height of release, h, the transport velocity of the plume, $\bar{u}$ (here taken as the mean wind speed at the height h), the source strength of the tracer, Q, the inversion height, z_i, and the vertical standard deviation, σ_z, as

$$\frac{\bar{u}\bar{\chi}_{CWI}}{Q} = \sqrt{\frac{2}{\pi}} \frac{1}{\sigma_z} \left\{ \exp\left[-\frac{1}{2} \left(\frac{h}{\sigma_z}\right)^2 \right] + \right. \qquad (7.3)$$

$$\left. \exp\left[-\frac{1}{2} \left(\frac{h}{\sigma_z}\right)^2 \left(1 - \frac{2z_i}{h}\right)^2 \right] + \exp\left[-\frac{1}{2} \left(\frac{h}{\sigma_z}\right)^2 \left(1 + \frac{2z_i}{h}\right)^2 \right] \right\}$$

This expression implies specular reflections of the tracer at both the ground and the inversion. Knowing $\bar{\chi}_{CWI}$, $\bar{u}$, h, and z_i an estimate of σ_z can be calculated. In these experiments, z_i is so large that its influence on the estimated value of σ_z is negligible. Precluding the z_i-effect by setting z_i as infinite reduces the expression to the common and widely used form

$$\frac{\bar{u}\bar{\chi}_{CWI}}{Q} = \sqrt{\frac{2}{\pi}} \frac{1}{\sigma_z} \exp\left[-\frac{1}{2} \left(\frac{h}{\sigma_z}\right)^2 \right] \qquad (7.4)$$

which constitutes a relation between σ_z and the normalized crosswind-integrated concentration, $\bar{u}\bar{\chi}_{CWI}/Q$, for a given value

of h. This relationship is illustrated in Fig. 7.1. It is noteworthy that there is a maximum value of $\bar{u}\bar{\chi}_{CWI}/Q$ for $\sigma_z = h$. Observed values of $\bar{u}\bar{\chi}_{CWI}/Q$ larger than this limit indicate that (7.4) cannot describe the vertical tracer concencentration distribution.

Values of $(\sigma_y)_{mea}$, $(\sigma_z)_{est}$, $(\bar{\chi}_{CWI})_{mea}$ for the 10 experiments are given in Table 7.1, together with other characteristic parameters. No value of $(\sigma_y)_{mea}$ for the experiment of April 30 has been included in Table 7.1, as in this experiment only runs 1 and

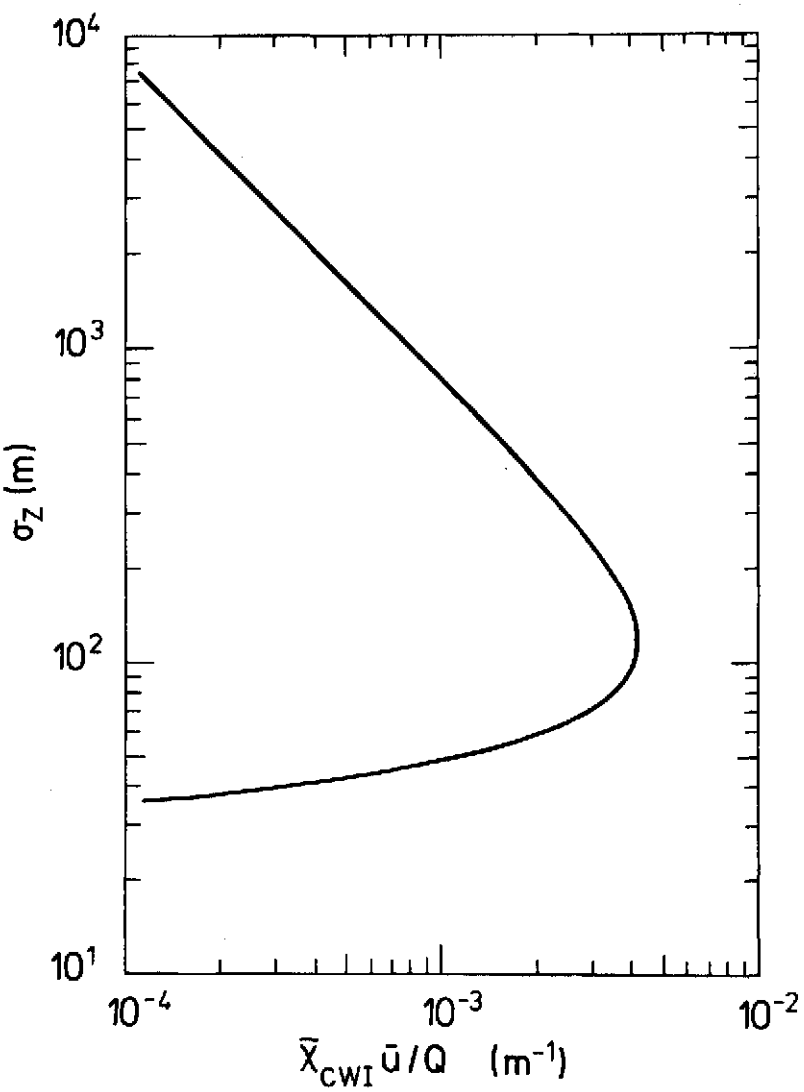

Fig. 7.1. Relation between σ_z and $\bar{u}\cdot\bar{\chi}_{CWI}/Q$ according to (7.4), for the release height h = 115 m. Note that $\bar{u}\cdot\bar{\chi}_{CWI}/Q$ has a maximum at $\sigma_z = h$.

Table 7.1. Results from the analysis of the measured tracer concentrations. The symbol *) indicates that it is impossible to determine $(\sigma_z)_{est}$.

Experiment 1978-1979	Time of experiment	Assigned distance (km)	Tracer release rate Q(g/s)	$(\sigma_y)_{mea}$ (m)	$(\sigma_z)_{est}$ (m)	$\frac{\bar{u}(\bar{\chi}_{CWI})_{mea}}{Q}$ $(10^{-9} \cdot m^{-1})$
Sep. 14	1523 1623	3.9	4.7	375	*)	4.4
Sep. 20	1317- 1417	1.9 3.7	3.2	254 444	342 1012	2.2 0.8
Sep. 26	1140- 1240	2.1 4.2	3.2	239 438	*) 223	5.7 3.1
Oct. 19	1213- 1313	1.9 3.7 5.4	3.2	184 283 404	136 225 351	4.1 3.1 2.2
Nov. 3	1320- 1420	4.0	2.3	301	*)	5.4
Nov. 9	1330- 1430	2.1 4.2 6.1	3.2	185 279 376	*) 155 205	4.5 3.9 3.3
Apr. 30	1302- 1342	2.0 4.2 5.9	3.1		*) 215 275	5.7 3.2 2.7
Jun. 27	1245- 1345	2.0 4.1 5.3	2.4	290 595 786	*) 300 456	5.1 2.5 1.7
Jul. 6	1250- 1350	1.9 3.6 5.3	3.0	190 402 580	155 405 568	3.9 1.9 1.4
Jul. 19	1215- 1318	2.1 4.2 6.0	3.3	236 460 623	*) 211 267	4.8 3.3 2.7

2 were well covered by the sampling unit network. It has been decided to include the 40-min averaged tracer concentration distribution in the analysis of the crosswind-integrated tracer concentrations only.

7.2. Comparison between measured and computed dispersion characteristics

The estimated values of $(\sigma_y)_{mea}$ and $(\bar{\chi}_{CWI})_{mea}$ will be compared to those derived from the computational methods that were introduced in Chapter 3. Methods for determining σ_y and σ_z, based on an indirect description of the atmospheric stability, have been reported by Turner (1970). We shall call these $(\sigma_y)_{PGT}$ and $(\sigma_z)_{PGT}$ (Pasquill, Gifford, Turner). In the ASME-guide by Smith (1973) other estimates, $(\sigma_y)_{Sm}$ and $(\sigma_z)_{Sm}$ have been given. In the PGT-method, the dispersion parameters are given as function of downwind distance as curves, separated according to the Pasquill stability classification scheme. The Sm-method constitutes a similar set of curves separated according to atmospheric stability (very unstable, unstable, neutral, and stable (see Fig. 2.13)). We chose to put the unstable class equal to Pasquill stability class B and C, and the neutral class equal to Pasquill class D.

From the measurements of the turbulent wind fluctuations the standard deviation of the turbulent wind fluctuations in the crosswind and vertical direction were estimated. These measurements were used for calculating σ_y and σ_z from: 1) Hay and Pasquill's (1959) approximation to the Taylor dispersion formula, $(\sigma_y)_\beta$ and $(\sigma_z)_\beta$, 2) the formulas suggested in Pasquill (1976), $(\sigma_y)_{EPA}$ and $(\sigma_z)_{EPA}$, 3) Draxler's (1976) suggestions, $(\sigma_y)_{Dr}$ and $(\sigma_z)_{Dr}$, and 4) the method proposed by Smith (1973), $(\sigma_y)_{S\theta}$ and $(\sigma_z)_{S\theta}$.

7.2.1. Analysis of lateral dispersion

Available for the analysis of the lateral dispersion parameter are 21 values of $(\sigma_y)_{mea}$ (60-min averaged tracer concentrations). Table 7.2 shows the estimates of σ_y that can be calculated from

Table 7.2. The lateral dispersion parameter derived from the computational methods.

Experiment 1978-1979	Distance (km)	$(\sigma_y)_\beta$ (m)	$(\sigma_y)_{Dr}$ (m)	$(\sigma_y)_{EPA}$ (m)	$(\sigma_y)_{S0}$ (m)	$(\sigma_y)_{PGT}$ (m)	$(\sigma_y)_{Sm}$ (m)
Sep. 14	3.9	362	321	207	414	240	202
Sep. 20	1.9	367	317	269	475	190	238
	3.7	-	532	425	842	340	422
Sep. 26	2.1	203	202	140	250	205	259
	4.2	360	362	224	454	390	470
Oct. 19	1.9	192	206	162	286	190	238
	3.7	394	365	267	528	340	422
	5.4	464	488	356	731	485	584
Nov. 3	4.0	267	228	168	338	370	451
Nov. 9	2.1	138	168	124	223	205	259
	4.2	242	295	200	404	390	470
	6.1	329	394	270	557	540	648
Jun. 27	2.0	362	281	206	366	245	248
	4.1	712	508	336	679	470	461
	5.3	875	623	412	846	588	574
Jul. 6	1.9	222	207	147	260	235	238
	3.6	404	353	229	450	415	412
	5.3	562	483	306	628	588	574
Jul. 19	2.1	240	257	178	319	135	125
	4.2	423	452	281	568	260	214
	6.0	581	603	374	772	350	283

the aforementioned methods. In Fig. 7.2, the values of $(\sigma_y)_{mea}$ have been plotted together with the PGT and Sm-curves, and it can be seen that the two methods reproduce the variation of $(\sigma_y)_{mea}$ with downwind distance fairly well. In the evaluation of Fig. 7.2, attention should be paid to the dissimilarity in averaging time for $(\sigma_y)_{mea}$ (60-min) and $(\sigma_y)_{PGT}$ (3-10 min). A correction on $(\sigma_y)_{PGT}$ to take this dissimilarity into account will increase the values of $(\sigma_y)_{PGT}$.

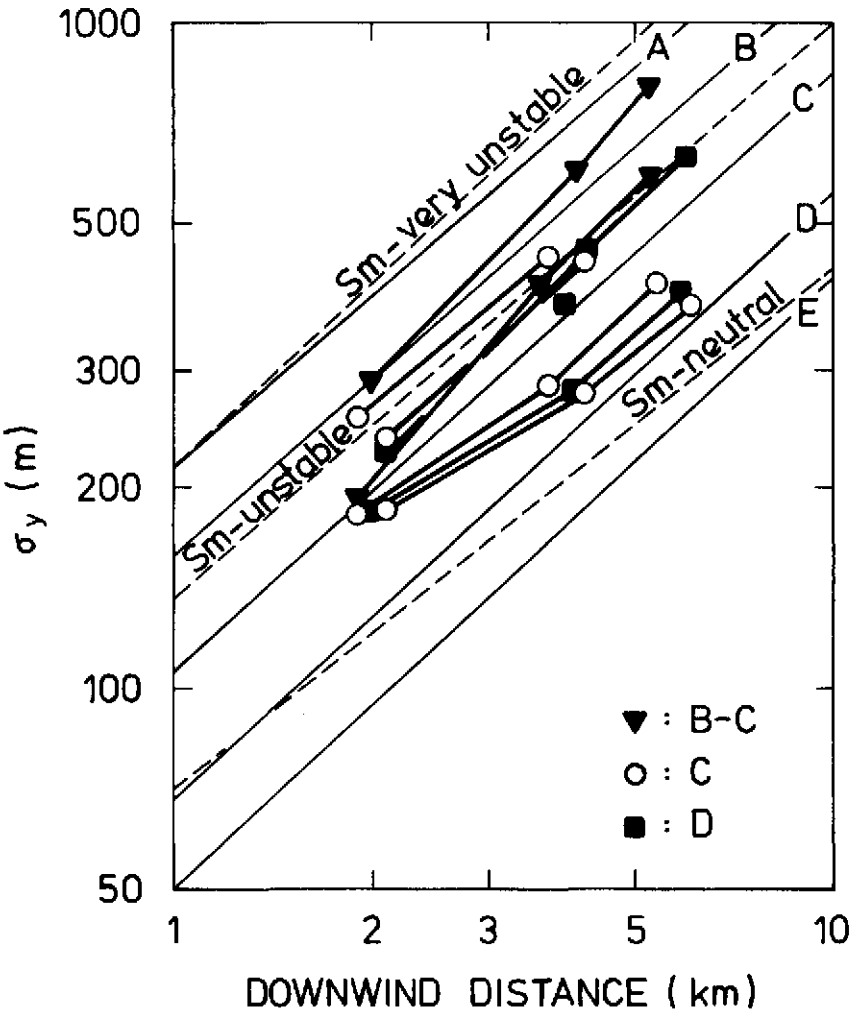

Fig. 7.2. Values of $(\sigma_y)_{mea}$, separated according to the Pasquill stability classification, plotted versus downwind distance. For comparison, the PGT-curves, (Turner, 1970), for the Pasquill stability classes A-E are shown. Also shown are the Sm-curves, (Smith, 1973), for neutral, unstable, and very unstable conditions.

The values of $(\sigma_y)_{mea}$ were compared to the estimates of the lateral spread parameter, calculated by the various methods, $(\sigma_y)_{..}$. The deviations between $(\sigma_y)_{..}$ and $(\sigma_y)_{mea}$ are evaluated by the fractional error, defined in the case of σ_y as

$$\text{fractional error} = \frac{(\sigma_y)_{..} - (\sigma_y)_{mea}}{0.5[(\sigma_y)_{..} + (\sigma_y)_{mea}]}$$

This quantity is used because it is logarithmically unbiased, i.e. a predicted value that is 1/n the measured value produces the same numerical fractional error as one that is n times the measured value.

Table 7.3 shows the fractional error between $(\sigma_y)_{mea}$ and σ_y, derived from the computational methods. The main results are illustrated further in Fig. 7.3, without taking notice of the differences in downwind distance. The β- and Dr-methods (based on wind variances) as well as the PGT- and Sm-methods (based on stability classification) are seen on the average to estimate the lateral dispersion parameter well, whereas the EPA-method

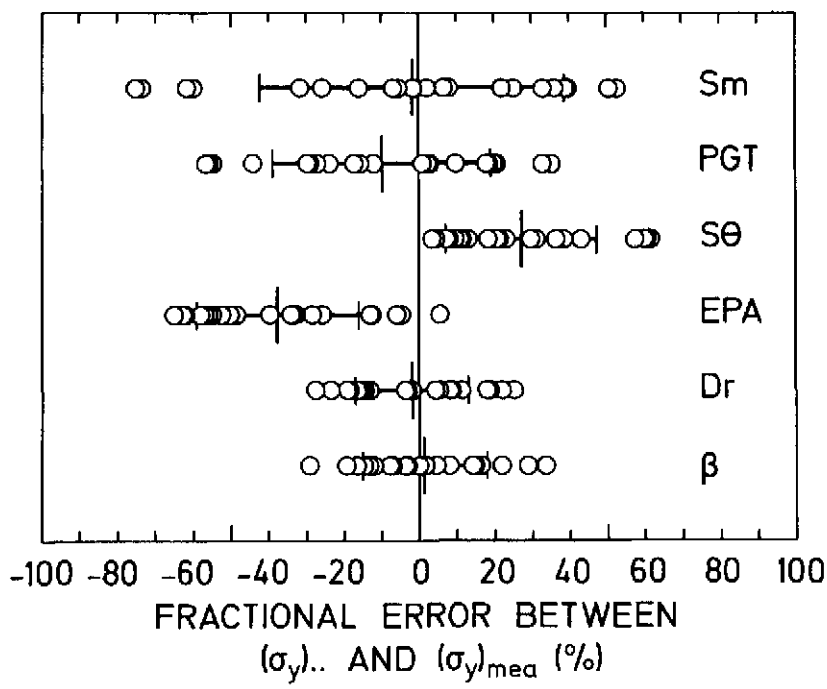

Fig. 7.3. Comparison of lateral dispersion parameters. The fractional error between the individual values of σ_y, computed from the various methods, and $(\sigma_y)_{mea}$ are indicated by o. Symbols refer to the computational methods, explained in the text. The center bar at each method indicates the mean fractional error. The spread in the distribution is evaluated by the root-mean-square fractional error. The outer bars indicate the mean fractional error plus or minus the root-mean-square fractional error.

Table 7.3. Results from the comparison between σ_y derived from the computational methods and $(\sigma_y)_{mea}$.

Experiment 1978-1979	Distance (km)	Fractional error (%) β-mea	Dr-mea	EPA-mea	Sθ-mea	PGT-mea	Sm-mea
Sep. 14	3.9	-4	-16	-58	10	-44	-60
Sep. 20	1.9	29	22	6	61	-29	-7
	3.7	-	18	-4	62	-27	-5
Sep. 26	2.1	-16	-17	-52	5	-15	8
	4.2	-19	-19	-65	4	-12	7
Oct. 19	1.9	5	11	-13	43	3	26
	3.7	34	25	-6	60	18	39
	5.4	14	19	-13	58	18	36
Nov. 3	4.0	-12	-28	-57	12	21	40
Nov. 9	2.1	-29	-10	-39	19	10	33
	4.2	-15	6	-33	37	33	51
	6.1	-13	5	-33	39	36	53
Jun. 27	2.0	22	-3	-34	23	-17	-16
	4.1	14	-16	-56	13	-23	-25
	5.3	8	-23	-62	7	-29	-31
Jul. 6	1.9	16	9	-26	31	21	22
	3.6	0	-13	-55	11	3	2
	5.3	-3	-18	-62	8	1	-1
Jul. 19	2.1	2	9	-28	30	-54	-62
	4.2	-8	-2	-48	21	-56	-73
	6.0	-8	-3	-50	21	-56	-75
Mean fractional error (%):		1	-2	-37	27	-9	-2
r.m.s. fractional error (%):		17	16	22	20	29	40

produces estimates of σ_y that are 37% too low on the average. In these experiments only one value of $(\sigma_y)_{EPA}$ out of 21 is larger than the corresponding value of $(\sigma_y)_{mea}$. In the mean the Sθ-method overpredicts $(\sigma_y)_{mea}$ by 27%; in the present experiment all values of $(\sigma_y)_{S\theta}$ are larger than $(\sigma_y)_{mea}$. It should be noted that $(\sigma_y)_{PGT}$ is actually characteristic of a sampling time of 3-10 min and therefore must be expected to be smaller than $(\sigma_y)_{mea}$. This is well in accordance with the average findings.

The root-mean-square (r.m.s.) fractional error clearly shows that the methods based on wind variances have the smaller scatter, a r.m.s. fractional error of about 20%, whereas the PGT- and Sm-methods based on stability classification produce results with an r.m.s. fractional error of ≃ 30% (PGT) and ≃ 40% (Sm). It is noted that the β- and Dr-methods, which have the smallest r.m.s. fractional error of all, are both based on Taylor's diffusion formula.

Those methods based on an atmospheric stability classification have, as expected, large scatter compared to the wind variance methods. From the comparison it is evident that the methods based on wind variances produce estimates with the smaller r.m.s. fractional error. This, therefore, might serve as a promising basis for further attempts to refine the methods to estimate σ_y from relatively simple measurements. It is equally evident that the use of certain of the wind variance-based methods in the Copenhagen area reveal biased estimates of σ_y. At present it is not obvious whether this is because the methods intentionally are calibrated to produce biased results in order, for instance, to be conservative (as could be the case for the EPA-method) or to some degree the methods are site specific and therefore need adjustment according to the individual sites.

To investigate Pasquill's (1976) and Draxler's (1976) methods in greater detail, the normalized lateral spread, S_y, has been calculated. In Chapter 2, S_y has been defined as

$$S_y \equiv \frac{\sigma_y}{\sigma_v T} \simeq \frac{\sigma_y}{\sigma_\theta x}$$

which, following Taylor's theory, can be argued to be a function of T and the Lagrangian time scale $t_{L,y}$ alone

$$S_y = f_y(T/t_{L,y})$$

Pasquill (1976) argues that S_y follows the expression

$$S_y \approx f_{y,\text{Pasquill}}(x)$$

fairly closely, and thus is a function mainly of downwind distance. In contrast, Draxler (1976) assumes that the f_y-function takes the dependence

$$S_y \approx f_{y,\text{ Draxler}}(T/T_y)$$

where, for the meaning of T_y, reference should be made to Chapter 2.

Figure 7.4 shows S_y as a function of x, which constitutes the dependence suggested by Pasquill (1976). The points display a rather large scatter. It is characteristic that all but one point lies above the f_y-function suggested by Pasquill (1976). The proposed x-dependence with no other parameters is seen to be a rather poor approximation to the actually measured normalized spread. At a downwind distance of approximately 2 km, Pasquill suggests $f_y(2\text{ km}) = 0.5$. The value of f_y in these experiments is seen to vary in the range 0.48-0.84. For a downwind distance of approximately 4 km, Pasquill suggests $f_y(4\text{ km}) = 0.4$. The experimental values of f_y covers the range 0.43-0.77, and for a distance of 6 km, Pasquill suggests $f_y(6\text{ km}) = 0.37$. The experimental values lie in the range 0.43-0.72.

As discussed in Chapter 2, it can be argued that the f_y-function, in addition to the x-dependence, also depends on the wind velocity; small values of f_y are associated with small wind velocities and vice versa. The measured f_y-values, shown in Fig. 7.4, indeed support the existence of this relationship, although the points do not vary with wind speed in a completely systematic manner; this suggests that more than downwind distance and wind

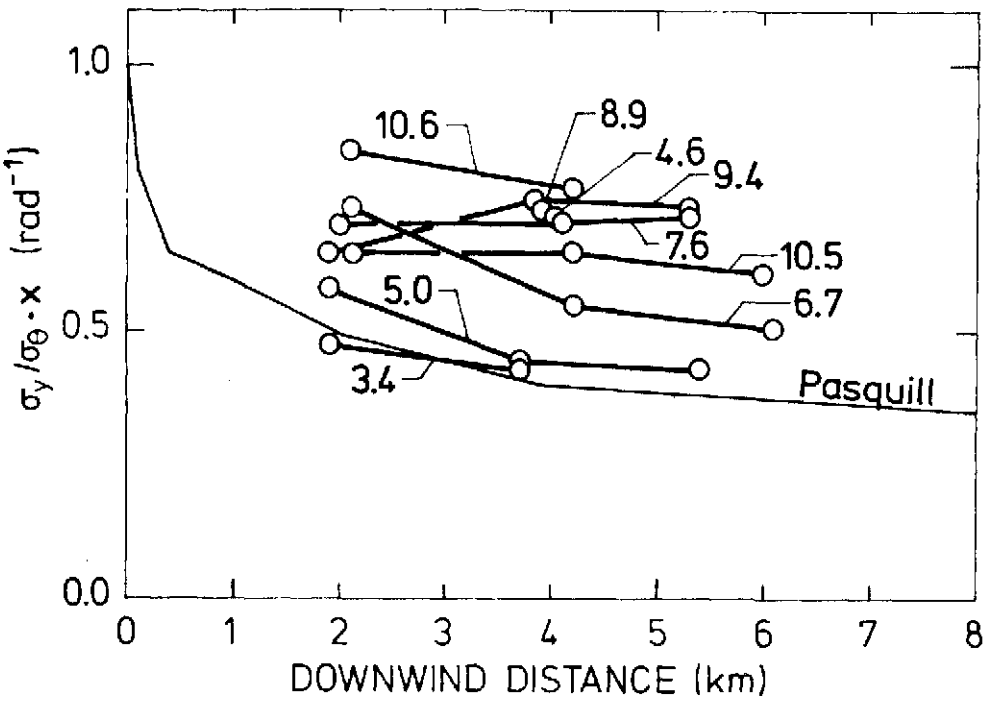

Fig. 7.4. The normalized lateral spread, $(\sigma_y)_{mea}/\sigma_\theta \cdot x$, as function of downwind distance. The mean wind velocity in units of m/s is indicated. Also shown is the f_y-function proposed by Pasquill (1976).

speed are required in order to describe the behaviour of the f_y-function. To throw the wind velocity dependence into relief, points characterized by wind velocities $\bar{u} > 9$ m/s, $6 < \bar{u} < 9$ m/s and $\bar{u} < 6$ m/s has been averaged and the results are illustrated in Fig. 7.5. The f_y-function suggested by Pasquill (1976), when used for one-hour-averaged concentrations, corresponds to situations that are characterized by very low wind velocities. This finding agrees with the results from the pilot dispersion experiments at Risø, reported by Gryning and Lyck (1980a).

Draxler (1976) suggested that the f_y-function depends primarily on the time of travel, $T = x/\bar{u}$, and introduces in that way the wind velocity in the f_y-function. This dimensionless spread is plotted in Fig. 7.6 as a function of time of travel. The points display substantial scatter, although obviously not as large as in Fig. 7.4. The points do not seem to move systematically with wind velocity. The f_y-function for unstable conditions and

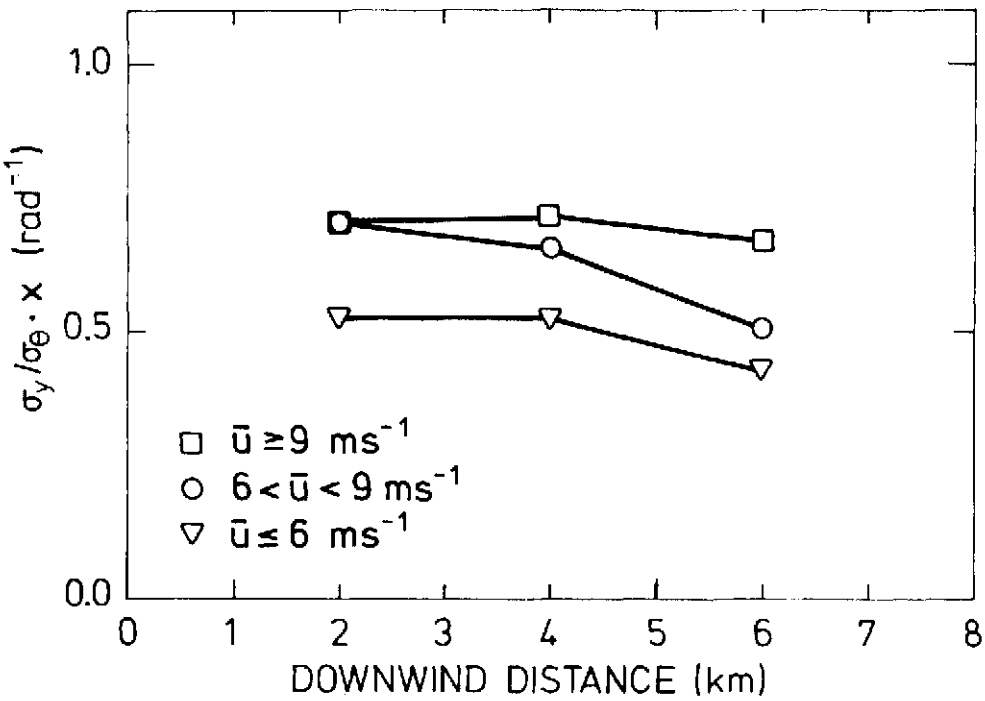

Fig. 7.5. Average values of the normalized lateral spread as function of downwind distance (~ 2 km, ~ 4 km, and ~ 6 km). The values are divided into 3 wind velocity classes, characterized by $\bar{u} \geq 9$ m/s, $6 < \bar{u} < 9$ m/s and $\bar{u} \leq 6$ m/s.

elevated sources as suggested by Draxler, are also shown, the overall fit is seen to be rather fair.

As in Fig. 7.4, the nondimensional spread from the experiment of November 3 completely falls outside the general pattern. This experiment differs from the other with respect to the inversion height, being only 390 m. This suggests a dependence between S_y and z_i or z_i/L. Figure 7.7 is identical with Fig. 7.6 but with z_i and z_i/L indicated. As can be seen, the points do not move systematically with respect to neither z_i nor z_i/L. The experimental results thus leave us with wind velocity dependence only, when the f_y-function is expressed as a function of downwind distance.

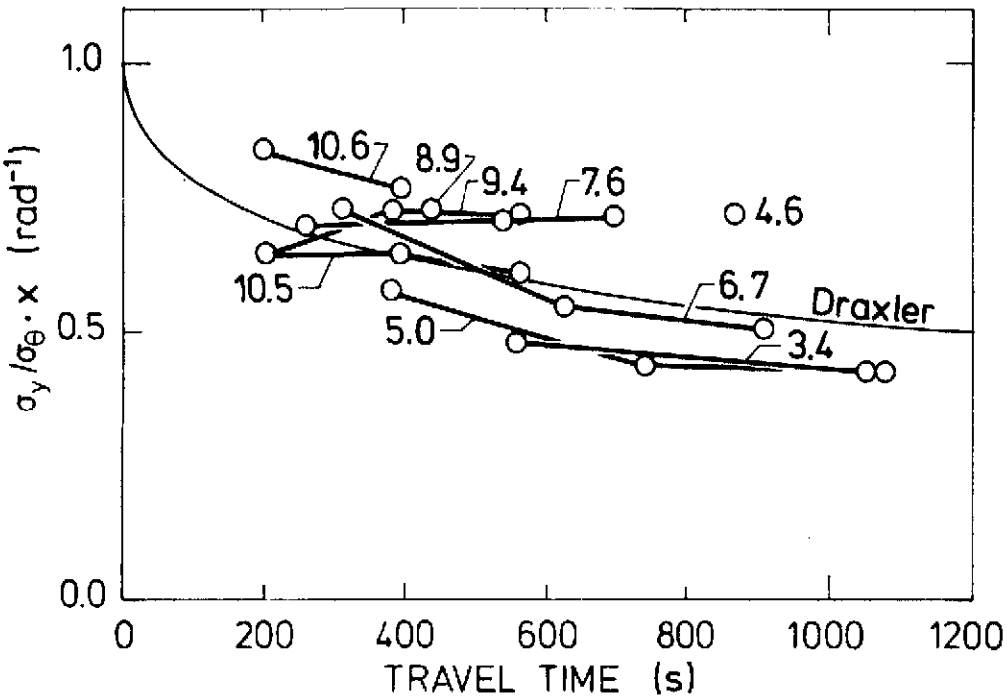

Fig. 7.6. The normalized lateral spread as function of the travel time, t = x/ū. The mean wind velocity in units of m/s is indicated. Also shown is the f_y-function proposed by Draxler (1976).

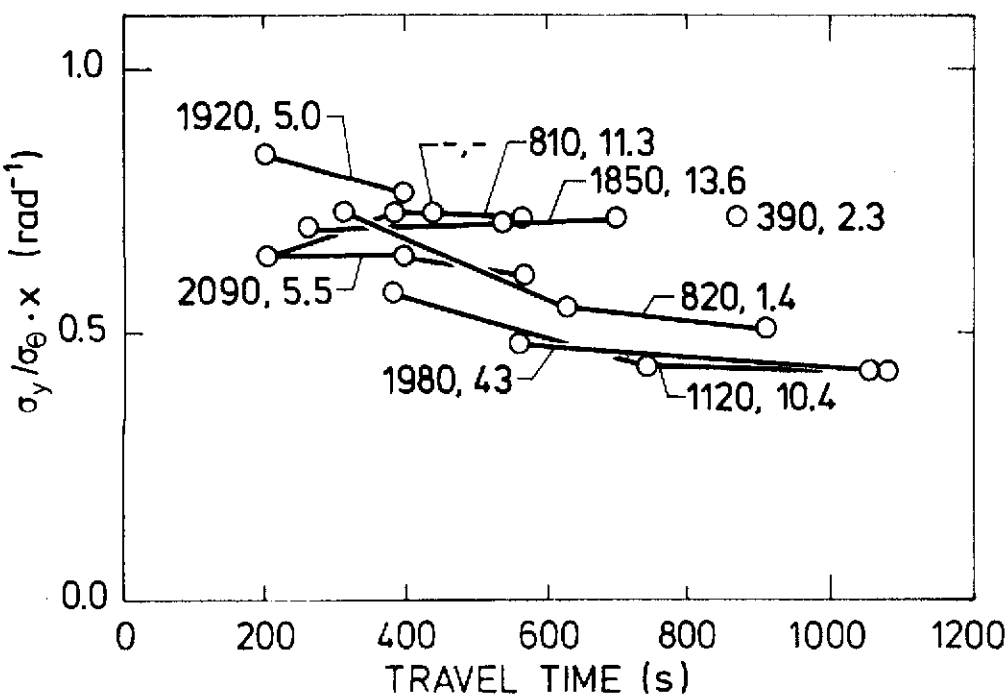

Fig. 7.7. The normalized lateral spread as function of the travel time, t = x/ū. The height of the lowest inversion, z_i, in units of meters, and - z_i/L are indicated.

7.2.2. Analysis of vertical dispersion

Twenty-four values of $(\sigma_z)_{est}$, of which three are based on 40-min averages and the rest are one-hour averages, are available for the analysis of vertical dispersion (Table 7.1). We recall that $(\sigma_z)_{est}$ is estimated by means of (7.3). The values of the vertical spread parameter that can be derived from the aforementioned methods, $(\sigma_z)_{..}$, are shown in Table 7.4. To estimate the uncertainty on $(\sigma_z)_{est}$ originating from the uncertainty in the absolute calibration of the gas chromatograph, Table 7.4 includes values of $(\sigma_z)_{est}$ that are derived by increasing and decreasing the measured tracer concentrations by 20%; $(\sigma_z)_{est}$ is seen to be very sensitive to variations in the absolute tracer concentrations. Owing to this substantial uncer-

Table 7.4. The vertical dispersion parameter, derived from the computational methods. The symbol *) indicates that it is not possible to determine $(\sigma_z)_{est}$.

Experiment 1978-1979	Distance (km)	$(\sigma_z)_{est}$ Measured concentration decreased 20% (m)	increased 20% (m)	$(\sigma_z)_\beta$ (m)	$(\sigma_z)_{DR}$ (m)	$(\sigma_z)_{EPA}$ (m)	$(\sigma_z)_{S\theta}$ (m)	$(\sigma_z)_{PGT}$ (m)	$(\sigma_z)_{Sm}$ (m)
Sep. 14	3.9	183	*)	74	278	186	245	76	139
Sep. 20	1.9	437	277	149	249	224	436	110	218
	3.7	1290	840	-	407	429	773	200	387
Sep. 26	2.1	*)	*)	129	145	249	201	120	237
	4.2	295	168	215	252	485	364	230	431
Oct. 19	1.9	209	*)	117	156	224	250	110	218
	3.7	298	170	162	253	429	432	200	387
	5.4	449	285	187	333	625	598	285	535
Nov. 3	4.0	*)	*)	129	201	468	356	220	413
Nov. 9	2.1	181	*)	85	137	249	207	120	237
	4.2	223	*)	135	233	485	376	230	431
	6.1	274	147	166	308	717	518	320	594
Apr. 30	2.0	*)	*)	96	134	116	175	56	83
	4.2	286	160	174	245	202	332	80	147
	5.9	356	218	203	321	261	444	98	192
Jun. 27	2.0	139	*)	143	147	313	216	173	228
	4.1	386	240	248	257	653	401	365	422
	5.3	577	374	278	312	883	500	485	526
Jul. 6	1.9	223	*)	90	100	299	140	165	218
	3.6	524	330	145	166	585	243	325	378
	5.3	1425	452	178	223	883	339	485	526
Jul. 19	2.1	164	*)	113	136	117	188	52	86
	4.2	281	155	202	235	202	340	80	147
	6.0	346	210	266	309	266	462	100	195

tainty in $(\sigma_z)_{est}$ it is not found reasonable to carry out a strict comparison between $(\sigma_z)_{..}$ and $(\sigma_z)_{est}$ along lines similar to the σ_y comparisons.

In a number of experiments, some values of $(\bar{u}\bar{\chi}_{CWI}/Q)_{mea}$ are too large to allow an estimate of $(\sigma_z)_{est}$ by means of (7.3). This is most pronounced for the series with sampling close to the TV mast. This deficiency cannot be ascribed to the calibration uncertainty on the measured concentrations, as it also appears when the tracer concentrations are increased and decreased by 20%. It might be due to the Gaussian assumption leading to (7.3), is a poor approximation to the actual vertical tracer concentration distribution. Thus, in order to obtain values of $(\sigma_z)_{est}$ for all experiments, either the shape of the vertical tracer concentration distribution must be altered and/or the plume centerline must be lowered and/or a wind velocity different from the one at the release height must be used in (7.3). Generally for the series furthest away (~ 6 km), it is always possible to estimate $(\sigma_z)_{est}$.

Due to the larger roughness of the urban area as compared to a rural area, larger values of σ_z are expected over a city than over a rural area. In an attempt to isolate this effect, Fig. 7.8 shows the values of $(\sigma_z)_{est}$, plotted together with the curves for $(\sigma_z)_{PGT}$ and $(\sigma_z)_{Sm}$. From the figure it can be seen that for the experiments assigned Pasquill stability class D, all values of $(\sigma_z)_{est}$ are considerably larger than $(\sigma_z)_{PGT}$, and also larger, but to a lesser extent, than $(\sigma_z)_{Sm}$. For the Pasquill stability class C experiments, $(\sigma_z)_{est}$ is seen to scatter around $(\sigma_z)_{PGT}$ with the main part of the values being smaller than $(\sigma_z)_{Sm}$. Concerning $(\sigma_z)_{est}$ for the experiments assigned Pasquill stability class B-C, the points are seen to scatter around $(\sigma_z)_{PGT}$ as well as $(\sigma_z)_{Sm}$. With the substantial uncertainty in $(\sigma_z)_{est}$ due to the calibration uncertainty, it is not possible at present to isolate the effect of the enhanced roughness in the city. Calibration work is in progress and this will hopefully reduce the uncertainty of $(\sigma_z)_{est}$ and make it possible to devise σ_z-curves corresponding to the roughness length and source height that are characteristic of the experiments. However, the funda-

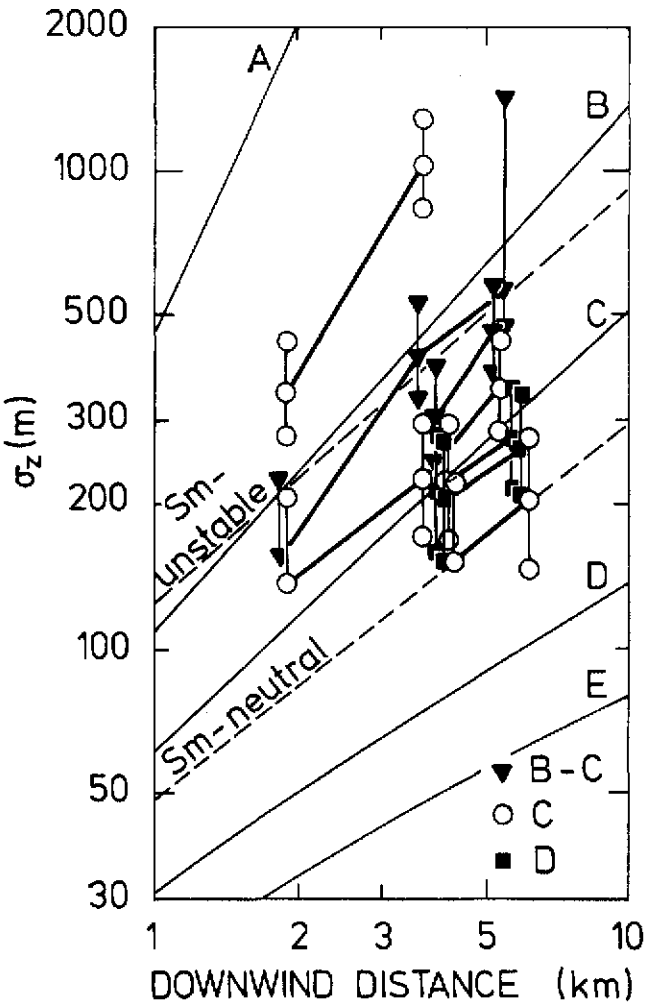

Fig. 7.8. Values of $(\sigma_z)_{est}$, separated according to the Pasquill stability classification, versus downwind distance. The effect on $(\sigma_z)_{est}$ from the uncertainty in the calibration of the gas chromatograph, is shown as bars. It was derived by increasing/decreasing the measured concentrations by 20%. For comparison, the PGT-curves (Turner, 1970) for the Pasquill stability classes A-E are shown. Also shown are the Sm-curves, (Smith, 1973) for neutral and unstable conditions.

mental lack of ability of the Gaussian distribution for some of the experiments to predict the measured tracer concentrations close to the TV-mast will stay unresolved as long as this distribution is applied.

7.2.3. Analysis of crosswind-integrated concentrations

Values of crosswind-integrated concentrations $(\bar{\chi}_{CWI})_{..}$ were estimated by means of (7.4) and the $(\sigma_z)_{..}$-values in Table 7.4 and then compared with the actually measured values of the crosswind-integrated concentrations. This analysis tests the ability of the computational methods to predict σ_z, as $(\bar{\chi}_{CWI})_{..}$ does not depend on $(\sigma_y)_{..}$. The fractional errors between the computed values of $\bar{\chi}_{CWI}$ and the actually measured ones are shown in Table 7.5 and illustrated in Fig. 7.9. As the average fractional error between $(\bar{\chi}_{CWI})_{..}$ and $(\bar{\chi}_{CWI})_{mea}$ derived from the β-, Dr-, PGT- and Sm-methods are less than

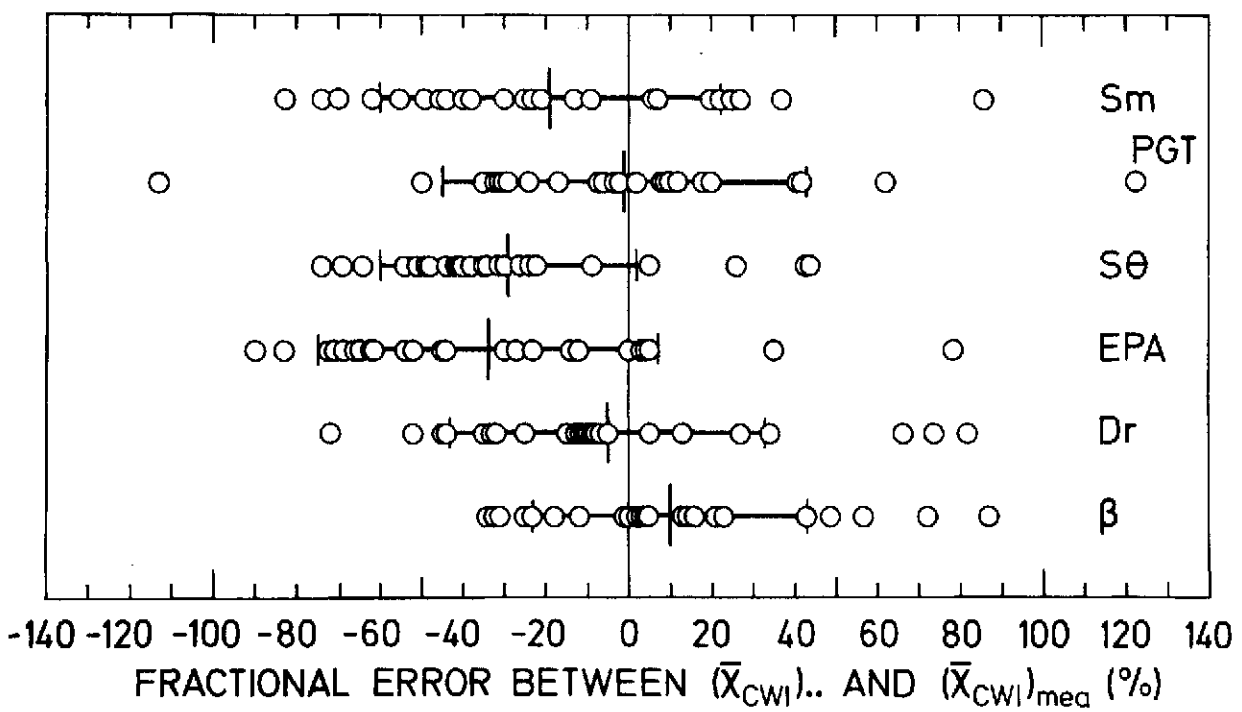

Fig. 7.9. Comparison of the crosswind-integrated concentration distributions. The fractional error between the individual values of $\bar{\chi}_{CWI}$, computed from the various methods and $(\bar{\chi}_{CWI})_{mea}$, are indicated by o. Symbols refer to the computational methods, explained in the text. The center bar at each method indicates the mean fractional error. The spread in the distribution is evaluated by the root-mean-square fractional error. The outer bars indicate the mean fractional error plus or minus the root-mean-square fractional error.

Table 7.5. Results from the comparison between $\bar{\chi}_{CWI}$, derived from the computational methods and $(\bar{\chi}_{CWI})_{mea}$.

Experiment 1978-1979	Distance (km)	Fractional error (%) β-mea	Dr-mea	EPA-mea	Sθ-mea	PGT-mea	Sm-mea
Sep. 14	3.9	-32	-52	-23	-42	-29	-9
Sep. 20	1.9	57	27	35	-22	62	37
	3.7	-	82	78	26	125	86
Sep. 26	2.1	-31	-35	-66	-51	-30	-62
	4.2	3	-9	-65	-40	-2	-55
Oct. 19	1.9	3	-5	-27	-35	2	-25
	3.7	21	-9	-54	-54	8	-45
	5.4	49	5	-52	-48	18	-38
Nov. 3	4.0	-25	-45	-71	-69	-50	-70
Nov. 9	2.1	-18	-9	-44	-31	-7	-40
	4.2	5	-25	-83	-64	-24	-74
	6.1	13	-32	-90	-74	-35	-83
Apr. 30	2.0	-34	-33	-62	-44	-31	-44
	4.2	14	-10	4	-35	10	22
	5.9	23	-13	4	-42	42	27
Jun. 27	2.0	-23	-73	-72	-24	-32	-49
	4.1	16	13	-69	-26	-17	-30
	5.3	43	34	-62	-9	-6	-13
Jul. 6	1.9	0	-45	-45	5	-3	-21
	3.6	72	66	-30	43	20	6
	5.3	87	74	-14	43	12	6
Jul. 19	2.1	-12	-15	-12	-30	-113	-23
	4.2	3	-8	3	-38	8	20
	6.0	0	-12	0	-48	41	25
Mean fractional error (%):		10	-5	-34	-29	-1	-19
r.m.s. fractional error (%):		33	38	41	31	44	41

20%, constituting the uncertainty in the absolute tracer concentrations, these 4 methods cannot be judged individually with respect to their ability to predict $(\bar{\chi}_{CWI})_{mea}$. It is noted that the σ_z-values that are used in the EPA-method (-34% fractional error) and the PGT-method (-1% fractional error) are based on the workbook values (Turner, 1970). However, in the EPA-method the values have been corrected for the enhanced roughness and heat islands effect at the experimental site. Without these corrections, of which the heat island effect is the dominant one, the EPA-method will produce exactly the same value of $\bar{\chi}_{CWI}$ as the PGT-method. This suggests that the enhancement of σ_z, as recommended by Pasquill (1976) for the EPA-method, due to the heat island effect, is too large for the residential area in Copenhagen, where the experiments take place. No explanation of the -29% mean fractional error for the Sθ-method is offered, but it seems that this method on the average simply produces values of σ_z which are too large.

The r.m.s. fractional error is seen to be fairly equal for all methods, ranging from 31% to 44%, which indicates that none of the methods, based on the analysis and the results from these dispersion experiments in the Copenhagen area, can be considered superior in predicting the variation of $(\bar{\chi}_{CWI})_{mea}$, although the methods based on the measured wind variances during the experiments do work a little better than the stability-based methods.

An interesting effect can be noted in the ability of the β-method to predict $(\bar{\chi}_{CWI})_{mea}$. The fractional error is clearly an increasing function of downwind distance. This is observed for all experiments in which measurements have been carried out in more than one series, except for the experiment on July 19, where there exists a minor decrease. To illustrate the effect, the fractional error has been plotted as a function of distance in Fig. 7.10. A large scatter is apparent, but it is demonstrated that close to the source there is a tendency for the fractional error to fall out negatively. There seems to be also a tendency for the curves to behave in an orderly manner after stability, with the smaller values of the fractional error associated with near

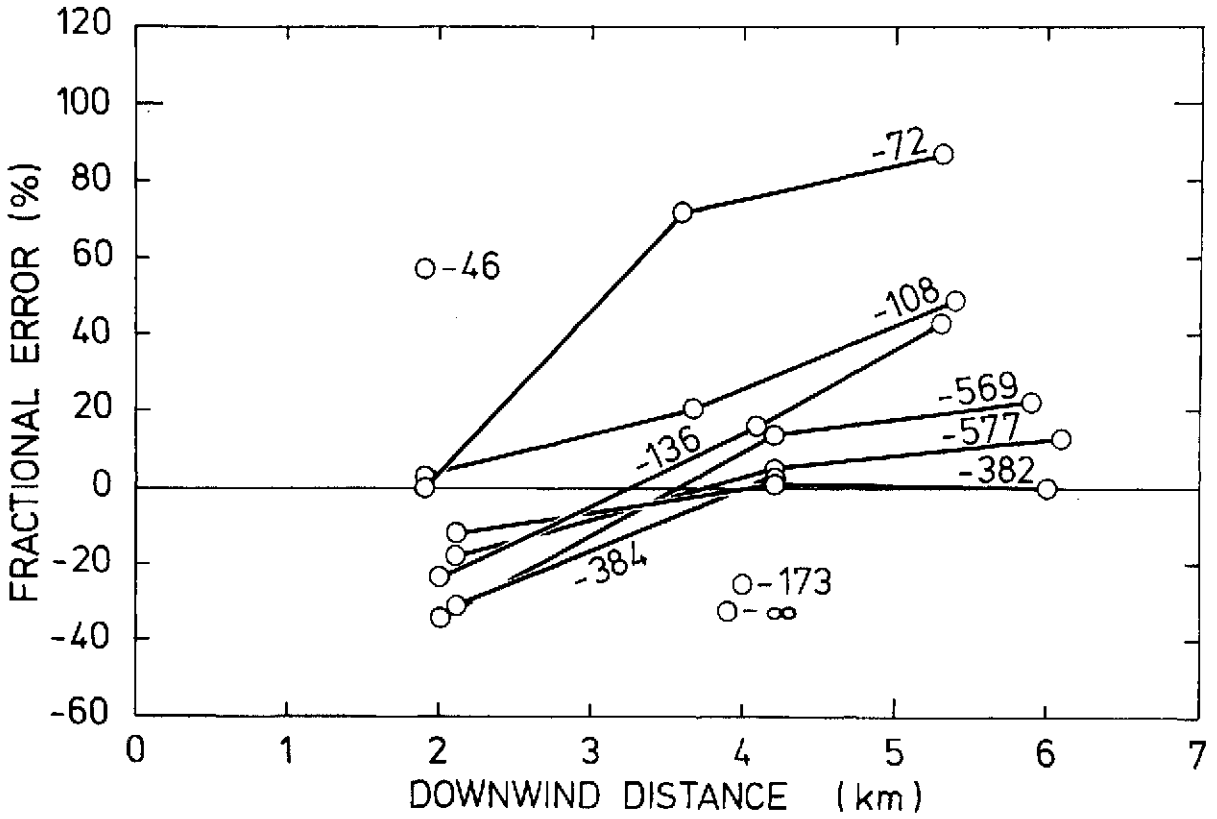

Fig. 7.10. The fractional error between $(\bar{\chi}_{CWI})_{\beta}$ and $(\bar{\chi}_{CWI})_{mea}$ versus downwind distance. The Monin-Obukhov lengths in meters are indicated for the individual experiments.

neutral conditions, and with the fractional error increasing with the instability.

A tentative explanation of the effect could be found in the Hay and Pasquill (1959) assumption of similarity between Lagrangian and Eulerian spectra, the cornerstone of the β-method. That the fractional error increases with increasing downwind distance indicates that the rate by which $(\sigma_z)_{\beta}$ grows is too small to describe the evolution in ground-level concentrations. This indicates, when looked upon from the viewpoint of the Hay and Pasquill (1959) theory, that the low frequency part of the Lagrangian spectrum of the vertical wind velocity is more energetic than the corresponding low frequency part of the Eulerian spectrum, from which $(\sigma_z)_{\beta}$ is actually computed. This indicates a systematic difference in the shape of the low frequency part of the

two types of spectra. The difference may also be ascribed to the shear layer, in which the dispersion in the vertical direction takes place. This effect is found only for the vertical dispersion. An equivalent effect for the lateral dispersion, which is performed in a flow-field that in the lateral direction can be considered much more homogeneous, is not observed.

7.2.4. Analysis of maximum concentrations

From an air pollution point of view, absolute concentrations are of particular interest. In this chapter we investigate how well it is possible to calculate the maximum ground-level concentrations at the experimental distances by applying σ_y and σ_z derived from the aforementioned methods. To do this the normalized, ground-level concentration at the centreline, $\bar{u}\bar{\chi}_{max}/Q$ were calculated. This quantity was compared to the normalized, measured tracer concentrations, $(\bar{u}\bar{\chi}_{max}/Q)_{mea}$, where for $\bar{\chi}_{max}$ the maximum measured tracer concentration in the various series have been inserted. Table 7.6 shows the values of $(\bar{u}\bar{\chi}_{max}/Q)_{..}/(\bar{u}\bar{\chi}_{max}/Q)_{mea}$ and the results have been illustrated in Fig. 7.11. In the ratio $(\bar{u}\bar{\chi}_{max}/Q)_{..}/(\bar{u}\bar{\chi}_{max}/Q)_{mea}$ the numerator is based purely on the individual methods and meteorological data, whereas the denominator is based solely on measured tracer concentrations. If perfect agreement were obtained, the ratio would turn out to be 1. However, $(\bar{u}\bar{\chi}_{max}/Q)_{mea}$ does not actually represent the real ground-level maximum concentration, because the measurements were made at discrete positions. The difference is believed to be minor, however. The concentrations derived with the use of the PGT-method have been corrected for the difference in averaging time. The correction is found following a formula in Turner (1970), $\bar{\chi}_{60\ min} = \bar{\chi}_{10\ min} \cdot (10/60)^p$ where p is in the range 0.17-0.20. Here p = 0.17 was used. For the β-, Dr- and EPA-methods, which are all based on wind variances, the mean fractional error is seen to be less than the 20% that constitutes the uncertainty in the measured, absolute tracer concentrations. Thus none of these three methods can be judged to be superior in their ability to predict the mean of $\bar{\chi}_{max}$. The wind variance-based Sθ-method has a mean fractional error of

Table 7.6. Results from the comparison between $(\bar{u}\bar{\chi}_{max}/Q)$, derived from the computational methods and $(\bar{u}\bar{\chi}_{max}/Q)_{mea}$. $\bar{\chi}_{max}$ represents the maximum ground-level concentration at the experimental distance.

		$(\bar{u}\bar{\chi}_{max}/Q)_{..}/(\bar{u}\bar{\chi}_{max}/Q)_{mea}$					
Experiment 1978-1979	Distance (km)	β mea	Dr mea	EPA mea	Sθ mea	PGT mea *)	Sm mea
Sep. 14	3.9	0.6	0.6	1.2	0.5	0.7	1.4
Sep. 20	1.9	1.2	1.0	1.3	0.4	1.8	1.5
	3.7	-	1.9	2.3	0.7	4.0	2.6
Sep. 26	2.1	0.8	0.8	0.8	0.5	0.6	0.4
	4.2	1.2	1.1	1.0	0.6	0.8	0.5
Oct. 19	1.9	1.1	0.9	0.9	0.5	0.8	0.7
	3.7	1.0	0.8	0.7	0.3	0.7	0.5
	5.4	1.6	1.0	0.8	0.4	0.8	0.5
Nov. 3	4.0	0.9	0.8	0.5	0.4	0.3	0.2
Nov. 9	2.1	1.3	1.2	1.1	0.7	0.7	0.6
	4.2	1.4	0.9	0.7	0.4	0.5	0.3
	6.1	1.4	0.8	0.5	0.3	0.4	0.3
Jun. 27	2.0	0.6	0.8	0.6	0.5	0.6	0.7
	4.1	0.8	1.1	0.7	0.6	0.7	0.8
	5.3	1.4	1.8	1.0	0.8	0.9	1.2
Jul. 6	1.9	0.8	0.9	0.7	0.7	0.5	0.6
	3.6	1.6	1.7	0.9	1.1	0.7	0.8
	5.3	2.8	2.8	1.3	1.5	0.9	1.1
Jul. 19	2.1	0.8	0.7	1.1	0.5	0.3	1.4
	4.2	1.1	1.0	1.7	0.6	1.4	2.7
	6.0	0.9	0.8	1.4	0.4	1.7	2.3
Mean fractional error (%):		8	1	-7	-58	-25	-22
r.m.s. fractional error (%):		35	37	36	35	53	64

*) corrected for differences in sampling time.

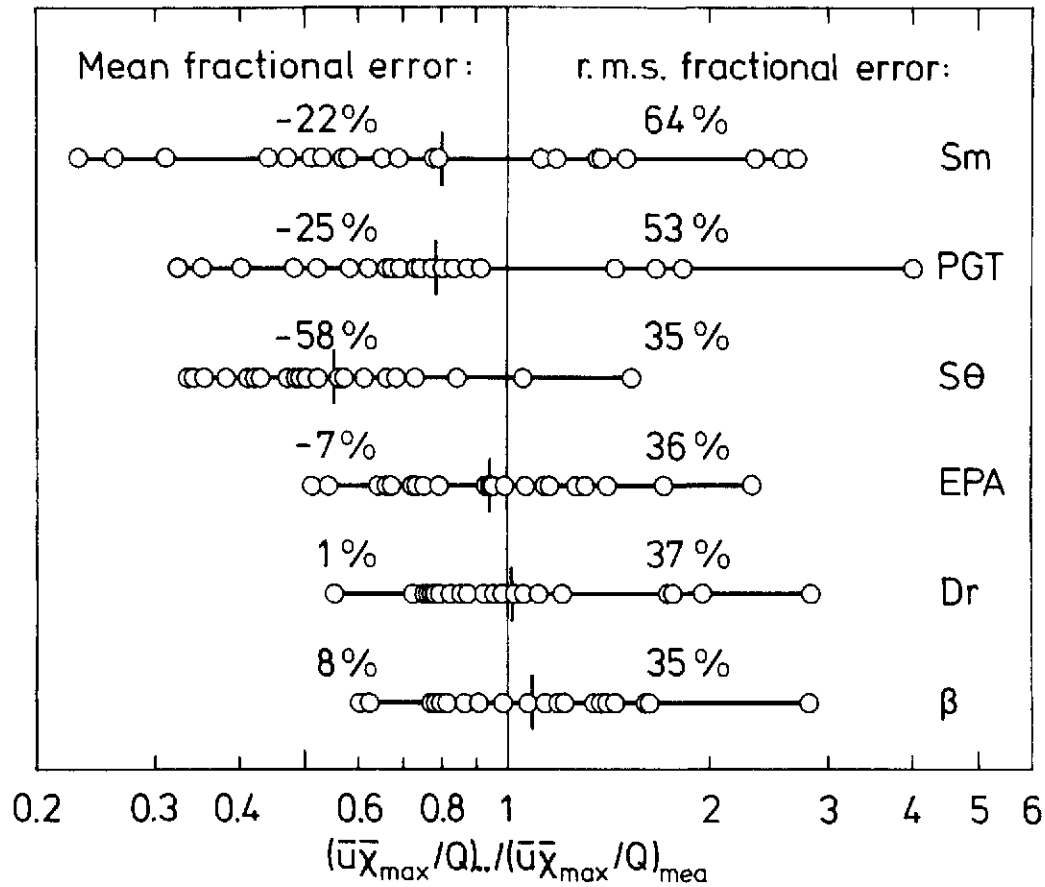

Fig. 7.11. The ratio of the computed maximum ground-level concentrations to measured maximum ground-level concentrations, $\left(\frac{\bar{u}\bar{\chi}_{max}}{Q}\right)../\left(\frac{\bar{u}\bar{\chi}_{max}}{Q}\right)_{mea}$, for all experimental distances. Symbols refer to the computational methods, explained in the text. The vertical bar at each method indicates the mean fractional error.

-58%, a result that is not surprising remembering the tendency of this method to overpredict both σ_y and σ_z. The stability-based methods, i.e. PGT and Sm, are seen to have a mean fractional error only slightly smaller than the lower limit of the uncertainty on the measured tracer concentrations.

The root-mean-square fractional error describes the ability of the methods to predict the variation of $\bar{\chi}_{max}$. Here, the wind variance-based methods, i.e. β, EPA, Dr, and Sθ, all come out with r.m.s. fractional errors of approximately 35%, whereas the

stability-based methods have substantially larger r.m.s. fractional errors, 64% for the Sm-method, and 53% for the PGT-method. It is interesting to note how well the EPA-method works, keeping in mind that this method on the average underpredicts σ_y with a mean fractional error of -37%, and also underpredicts the cross-wind-integrated concentrations by -34%. As the maximum concentration is inversely proportional to σ_y, these effects to a certain extent cancel each other in calculations of the centreline concentrations, rendering the final result as good as the results from the β- and Dr-method.

For these experiments, $(\bar{u}\bar{\chi}_{max}/Q)_{..}/(\bar{u}\bar{\chi}_{max}/Q)_{mea}$ is seen to vary in the range 0.6-2.8 for the β-method, in the range 0.5-2.4 for the EPA-method, 0.6-2.8 for the Dr-method, 0.3-1.5 for the Sθ-method, and 0.2-2.7 for the Sm-method. The ratio for the widely used PGT-method is seen to vary in the range 0.3-4.0, or more than an order of magnitude.

7.2.5. Analysis of dispersion in convective conditions

Results from the dispersion experiments also were compared to Deardorff and Willis's measurements of the dispersion of oil-droplets in a water tank during fully convective conditions.

Convective scaling of the atmosphere applies at levels high enough for mechanical turbulence to be neglected in comparison with turbulence of convective origin. The height for this condition to be fulfilled is not well known. Priestly (1955) argued that the condition is satisfied for $z > -0.03$ L and Panofsky (1978) assumed that convective scaling is applicable provided $z > -L$. Willis and Deardorff's requirements on z_i/L and $\bar{u}/w_*$ for validity of their model of the convective turbulence statistics is given in Chapter 2, (2.46) and (2.48). Here z_i is the height of the lowest inversion.

In order to perform the analysis, the characteristic vertical velocity w_* has to be estimated. From the expression of the Monin-Obukhov length

$$L = - \frac{\bar{T} \; u_*^3}{g \; k \, (w'T')_o}$$

and from (2.45), we get the expression

$$w_* = \left(\frac{z_i \; u_*^3}{-L \; k} \right)^{1/3}$$

which contains only quantities already known from Table 6.1. The estimated values of w_*, $\bar{u}/w_*$, z_i/L and L are given in Table 7.7. Only those experiments for which $-z_i/L \geq 5$ are included. The conditions concerning $\bar{u}/w_*$ are seen to be fulfilled for all ex-

Table 7.7. Results of the analysis of the fulfilment of the conditions required for convective scaling of the experiments. Included are experiments only for which $- z_i/L \geq 5$. The requirements for convective scaling to be applicable are $1.2 \leq \bar{u}/w_* < 6$ and $- z_i/L > 10$. For $\bar{u}$ the mean wind speed at 115 m height was used.

Experiment 1978-1979	w_* (m/s)	$\frac{\bar{u}}{w_*}$	$- \frac{z_i}{L}$	-L (m)	$\frac{h}{z_i}$
Sep. 20.	1.7	2.0	43	46	0.058
Sep. 26.	1.7	6.2	5.0	384	0.060
Oct. 19	1.1	4.5	10.4	108	0.103
Jun. 27	2.1	3.6	13.6	136	0.062
Jul. 6	2.1	4.5	11.3	72	0.142
Jul. 19	1.8	5.7	5.5	382	0.055

periments included in Table 7.7 except for one of September 26. The condition regarding z_i/L, which secures a fully convective flow field, is fulfilled, except for the experiments on September 26 and July 19 where $-z_i/L$ is below the recommended limit. This

indicates that the flow field cannot be considered as completely dominated by the convective scale motion throughout the mixed layer, but that wind shear also plays a certain role in the dispersion process. For the experiments of September 20, October 19, June 27, and July 19 both requirements are fulfilled.

Figure 7.12 shows the dimensionless crosswind-integrated tracer concentration plotted as a function of the dimensionless distance The dimensionless source height varies from experiment to exper-

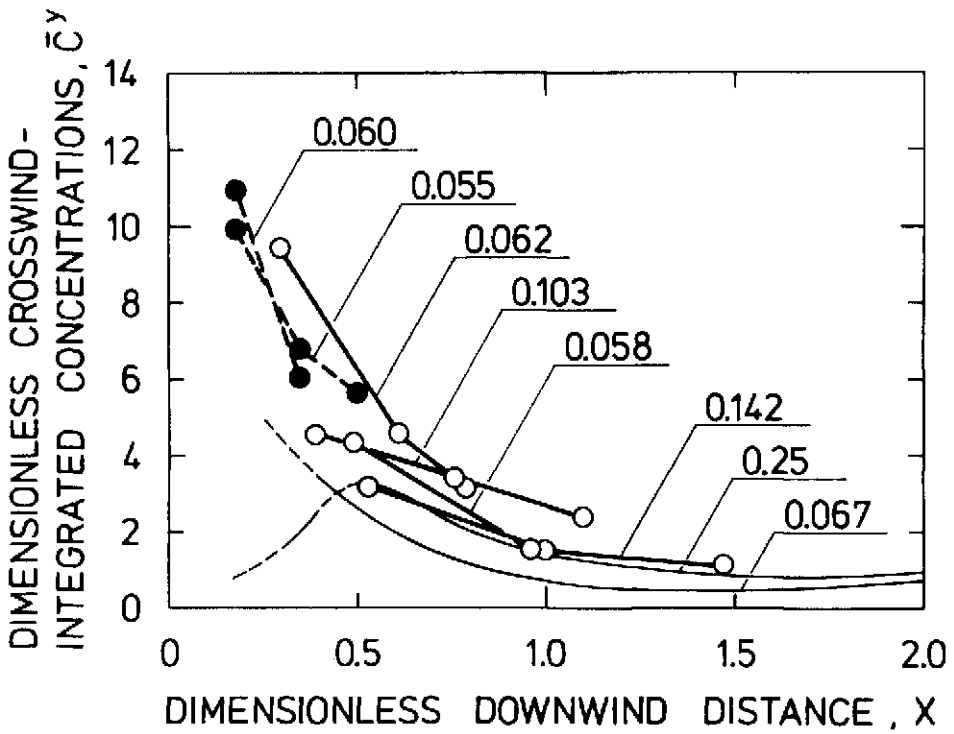

Fig. 7.12. Dimensionless crosswind integrated ground-level concentrations, $\bar{C}^y$, versus dimensionless downwind distance, X. Results from experiments, where the requirements for convective scaling are fulfilled are indicated by (o); if the conditions are "close" to be fulfilled, the results are indicated by (●) and the connecting line is dashed. The dimensionless release height, h/z_i, is shown for each experiment. For comparison, results are shown from two tank experiments (Deardorff and Willis, 1975; Willis and Deardorff, 1978) with h/z_i = 0.067 and 0.25, respectively.

iment because the actual source height is normalized with the height of the convective boundary layer. This makes comparison with Deardorff and Willis's experiments for the near ground-level source troublesome. Therefore, results from Deardorff and Willis's experiments for a "near ground-level source", with h/z_i = 0.067 as well as for a high source with h/z_i = 0.25 has been plotted in Fig. 7.12. No tank experiments with dimensionless source heights between these values have yet been reported. For all experiment the dimensionless source height for the experiments are seen to be closer to 0.067 than to 0.25; 4 experiments have indeed dimensionless source heights very close to 0.067. Thus, the experiments must be considered in convective boundary layer parameterization as performed as near groundlevel releases. By inspecting Fig. 7.12 it is seen that the results from the experiments of September 26 and July 19 are seen to not separate from the other experiments in any systematic manner in spite of the lacks of fulfilment of the required conditions to secure that the flow-field can be considered to be fully convective.

Deardorff and Willis's curve for the nondimensional crosswind-integrated concentrations for near surface releases has a rather characteristic shape. Due to the small but significant release height, the curve has to be at zero for X = 0 corresponding to a situation in which the plume passes above the position without reaching the ground level. At the position where the plume reaches ground level, the dimensionless crosswind concentration will have have a maximum. Thereafter it rapidly decreases, gradually leaving the curve almost flat for a substantial period of the dimensionless time.

The general behaviour of the curve for near-surface releases in the range $0.2 < X < 1.5$ is supported by the results from the experiment in Copenhagen, but it is characteristic that even with substantial scatter in the points they all are situated above Willis and Deardorff's curve for near-surface releases. This means that the values of the actually measured crosswind-integrated concentrations for the full-scale experiments are larger than values found in the tank experiments, indicating that the

vertical dispersion process in the full-scale experiments is less effective in diluting near surface concentrations than in the water-tank experiments. A tentative explanation for this difference is that a substantial part of the dispersion takes place in the lower part of the convective boundary layer before the ultimate ground-level sampling by the sampling units. At smaller distances from the ground the mechanical contribution to the turbulent energy becomes increasingly important compared with the convective energy in the dispersion process. Close to the ground the mechanical turbulence will be dominant in the vertical process. Because of the relative reduction in the convective motion it will take a larger dimensionless downwind distance to mix-up pollutants (sweep-up) close to the surface than is the case under fully convective flow conditions in a water tank experiment. In the water tank the mechanical turbulence is absent close to the bottom of the tank due to the special technique used.

7.3. Proposed models for the prediction of σ_y and σ_z for elevated point sources in an urban area under neutral and unstable conditions

In this chapter we will devise improvements to the methods of predicting σ_y and σ_z. The σ_y- and σ_z-values are calibrated for use in connection with the Gaussian plume model for calculations of concentrations of the effluents. The estimated concentrations can be expected to be most reliable close to the ground. The proposed models rests on the experience and results from the dispersion experiments in Copenhagen, thus covering only neutral and unstable atmospheric conditions.

The computational schemes are the so-called "split sigma" models, indicating that the determination of σ_y and σ_z is based on different principles.

7.3.1. Lateral dispersion parameter.

An inspection of Table 7.3 reveals that for predictions of the variation of σ_y, methods based on the measured wind variances clearly are superior compared with stability index-based methods. This judgement is based on the r.m.s. fractional error. In this context the mean fractional error is of no interest; biased values can simply be scaled to give a correct mean value. The best of the variance-based methods turned out to be the Dr-method, having a r.m.s. fractional error of 16%. The β-method also should be considered, but the requirement for extensive on-line computational facilities for calculating $(\sigma_y)_\beta$ on a routine basis leaves this method too demanding to be recommended for routine measurements at the present state of technology.

The EPA-method does not immediately call for attention due to its high r.m.s. fractional error, but the performance is vastly improved when taking into account the wind velocity dependence of the f_y-function demonstrated in Fig 7.5. For practical calculations of σ_y, it is suggested to take into account the wind velocity dependence of the f_y-function as shown in Table 7.8.

Table 7.8. Values of $f_y(x,u)$ to be used in the proposed procedure for evaluating $\sigma_y = \sigma_\theta \cdot x \cdot f_y(x,u)$ with σ_θ in radians.

$x(m \times 10^3)$	0	1	2	4	6
$\bar{u} \geq 9$ m/s	1	0.85	0.75	0.70	0.65
$6 < \bar{u} < 9$ m/s	1	0.80	0.70	0.60	0.55
$\bar{u} \leq 6$ m/s	1	0.70	0.55	0.45	0.40

The fractional error between $(\sigma_y)_{mea}$ and σ_y calculated by use of this revised f_y-function, is shown in Table 7.9. The mean fractional error turns out to be -3%, and the r.m.s. fractional error 15%.

Table. 7.9. Comparisons between predicted and measured values of σ_y and $\bar{\chi}_{CWI}$. The predicted values were obtained from the new method devised in this chapter.

Experiment 1978-1979	Distance (km)	σ_y new method (m)	Fractional error*) (%)	σ_z new method (m)	$\left(\frac{\bar{u}\bar{\chi}_{CWI}}{Q}\right)$ new method ($10^{-9}m^{-1}$)	Fractional error**) (%)
Sep. 14	3.9	309	-19	210	3.3	-31
Sep. 20	1.9	299	-16	110	4.2	62
	3.7	479	8	200	3.4	125
Sep. 26	2.1	212	4	120	4.2	-30
	4.2	394	-11	230	3.1	-2
Oct. 19	1.9	180	-2	110	4.2	2
	3.7	289	2	200	3.4	8
	5.4	377	-7	286	2.6	18
Nov. 3	4.0	188	-46	220	3.2	-52
Nov. 9	2.1	175	24	120	4.2	-7
	4.2	300	7	230	3.1	-24
	6.1	400	6	320	2.3	-35
Apr. 30	2.0			115	4.2	-31
	4.2			230	3.1	-5
	5.9			310	2.4	-10
Jun. 27	2.0	288	-1	173	3.7	-32
	4.1	504	-17	365	2.1	-17
	5.3	617	-24	485	1.6	-6
Jul. 6	1.9	221	25	165	3.8	-3
	3.6	388	-4	325	2.3	20
	5.3	541	-7	485	1.6	11
Jul. 19	2.1	265	12	120	4.2	-13
	4.2	493	7	230	3.1	-6
	6.0	658	5	315	2.4	-14
Mean fractional error (%):			-3			-3
r.m.s. fractional error (%):			15			35

*) $\dfrac{\sigma_y - (\sigma_y)_{mea}}{\frac{1}{2}(\sigma_y + (\sigma_y)_{mea})} \cdot 100$ (%)

**) $\dfrac{\chi_{CWI} - (\chi_{CWI})_{mea}}{\frac{1}{2}(\chi_{CWI} + (\chi_{CWI})_{mea})} \cdot 100$ (%)

Whether this new method or the Dr-method should be preferred or not when calculating σ_y for elevated sources under neutral and unstable atmospheric conditions, is purely a matter of taste and prejudice. The new method describes the lateral dispersion in terms of downwind distance, which is more direct and easy to survey than a description in terms of travel time as in the Dr-method. Also, from the theoretical considerations in Chapter 2, it is argued that the f_y-function depends on both x and $\bar{u}$.

However, it is not obvious that this dependence should take the simple form $f_y(x/\bar{u}) = f_y(T)$. This form expresses the assumption that the Lagrangian time scale is constant and independent of meteorological conditions. The new method keeps both x and $\bar{u}$ as free parameters. These methods require measurements of σ_θ, which fortunately are relatively easy to perform; it can, for example, be done with a well-designed wind vane.

7.3.2. Vertical dispersion parameter.

Although the wind variance-based methods were substantially better for predicting σ_y than were the stability-based ones, this is not the case for the prediction of the vertical dispersion parameter, judged from the ability to predict the measured crosswind-integrated ground-level tracer concentration. From Table 7.5 it can be seen that the r.m.s. fractional error for the individual methods for all practical purposes may be judged to be equivalent, although the wind variance-based methods are seen to work a little better.

Concerning the stability-based methods, an increase of σ_z compared with $(\sigma_z)_{PGT}$ is expected due to the difference in surface roughness between the experimental site and the characteristic surface roughness for the PGT-curves. This effect is expected to be most pronounced under neutral conditions, and insignificant under fully convective conditions. It can be seen from Fig. 7.8 that the values of $(\sigma_z)_{est}$ in Pasquill stability class D are positioned above the PGT D-curve, even when taking into account the ±20% calibration uncertainty in the absolute tracer concentrations. Values of $(\sigma_z)_{est}$ in Pasquill stability class C are seen to scatter around the C-curve. Whether the values of $(\sigma_z)_{est}$ on the average lie above the C-curve or not cannot be judged, as this information is hidden in the uncertainty of $(\sigma_z)_{est}$ that originates from the error in the absolute tracer concentrations. For values of $(\sigma_z)_{est}$ in Pasquill stability class B-C, an equal conclusion must be drawn. A final proposition to enable a model to predict σ_z should wait for the results from a thorough calibration of the gaschromatograph. In the meantime it is suggested that predictions of σ_z should be based on the PGT-curves, using

the C-curve for experiments assigned Pasquill stability class D as well as C, while the A and B curves should be employed in the usual way. This proposal is limited to neutral and unstable meteorological conditions and release heights and surface roughness as existing in these experiments.

The fractional error between the value of the crosswind-integrated concentrations that can be calculated by this new method, and the actually measured values are given in Table 7.9. The mean fractional error is -3% and the r.m.s. fractional error turns out to be 35%.

A substantial drawback of the wind variance-based methods is that reliable measurements of the variance of the vertical wind fluctuations, σ_ϕ^2, are difficult to achieve. They can be made by the use of bi-directional vanes, but this instrument is troublesome to operate on a routine basis due to problems associated with balancing the fluctuating part of the instrument. The instrument will be influenced by deposition of dust, dirt, dew, etc., and rain and snow may cause very large errors. Use of vertical propellers to measure σ_ϕ requires on-line computational facilities in order to correct for the lack of a cosine response characteristic for this instrument. If reliable measurements of σ_ϕ are available, then the experiments in Copenhagen indicate that the most accurate predictions of σ_z are obtained from the Dr-method. Recently Balser and Netterville (1981) have reported that acustic sounders now are developed to such a stage that this instrument can be used to measure σ_ϕ on routine basis.

If possible, σ_z could also be predicted from the β-method, but this would require extensive computational facilities.

8. CONCLUSIONS

Results are reported from 10 elevated-source, urban-scale tracer dispersion experiments in the Copenhagen area, performed under neutral and unstable meteorological conditions. The tracer is released at a height of 115 m from the TV tower in Gladsaxe, a suburb of Copenhagen, with tracer sampling units ground-level positioned in 1-3 crosswind series, 2-6 km downwind from the tower. The roughness length for the site was estimated to be 0.6 m from measurements of the variance of the vertical wind velocity fluctuations as well as from mean wind profiles.

The lateral dispersion parameter, σ_y, was estimated from the measured tracer concentration distribution and compared with values of σ_y computed by methods based on the measured wind variance in the experiments and methods based on a stability classification of the atmospheric conditions. Both the β- and Dr-methods (based on wind variances) as well as the PGT- and Sm-methods (based on stability classifications) gave good estimates on the average of the lateral dispersion parameter, whereas the EPA-method (based on wind variance) produces estimates of σ_y that are 37% too low on the average. In these experiments, only one value of $(\sigma_y)_{EPA}$ out of 21 is larger than the corresponding value of $(\sigma_y)_{mea}$. The Sθ-method (based on wind variances) overpredicts $(\sigma_y)_{mea}$ by 27% in the mean. In the present experiments all values of $(\sigma_y)_{S\theta}$ are greater than $(\sigma_y)_{mea}$.

The root-mean-square (r.m.s.) fractional error clearly shows that the methods based on wind variances have the smallest scatter, (r.m.s. fractional error about 20%), whereas the PGT- and Sm-methods based on stability classification produce results with r.m.s. fractional errors of $\simeq$ 30% (PGT) and $\simeq$ 40% (Sm). The normalized lateral spread, f_y, was calculated. It is argued that the f_y-function in addition to being dependent on downwind distance must also be an explicite function of the wind velocity. Results

from the experiments support this wind velocity dependence, which is absent in Pasquill's method (1976).

Also, the measured tracer concentration distribution were cross-wind-integrated, $(\bar{\chi}_{CWI})_{mea}$. Estimates of $\bar{\chi}_{CWI}$ were computed by means of the vertical dispersion parameter, σ_z, derived according to the aforementioned methods, and assuming a Gaussian-type vertical tracer concentration distribution. The mean fractional error between calculated and measured values of $\bar{\chi}_{CWI}$ for the β-, Dr-, PGT- and Sm-method fell within the range of 20% to -20%; this constituted the uncertainty in the absolute tracer concentration associated with the calibration of the gaschromatograph for tracer analysis. The Sθ-method produced a mean fractional error of -29%; the large negative value of the mean fractional error of the EPA-method (-34%) suggests that the corrections of σ_z, recommended in the EPA-method due to the heat island effect, are too large for the residential area where the experiments are performed. The r.m.s. fractional error is seen to be almost equal for all methods, ranging from 31% to 44%. This indicates that none of the methods based on this analysis and the results from these dispersion experiments in the Copenhagen area can be considered superior in predicting the variation of $(\bar{\chi}_{CWI})_{mea}$. The methods based on the measured wind variances during the experiments, however, perform a little better than the stability based methods. An interesting effect was noted when using the β-method to predict $(\bar{\chi}_{CWI})_{mea}$. The fractional error systematically increases as a function of downwind distance. A tentative explanation of this might lie in the Hay and Pasquill (1959) assumption of similarity between the Lagrangian and Eulerian spectra. The effect implies that the low frequency part of the Lagrangian spectrum of the vertical wind velocity is more energetic than the corresponding part of the Eulerian spectrum. The difference may be ascribed to the effect of the shear layer in which dispersion in the vertical direction takes place.

The assumed Gaussian distribution of the tracer concentrations was found in some situations to be unable to reproduce values of $\bar{\chi}_{CWI}$ consistent with those measured in the series closer to the source.

The ability to successfully predict the maximum ground-level concentrations at the experimental distances were investigated by means of the normalized, ground-level concentration at the centerline, $(\bar{u}\bar{\chi}_{max}/Q)_{..}$. This quantity was compared with the normalized, measured tracer concentrations, $(\bar{u}\bar{\chi}_{max}/Q)_{mea}$, where for $\bar{\chi}_{max}$ the maximum measured tracer concentration in the various series have been inserted. For the β-, EPA- and Dr-methods the mean fractional error of the values of $(\bar{u}\bar{\chi}_{max}/Q)_{..}/(\bar{u}\bar{\chi}_{max}/Q)_{mea}$ is seen to be less than 20%. This constitutes the uncertainty in the measured, absolute tracer concentrations, and thus none of these three methods can be judged to be superior in the ability to predict the mean of $\bar{\chi}_{max}$. The wind variance-based Sθ-method has a mean fractional error of -58%. The stability-based methods, i.e. PGT and Sm, are seen to have a mean fractional error only slightly smaller than the lower limit of the uncertainty on the measured tracer concentrations. The root mean square of the fractional error describes the ability of the methods to predict the variation of $\bar{\chi}_{max}$. Here, the wind variance-based methods, β, EPA, Dr, and Sθ all come out with r.m.s. fractional errors of approximately 35%, whereas the stability-based methods have substantially larger r.m.s. fractional errors, 64% for the Sm-method and 53% for the PGT-method. For the experiments reported here, $(\bar{u}\bar{\chi}_{max}/Q)_{mea}$ is seen to vary in the range 0.6-2.8 for the β-method, in the range 0.6-2.8 for the Dr-method, 0.5-2.3 for the EPA-method, 0.3-1.5 for the Sθmethod, and 0.2-2.7 for the Sm-method. The ratio for the widely used PGT-method is seen to change in the range 0.3-4.0, thus varying more than an order of magnitude.

The experimental results also were compared to Willis and Deardorff's water-tank experiments modelling dispersion during fully convective conditions. The general behaviour as reported by Willis and Deardorff of the ground-level crosswind-integrated concentrations for near-surface releases is supported by the results from the experiments in Copenhagen, but it is characteristic that, even considering the substantial scatter, they all are larger than the values reported by Willis and Deardorff for near-surface releases. This means that the values of the actually measured crosswind-integrated concentrations for the

experiments in full scale are larger than those reported from the tank experiments. A tentative explanation for this difference might be found in the circumstance that a substantial part of the dispersion takes place in the lower region of the boundary layer, where mechanical turbulence is not negligible.

Based on the experiments, a semi-empirical model is devised for predicting the lateral and vertical dispersion parameters for elevated point sources in an urban area under neutral and unstable conditions.

ACKNOWLEDGEMENTS

The never failing support and interest of H. Flyger, the Air Pollution Laboratory, and N.E. Busch, Risø, are fully appreciated. I am much indebted to S. Hadvig, the Technical University of Denmark, for his help.

During my work I benefitted much from the advice of my colleagues at Risø, especially N.O. Jensen, L. Kristensen, S.E. Larsen and E.L. Petersen. Further, I gained much experience through collaboration with D.W. Thomson and H.A. Panofsky, both of Pennsylvania State University. L. Kristensen and D.W. Thomson also supplied valuable comments on the manuscript. The co-operation with E. Lyck, and the careful calibration and maintenance of the gas chromatograph by E. Lund Thomsen, both of the Air Pollution Laboratory, are acknowledged. The painstaking maintenance of the meteorological instruments by A. Hansen at the Meteorology Section is fully appreciated.

A number of persons and institutions were involved in the carrying out of the experiments. U. Torp of the Air Pollution Laboratory furnished routine meteorological measurements. H.S. Buch of the Danish Meteorological Institute provided forecasts for the experiments. The technical staff at the Air Pollution Laboratory and Meteorology Section provided practical support.

The routine meteorological measurements at the TV tower are performed by the Danish Meteorological Institute. The TV tower belongs to the Danish Department of Post and Telecommunication.

The study was sponsored by the Danish National Agency of Environmental Protection and Risø National Laboratory.

LIST OF SYMBOLS

a constant

A constant

a_n constant in Fourier-expansion

A^* characteristic function, $[A^* = \frac{1}{2}(\sigma_u^2 + \sigma_v^2)/(u_*^2\ \phi_\varepsilon^{2/3})]$

b slowly varying function of stability used in Lagrangian similarity theory, in practice $b = k$.

B bulk Richardson number

B^* characteristic height

B_r parameter describing the vertical concentration distribution

b_n constant in Fourier expansion

c function relating advection wind to $\bar{z}$

C constant

c_p specific heat of air at constant pressure

$\bar{C}$ dimensionless mean concentration, [time average]

$\bar{C}^y$ dimensionless crosswind-integrated mean concentration, [time average]

D constant

$\bar{E}$ mean turbulent kinetic energy, [time average]

f dimensionless frequency

F normalized power spectrum function

F_E normalized Eulerian power spectrum function

f_j function describing the dimensionless spread; $j = y$ (cross-wind spread), $j = z$ (vertical spread)

F_L normalized Lagrangian power spectrum function

$F^*_{L,i}$ dimensionless power spectrum function of dimensionless frequency $nt_{L,j}$, $(i,j) = (v,y),(w,z)$

$F_{L,v}$ normalized Lagrangian power spectrum function for the lateral wind velocity

f_s similarity function describing the vertical contration distribution

f_T dimensionless low-pass filtering frequency due to time of travel

f_{t_i} dimensionless low-pass filtering frequency due to instrument response

$f_{y,Draxler}$ Draxler's (1976) function of the dimensionless spread in the crosswind direction

$f_{y,Pasquill}$ Pasquill's (1976) function of the dimensionless spread in the crosswind direction

f_τ dimensionless high-pass filtering frequency due to sampling time

g acceleration of gravity

G function describing the influence of atmospheric stability on $d\hat{z}/dt$

h source height

H vertical flux of sensible heat

H_p transfer function for vertical propeller

H_v transfer function for wind vane

i intensity of turbulence

k von Kármán constant

K calibration factor for vertical propeller

K_H eddy diffusivity for heat

K_{ij} eddy diffusivity tensor

K_M eddy diffusivity for momentum

K_1 eddy diffusivity in the x_1-direction

K_{11} $K_{11} = K_1$

K_2 eddy diffusivity in the x_2-direction

K_{22} $K_{22} = K_2$

K_3 eddy diffusivity in the x_3-direction

K_{33} $K_{33} = K_3$

$(K_3)_o$ value of K_3 at the height $(x_3)_o$

ℓ characteristic lateral length scale

l instrument distance constant

L Monin-Obukhov length

m exponent in power law representation of the wind profile

$M\sigma_y$ used in Raynor et al.(1978) to represent the distribution of the location of the plume centerline

n frequency, (Hertz)

N number of terms in a Fourier expansion

n_E limiting frequency for Eulerian power spectrum

n_L limiting frequency for Lagrangian power spectrum

N_1 characteristic number of terms in a Fourier expansion

p exponent in power laws

q exponent in power law

Q release rate

r exponent of vertical concentration distribution

R_E Eulerian autocorrelation function

R_L Lagrangian autocorrelation function

$R^*_{L,i}$ Lagrangian autocorrelation function of dimensionless time lag $t/t_{L,i}$, $(i,j) = (v,y),(w,z)$

$R_{L,v}$ Lagrangian autocorrelation function of v

Ri gradient Richardson number

Ri_f flux Richardson number

s constant

S angular response function for vertical propeller, used in general derivations

$S(n)$ power spectrum function

S_{cup} angular response function for cup anemometer

S_E Eulerian power spectrum function

$S_{E,v}$ Eulerian power spectrum function for lateral wind velocity fluctuations

S_j dimensionless spread, j = y (crosswind spread), j = z (vertical spread)

S_L Lagrangian power spectrum function

S_{prop} angular response function for the vertical propeller

t time

T travel time

$\bar{T}$ mean temperature, [time average]

T' fluctuation of temperature

t_E Eulerian integral time scale

t_i instrument response time

t_L Eulerian integral time scale

$t_{L,v}$ Lagrangian integral time scale for v

T_y characteristic lateral time scale used by Draxler (1976)

T_z characteristic vertical time scale used by Draxler (1976)

T_o characteristic time for the transition between the initial and inertial stage of puff dispersion

T_* Monin-Obukhov temperature scale

u instantaneous wind velocity in the x_1-direction

$\bar{u}$ mean value of u, [time average]

u' fluctuation of u, $\overline{u'^2}$ is the variance of u', [time average]

u_1 instantaneous wind velocity in the x_1-direction, $u_1 = u$

$\bar{u}_1$ mean value of u_1, [time average]

u_1' fluctuation of u_1

u_2 instantaneous wind velocity in the x_2-direction, $u_2 = v$

$\bar{u}_2$ mean value of u_2, [time average]

u_2' fluctuation of u_2

u_3 instantaneous wind velocity in the x_3-direction, $u_3 = w$

$\bar{u}_3$ mean value of u_3, [time average]

u_3' fluctuation of u_3

$(\bar{u}_1)_o$ value of $\bar{u}_1$ at height $(x_3)_o$

u_* friction velocity

v instantaneous wind velocity in the x_2-direction, $v = u_2$

V output voltage from vertical propeller

$\bar{v}$ mean value of v, [time average]

v' fluctuation of v, $\overline{v'^2}$ is the variance of v', [time average]

v_g geostrophic wind

v_1 crosswind velocity of particle 1

v_2 crosswind velocity of particle 2

w instantaneous wind velocity in the x_3-direction, $w = u_3$

w' fluctuation of w, $\overline{w'^2}$ is the variance of w', [time average]

w_* convective velocity scale

x $x = \phi_m(Ri)^{-1}$

x downwind distance

X dimensionless downwind distance

x_1 co-ordinate for the horizontal along-wind direction, (Cartesian co-ordinate system)

x_2 co-ordinate for the horizontal crosswind direction (Cartesian co-ordinate system)

x_3 co-ordinate for the vertical direction (Cartesian co-ordinate system)

$(x_3)_o$ characteristic height

Y crosswind distance traversed by an air parcel, $\overline{Y^2}$ is the mean-square crosswind distance travelled by the air parcels, [ensemble average]

Y dimensionless crosswind distance

Y_c crosswind distance between a pair of particles, $\overline{Y_c^2}$ is the mean square separation between a pair of particles, [ensemble average]

y_i crosswind distance to position i

Y_o initial separation of a pair of particles

Y_1 crosswind distance traversed by particle 1

Y_2 crosswind distance traversed by particle 2

z height above the ground

Z dimensionless height

$\hat{z}$ mean plume height

z_i height of the lowest inversion

z_m geometric mean of z_1 and z_2

z_o roughness length

z_1 measuring height

z_2 measuring height

α angle

β ratio between Lagrangian and Eulerian integral time scales

β^+ estimate for the lateral windspeed sensed by the cup anemometer

β_y β for the lateral direction

γ angle between the wind vector and a vertical plane

Γ dry adiabatic lapse rate

δv relative crosswind velocity of a pair of particles

Δ indicate difference

Δw starting speed for vertical propeller

ε dissipation rate of turbulent kinetic energy

ζ damping ratio for wind vane

θ wind direction sensed by wind vane

$\bar{\theta}$ mean potential temperature, [time average]

κ wave number

λ wavelength

λ_p distance constant for the vertical propeller

λ_v characteristic length for the wind vane

Λ function of lateral position and shape of the vertical concentration distribution to secure fulfilment of the continuity equation

ξ time lag in $R_{L,v}(\xi)$

ρ density of air

Σ indicate summation

σ_E standard deviation of Eulerian wind velocity fluctuations, $\sigma_E^2 = \int_0^\infty S_E(n)\,dn$

σ_L standard deviation of Lagrangian wind velocity fluctuations, $\sigma_{L_2}^2 = \int_0^\infty S_L(n)\,dn$

σ_u $[\sigma_u^2 \equiv \overline{u'^2}]$

σ_v $[\sigma_v^2 \equiv \overline{v'^2}]$

σ_w $[\sigma_w^2 \equiv \overline{w'^2}]$

σ_y standard deviation of crosswind concentration distribution

$(\sigma_y)_{Dr}$ σ_y derived from Draxler (1976)

$(\sigma_y)_{EPA}$ σ_y derived from Pasquill (1976)

$(\sigma_y)_{mea}$ σ_y derived from the measured concentrations

$(\sigma_y)_{PGT}$ σ_y derived from Turner (1970)

$(\sigma_y)_{Sm}$ σ_y derived from Smith (1973), based upon a stability classification

$(\sigma_y)_{S\Theta}$ σ_y derived from Smith (1973), based upon measured wind variances

$(\sigma_y)_\beta$ σ_y derived from Hay and Pasquill (1959)

$(\sigma_y)_{..}$ σ_y derived from the various methods

σ_z characteristic standard deviation of the vertical concentration distribution

$(\sigma_z)_{Dr}$ σ_z derived from Draxler (1976)

$(\sigma_z)_{EPA}$ σ_z derived from Pasquill (1976)

$(\sigma_z)_{est}$ σ_z estimated from the measured concentrations

$(\sigma_z)_{PGT}$ σ_z derived from Turner (1970)

$(\sigma_z)_{Sm}$ σ_z derived from Smith (1973), based upon a stability classification

$(\sigma_z)_{S\Theta}$ σ_z derived from Smith (1973), based upon measured wind variances

$(\sigma_z)_\beta$ σ_z derived from Hay and Pasquill (1959)

$(\sigma_z)_{..}$ σ_z derived from the various methods

σ_Θ standard deviation of the lateral wind direction fluctuations

$\Sigma\sigma_y$ used in Raynor et al. (1978) to describe the spread of a plume, including the effect of meandering and dispersion

σ_ϕ standard deviation of the vertical wind direction fluctuations

τ sampling time

τ surface shear stress

Φ dimensionless function relating Ri_f to z/L

ϕ angle between the wind vector and a horizontal plane

ϕ_h dimensionless temperature gradient

ϕ_m dimensionless wind shear

ϕ_ε dimensionless dissipation

χ instantaneous concentration

$\bar{\chi}$ mean value of χ, [time average]

χ' fluctuation of χ

$\bar{\chi}_{CWI}$ crosswind-integrated mean concentration, [time average]

$(\bar{\chi}_{CWI})_{EPA}$ $\bar{\chi}_{CWI}$ derived from Pasquill (1976)

$(\bar{\chi}_{CWI})_{mea}$ $\bar{\chi}_{CWI}$ derived from the measured concentrations

$(\bar{\chi}_{CWI})_{PGT}$ $\bar{\chi}_{CWI}$ derived from Turner (1970)

$(\bar{\chi}_{CWI})_{Sm}$ $\bar{\chi}_{CWI}$ derived from Smith (1973), based on a stability classification

$(\bar{\chi}_{CWI})_{S\Theta}$ $\bar{\chi}_{CWI}$ derived from Smith (1973), based on measured wind variances

$(\bar{\chi}_{CWI})_{\beta}$ $\bar{\chi}_{CWI}$ derived from Hay and Pasquill (1959)

$(\bar{\chi}_{CWI})_{..}$ $\bar{\chi}_{CWI}$ derived from the various methods

$\bar{\chi}_i$ measured tracer concentration at position i

$\bar{\chi}_{max}$ maximum ground-level concentration at a certain distance from the source. Whether it is measured or derived from one of the various methods is indicated by subscripts.

$\bar{\chi}_o$ mean concentration at ground level, [time average]

Ψ dimensionless function describing the effect of stability on the wind profile

Ψ_u dimensionless function describing the effect of stability on σ_u

Ψ_v dimensionless function describing the effect of stability on σ_v

Ψ_w dimensionless function describing the effect of stability on σ_w

ω frequency, (rad/s)

Ω angular velocity, the argument indicates the angle of attack of the wind vector

ω_e characteristic frequency, (rad/s), for wind vane

Ω^+ estimate of the vertical velocity as sensed by the vertical propeller

I subscript indicating a specific area

II subscript indicating a specific area

REFERENCES

BARAD, M.L. (1958). Project Prairie Grass, a field program in diffusion. Geophys. Res. Pap., no. 59, vol. 1 and 2. (U.S. Air Force Cambridge Research Center, Bedfort, Mass.) AFCRC-TR-58-235. 280 + 209 pp.

BALSER, M., and NETTERVILLE, D. (1981). Measuring wind turbulence with doppler-acoustic radar. J. Appl. Meteorol., 20, 27-35.

BATCHELOR, G.K. (1952). Diffusion in a field of homogeneous turbulence, II. The relative motion of particles. Proc. Camb. phil. Soc., 48, 345-362.

BERKOWICZ, R., and PRAHM, L.P. (1979). Generalization of K theory for turbulent diffusion. Part I: Spectral turbulent diffusivity concept. J. Appl. Meteorol., 18, 266-272.

BRIER, G.W. (1950). The statistical theory of turbulence and the problem of diffusion in the atmosphere. J. Meteorol. 7, 283-290.

BRIGGS, G.A., and McDONALD, K.R. (1978). Prairie grass revisited: Optimum indicators of vertical spread. (Environmental Research Laboratories. Air Resources, Atmospheric Turbulence and Diffusion Laboratory, Oak Ridge, Tennessee), ATDL contribution no. 78/8, 31 pp.

BROOK, R.R. (1977). Effective dynamic response of paired Gill anemometers. Boundary-Layer Meteorol., 11, 33-37.

BUSCH, N.E., and KRISTENSEN, L. (1976). Cup anemometer overspeeding. J. Appl. Meteorol., 15, 1328-1332.

BUSCH, N.E., CHRISTENSEN, O., KRISTENSEN, L., LADING, L., and LARSEN, S.E. (1979). Meteorological field instrumentation. Wind speed and direction by means of cups, vanes, propellers and lasers. Risø-R-400, 49 pp.

BUSINGER, J.A. (1973). Turbulent transfer in the atmospheric surface layer. In: Workshop on micrometeorology. Ed. by D.A. Haugen. (American Meteorological Society, Boston, Mass.), 67-100.

CHAUDHRY, F.H., and MERONEY, R.N. (1973). Similarity theory of diffusion and the observed vertical spread in the diabatic surface layer. Boundary-Layer Meteorol., 3, 405-415.

CHRISTENSEN, O. (1971). Wind velocity sensing by means of four-bladed helocoid propellers. Report, University of Michigan, Department of Meteorology and Oceanography, 100 pp.

CORRSIN, S. (1963). Estimates of the relations between Eulerian and Lagrangian scales in large Reynolds number turbulence. J. Atmos. Sci., 20, 115-119.

CORRSIN, S. (1974). Limitations of gradient transport models in random walks and in turbulence. In: Turbulent diffusion in environmental pollution. Proceeding of a symposium held at Charlottesville, Va., April 8-19, 1973. Ed. by F.N. Frenkiel and R.E. Munn. (Advances in Geophysics, 18A), (Academic Press, London), 25-60.

CRAMER, H.E. (1959). Engeneering estimates of atmospheric dispersal capacity. Am. Ind. Hyg. Assoc. J., 20, 183-189.

CRAMER, H.E., RECORD, F.A., and VAUGHAN, H.C., (1958). The study of the diffusion of gases or aerosols in the lower atmosphere. (U.S. Air Force Cambridge Research Center, Bedford, Mass.) AFCRC-TR-58-239. 70 pp.

DE FÉRIET, J.K. (1939). Les fonctions aléatories stationnaires et la théorie statistique de la turbulence homogene. Ann. Soc. Sci., Bruxelles, Ser. 1, 59, 145-194.

DEARDORFF, J.W., and WILLIS, G.E. (1975). A parameterization of diffusion into the mixed layer. J. Appl. Meteorol., 14, 1451-1458.

DORAN, J.C., HORST, T.W., and NICKOLA, P.W. (1978). Variations in measured values of lateral diffusion parameters. J. Appl. Meteorol., 17, 825-831.

DRAXLER, R.R. (1976). Determination of atmospheric diffusion parameters. Atmos. Environ., 10, 99-105.

ELLIOTT, W.P. (1961). The vertical diffusion of gas from a continuous source. Int. J. Air Water Pollut., 4, 33-46.

FRANCEY, R.J., and SAHASHI, K. (1979). Gill propeller anemometer frequency response over the sea. J. Appl. Meteorol., 18, 1083-1086.

GIFFORD, F.A. (1961). Use of meteorological observations for estimating atmospheric dispersion. Nucl. Saf. 2(4), 47-51.

GOLDER, D. (1972). Relations among stability parameters in the surface layer. Boundary-Layer Meteorol., 3, 47-58.

GRYNING, S.E., LYCK, E., and HEDEGAARD, K. (1978). Short-range diffusion experiments in unstable conditions over inhomogeneous terrain. Tellus, 30, 392-403.

GRYNING, S.E. and THOMSON, D.W. (1979). A tall-tower instrument system for mean and fluctuating velocity, fluctuating temperature and sensible heat flux measurements. J. Appl. Meteorol., 18, 1674-1678.

GRYNING, S.E., and LYCK, E. (1980a). Medium-range dispersion experiments downwind from a shoreline in near neutral conditions. Atmos. Environ., 14, 923-931.

GRYNING, S.E., PETERSEN, E.L., and LYCK, E. (1980b). Elevated source SF_6-tracer dispersion experiments in the Copenhagen area. Preliminary results I. Proceedings of the tenth international technical meeting on air pollution modelling and its application. NATO/CCMS Air Pollution Pilot Study, Rome, Italy, October 22-26, 1979, 119-132.

GRYNING, S.E., and LYCK, E. (1980c). Elevated source SF_6-tracer dispersion experiments in the Copenhagen area. Preliminary results II. In: Seminar on radioactive releases and their dispersion in the atmosphere following a hypothetical reactor accident. Vol. 2. Risø, April 22-25, 1980. (Commission of the European Communities, Luxembourg), 905-924.

GRYNING, S.E., and LYCK, E. (1980d). Comparison between dispersion calculation methods based on in-situ meteorological measurements and results from elevated-source tracer experiments in an urban area. Danish National Agency of Environmental Protection, Air Pollution Laboratory, MST LUFT A40, 32 pp.

GRYNING, S.E., and LARSEN, S.E. (1981). Relation between dispersion characteristics over surfaces with dissimilar roughness and atmospheric stability, under conditions of equal geostrophic winds. Atmos. Environ., 15, 983-987.

HAMILTON, P.M. (1969). The application of a pulsed-light rangefinder (lidar) to the study of chimney plumes. Philos. Trans. R. Soc. London, Ser. A 265, 153-172.

HAY, J.S., and PASQUILL, F. (1957). Diffusion from a fixed source at a height of a few hundred feet in the atmosphere. J. Fluid Mech., 2, 299-310.

HAY, J.S. and PASQUILL, F. (1959). Diffusion from a continuous source in relation to the spectrum and scale of turbulence. In: Atmospheric diffusion and air pollution. Proceedings of a symposium held at Oxford, August 24-29, 1958. Ed. by F.N. Frenkiel and P.A. Sheppard (Advances in Geophysics, 6), (Academic Press, London), 345-365.

HORST, T.W. (1979). Lagrangian similarity modeling of vertical diffusion from a ground-level source. J. Appl. Meteorol., 18, 733-740.

KAIMAL, J.C., WYNGAARD, J.C., HAUGEN, D.A., COTÉ, O.R., and IZUMI, Y. (1976). Turbulence structure in the convective boundary layer. J. Atmos. Sci., 33, 2152-2169.

KAIMAL, J.C. (1978). Horizontal velocity spectra in an unstable surface layer. J. Atmos. Sci., 35, 18-24.

KLUG, W. (1969). Ein verfahren zur bestimmung der ausbreitungsbedingungen aus synoptischen beobachtungen. Staub-Reinhalt. Luft, 29, 143-147.

LAMB, R.G. (1978). A numerical simulation of dispersion from an elevated point source in the convective planetary boundary layer. Atmos. Environ., 12, 1297-1304.

LARSEN, S.E., and BUSCH, N.E. (1974). Hot-wire measurements in the atmosphere. Part 1: Calibration and response characteristics. DISA Information No. 16, 15-34.

LEMONE, M.A. (1973). The structure and dynamics of horizontal roll vortices in the planetary boundary layer. J. Atmos. Sci., 30, 1077-1091.

LETTAU, H. (1952). On eddy diffusion in shear zones. (U.S. Air Force Cambridge Research Center, Bedford, Mass.), Geophys. Res. Pap., No. 19, 437-445.

LUMLEY, J.L., and PANOFSKY, H.A. (1964). The structure of atmospheric turbulence. (Interscience monographs and texts in physics and astronomy, XII), (Interscience, New York) 239 pp.

MACCREADY, P.B., Jr. (1965). Dynamic response characteristics of meteorological sensors. Bull. Am. Meteorol. Soc., 46, 533-538.

MCELROY, J.L., and POOLER, F. JR. (1968) St. Louis dispersion study, Vol. 2. Analysis. NAPCA-Pub-AP-53. PB-190-255. 56 pp.

MCELROY, J.L. (1969). A comparative study of urban and rural dispersion. J. Appl. Meteorol., 8, 19-31.

MONIN, A.S. (1959). Smoke propagation in the surface layer of the atmosphere. In: Atmospheric diffusion and air pollution. Proceeding of a symposium held at Oxford, August 24-29, 1958. Ed. F.N. Frenkiel and P.A. Sheppard. (Advances in Geophysics, 6), (Academic Press, London), 331-343.

NIEUWSTADT, F.T.M., and ULDEN, A.P. van (1978). A numerical study on the vertical dispersion of passive contaminants from a continuous source in the atmospheric surface layer. Atmos. Environ., 12, 2119-2124.

NIEUWSTADT, F.T.M., and DUUREN, H. van (1979). Dispersion experiments with SF_6 from the 213 m high meteorological mast at Cabauw in the Netherlands. In: Fourth symposium on turbulence, diffusion and air pollution, January 15-18, 1979. Reno, Nev. (American Meteorological Society, Boston, Mass.), 34-40.

NIEUWSTADT, F.T.M. (1980). Application of mixed-layer similarity to the observed dispersion from a ground-level source. J. Appl. Meteorol., 19, 157-162.

NRC REGULATORY GUIDE (1972). Onsite meteorological programs. Regulatory Guide 1.23. U.S. Nuclear Regulatory Commission.

OGURA, Y. (1957). The influence of finite observation intervals on the measurement of turbulent diffusion parameters. J. Meteorol., 14, 176-181.

PANOFSKY, H.A. (1973). Tower micrometeorology. In: Workshop on micrometeorology. Ed. by D.A. Haugen. (American Meteorological Society, Boston, Mass.), 151-176.

PANOFSKY, H.A. (1978). Matching in the convective planetary boundary layer. J. Atmos. Sci., 35, 272-276.

PANOFSKY, H.A. (1979). Lecture notes for Meteo 555 (Atmospheric Diffusion) at the Pennsylvania State University.

PASQUILL, F. (1961). The estimation of the dispersion of windborne material. Meteorol. Mag., 90, 33-49.

PASQUILL, F. (1962). Atmospheric diffusion. The dispersion of windborne materials from industrial and other sources. (van Nostrand, London), 297 pp.

PASQUILL, F. (1974). Atmospheric diffusion. The dispersion of windborne materials from industrial and other sources. 2. edition. (Wiley, London), 429 pp.

PASQUILL, F. (1975a). The dispersion of materials in the atmospheric boundary layer - the basis for generalizations. In: Lectures on air pollution and environmental impact analyses. Boston, Mass., September 29 - October 3, 1975. Ed. by D.A. Haugen. (American Meteorological Society, Boston, Mass.), 1-34.

PASQUILL, F. (1975b). Some topics relating to modelling of dispersion in boundary layer. EPA-650/4-75-015. PB-243524/6 GA. 69 pp.

PASQUILL, F. (1976). Atmospheric dispersion parameters in gaussian plume modeling. Part II. Possible requirements for change in the Turner workbook values. EPA-600/4-76-030B. PB-258036/3 GA. 55 pp.

PAULSON, C.A. (1970). The mathematical representation of windspeed and temperature profiles in the unstable surface layer. J. App. Meteorol., 9, 857-861.

PRIESTLEY, C.H.B. (1955). Free and forced convection in the atmosphere near the ground. Q. J. R. Meteorol. Soc., 81, 139-143.

RAYNOR, G.S., MICHAEL, P., BROWN, R.M., and SETHURAMAN, S. (1975). Studies of atmospheric diffusion from a nearshore oceanic site. J. Appl. Meteorol., 14, 1080-1094.

RAYNOR, G.S., BROWN, R.M., and SETHURAMAN, S. (1978). A comparison of diffusion from a small island and an undisturbed ocean site. J. Appl. Meteorol., 17, 129-139.

RAYNOR, G.S. (1978). A radio-controlled air sampling system for diffusion experiments. J. Appl. Meteorol., 17, 1619-1624.

ROBERTS, O.F.T. (1923). The theoretical scattering of smoke in a turbulent atmosphere. Proc. Roy. S. London, Ser. A, 104, 640-654.

SAGENDORF, J.F., and DICKSON, C.R. (1974). Diffusion under low windspeed inversion conditions. NOAA TM-ERL-ARL-52. 93 pp.

SHEIH, C.M. (1980). On the lateral dispersion coefficients as functions of averaging time. J. Appl. Meteorol., 19, 557-561.

SMITH, F.B. (1957). The diffusion of smoke from a continuous elevated point-source into a turbulent atmosphere. J. Fluid Mech., 2, 49-76.

SMITH, F.B., and HAY, J.S. (1961). The expansion of clusters of particles in the atmosphere. Q. J. R. Meteorol. Soc., 87. 82-101.

SMITH, F.B. (1973). A scheme for estimating the vertical dispersion of a plume from a source near ground level. In: Proceedings of the third meeting of the expert panel on air pollution modeling. Paris, October 2-3, 1972 A report of the air pollution pilot study (Nato Comittee on the Challenges of Modern Society, Bruxelles) Chapter XVII, 14 pp.

SMITH, F.B. (1979). The relation between Pasquill stability P and Kazanski-Monin stability μ (in neutral and unstable conditions). Atmos. Environ., 13, 879-881.

SMITH, M.E. (1956). The variation of effluent concentrations from an elevated point source. A.M.A. Arch. Ind. Health, 14, 56-68.

SMITH, M.E. (Ed.) (1973). Recommended guide for the prediction of the dispersion of airborne effluents. 2. (American Society of Mechanical Engineers, New York). 85 pp.

SUTTON, O.G. (1953). Micrometeorology, (McGraw-Hill, New York), 333 pp.

TAYLOR, G.I. (1921). Diffusion by continouos movements. Proc. Lond. Math. Soc. 2, 196-211.

TENNEKES, H., and LUMLEY, J.L. (1972). A first course in turbulence. (MIT Press, Cambridge, Mass.) 300 pp.

THOMAS, P., and NESTER, K. (1976). Experimental determination of the atmospheric dispersion parameters over rough terrain, part 2, evaluation of measurements. KFK-2286. 25 pp.

TURNER, D.B. (1970). Workbook of atmospheric dispersion estimates. (National Air Pollution Control Administration, Cincinnati, Ohio) HPS Pub. 999-AP-26. 88 pp.

ULDEN, A.P. van (1978). Simple estimates for vertical diffusion from sources near the ground. Atmos. Environ., 12, 2125-2129.

VOGT, K.J., and GEISS, H. (1974). Tracer experiments on the dispersion of plumes over terrain of major surface roughness. JÜL-1131-ST. 19 pp.

WANDEL, C.F., and KOFOED-HANSEN, O. (1962). On the Eulerian-Lagrangian transform in the statistical theory of turbulence. J. Geophys. Res., 67, 3089-3093.

WILLIS, G.E., and DEARDORFF, J.W. (1976). A laboratory model of diffusion into the convective planetary boundary layer. Q. J. R. Meteorol. Soc., 102, 427-445.

WILLIS, G.E., and DEARDORFF, J.W. (1978). A laboratory study of dispersion from an elevated source within a modeled convective planetary boundary layer. Atmos. Environ., 12, 1305-1311.

YANSKEY, G.R., MARKEE, E.H., and RICHTER, A.P. (1966). Climatology of the national reactor testing station. IDO-12048. 220 pp.

ZILITINKEVICH, S.S., and MONIN, A.S. (1974). Similarity theory for the planetary boundary layer of the atmosphere. Izv. Acad. Sci. USSR, Atmos. Oceanic Phys. 10, 353-359.

ZILITINKEVICH, S.S. (1975). Resistance laws and prediction equations for the depth of the planetary boundary layer. J. Atmos. Sci., 32, 741-752.

APPENDIX

Prior to the dispersion experiments in Copenhagen, two experimental campaigns were carried out at Risø National Laboratory in order to test the developed tracer sampling units and the devised experimental procedure.

In the first campaign, reported by Gryning et al. (1978), the first generation tracer sampling units, developed to measure the dispersion of a release of the tracer sulphur hexafluoride, were tested in nine experiments during the period April to July 1976.

The tracer was released at a high of 60 m from the Risø meteorological tower, situated on a peninsula in the Roskilde Fjord, Denmark, and was sampled at ground-level positions distributed along a crosswind line about 1 km downwind. During the experiments, the turbulent wind velocity components were measured at the height of release with a three-dimensional ultrasonic anemometer. The experiments were performed in westerly winds; hence the dispersion was influenced by the internal boundary layer developing downwind from the inhomogeneity in surface roughness between the fjord and the site. Five of the experiments, performed under neutral and slightly unstable conditions, were accepted as cases of purely turbulent dispersion of the tracer. Because of wind direction shifts the others were discarded.

The tracer concentration measurements allowed for a direct estimate of the lateral dispersion parameter, σ_y. The working approximation of Taylor's dispersion formula, described by Hay and Pasquill (1959), using the wind velocity measurements at the height of release, was found to give a good prediction of the values of σ_y derived from the measured tracer concentrations. However, the tracer was released and the sonic measurements were performed above the internal boundary layer, but a substantial part of the dispersion of the tracer took part

inside. The good agreement shows that the lateral dispersion at 1 km is rather insensitive to the developing internal boundary layer. It is argued that this can be a consequence of the fact that the increase in variance inside the internal boundary layer almost entirely takes place at frequencies so high that they will be eliminated to a large extent by the low-pass filtering implied in Taylor's formula.

Because the estimates of the vertical parameter σ_z were inferred only from continuity considerations, they could not be used to check the validity of calculating σ_z from Taylor's formula, but on the other hand, no inconsistency with this formula was found.

A second, rather similar, experimental campaign, reported by Gryning and Lyck (1980a), was carried out at Risø in the fall, winter, and spring seasons of 1976-77. A greater number of slightly modified tracer sampling units were now available, and a factor of ten improvement in the sensitivity of the gaschromatograph for tracer analysis allowed the dispersed tracer to be sampled at ground level about 5 km downwind from the source at the same tracer release rate as in the first campaign. No changes were made in the tracer release system and the meteorological instrumentation.

Five atmospheric dispersion experiments out of a total of six, all assigned Pasquill stability class D, were suitable for this analysis. The experiments were performed with westerly winds, so the dispersion was influenced by the internal boundary layer that develops downwind from the inhomogeneity between Roskilde Fjord and the Risø site.

The lateral dispersion parameters, σ_y, were estimated according to three methods based on quantitative descriptions of the flow and compared with the measured values of σ_y. Hay and Pasquill's approximation (1959) of Taylor's formula was again found to work well in predicting σ_y, which also applied to the method described by Draxler (1976).

Equivalent comparisons of the vertical dispersion parameter, σ_z, were troublesome as the sampling unit set-up allowed only for an indirect estimate of σ_z. A tentative correction based on Draxler's method (1976) was devised for the effect of change of surface roughness on the estimates of σ_z. Applying this correction, Draxler's method was found to predict the indirect measured σ_z-values reasonably well.

The ability of the various methods to predict the maximum ground-level tracer concentrations was also investigated. The agreement between the estimated maximum ground-level concentrations derived from Draxler, when applying the devised correction on σ_z, and the concentrations actually measured was found to be better in most cases than the absolute calibration uncertainty in the tracer analysis.